SWITCHED CAPACITOR NETWORKS

(A NOVEL PREWARPING PROCEDURE)

Charles Robert Weston Campbell

Thesis submitted to the Department of Electrical and Electronic Engineering, Faculty of Engineering at the University of Cape Town for the degree of Doctor of Philosophy of Engineering.

Cape Town, December 1984.

SWITCHED CAPACITOR NETWORKS

(A NOVEL PREWARPING PROCEDURE)

Charles Robert Weston Campbell

ABSTRACT

Novel methods for prewarping filter specifications prior to realization in Switched Capactior (SC) form are presented. These allow the design of arbitrary response requirements, exhibiting a low amount of error that normally results from the frequency warping associated with sampled-data networks.

Adjustment is applied to the pole and zero locations of a reference filter, using three distinct approaches (Center Frequency "CF", Selectivity "S" and Complex Mapping "CM" pole/zero prewarping), developed for both the Lossless Discrete Integrator (LDI) and Bilinear (Bil) analog to digital transformations. The derivation of the prewarping expressions is explained with reference to these mappings, and the effect they have on the apparent pole and zero locations of an SC filter realization.

The success of each approach in yielding an accurate approximation to a required response is then assessed by calculating the error that each pole and zero contributes to the magnitude response of the prewarped realization. By plotting this error as a function of pole (or zero) location and signal frequency, general observations follow, regarding the use of pole/zero prewarping, and the suitability of each approach for particular filter applications.

Accordingly, CM prewarping is seen to exhibit an error characteristic associated with low distortion of the filter

magnitude response shape, while those of CF and S prewarping have error characteristics associated with reduced magnitude error in the vicinity of the poles and zeros of the filter function. In a similar way the LDI and Bil transformations are compared, showing that poorer approximations result when using the Bil transformation.

The pole error contribution analysis is also used for optimizing the response, by allowing selective use, within a single filter, of the three pole/zero prewarping approaches. Another technique for this optimization involves increasing the filter order, and methods for its application, based on the error analysis, are described.

Computer-simulated examples are used to demonstrate the application of pole/zero prewarping and some of the optimization techniques available. Using one of these examples, pole/zero prewarping is compared with classical prewarping, showing that, although both yield very good approximations, classical prewarping is to be preferred, because of its reliability and ease of application. However, the advantages of pole/zero prewarping become evident in filter designs requiring non-piecewise-constant-magnitude responses, where classical prewarping can no longer be applied. Such an example is given showing that very close agreement between an analog reference filter and its SC realization is possible when using pole/zero prewarping.

The application of pole/zero prewarping in Forward-Difference (FD) and Backward-Difference (BD) transformed structures is also demonstrated, and the results compared with those obtained by using the LDI and Bil transformations. Comparable results are shown to be possible. However, the FD and BD transformations are

not recommended because of the large amount of prewarping necessary, and the possible adverse effects this may have on the filter design and performance.

For high frequency applications, and those which employ variable sampling frequency, a new approach to prewarping is suggested, involving adjustment of the signal in Complementary Frequency Conversion (COFREC) pre- and post-filters. Ways of implementing these COFREC filters, using Surface Acoustic Wave (SAW) devices, are studied, and limitations to their immediate application identified.

The noise behaviour of SC networks is also discussed, and results are presented, showing that accurate prediction of the noise at the output of a filter is possible. Two prediction methods are used for comparison with experimental results : (i) a frequency-domain approach based on z-domain analysis of the circuit, and (ii) SPICE simulation. In addition, a third approach is described that involves a time-domain simulation of the circuit. However, problems related to the time-varying nature of SC networks were encountered when applying this method to filter examples other than a first order integrator. For the experimental noise measurement, a new expression is derived, enabling characterization of the equivalent input noise current and voltage of an operational amplifier.

Finally, a brief summary of the operations of interpolation and decimation is given, showing how these may be used to improve the design and performance of SC networks. Existing interpolation and decimation circuits are given, and the way in which these may be used in general sample rate conversion systems is described.

DECLARATION

I declare that this Thesis is my own unaided work. It is being submitted for the degree of Doctor of Philosophy of Engineering in the University of Cape Town. It has not been submitted previously for any degree or examination in any other University.

Signature removed

C.R.W.Campbell

20th day of December , 1984.

ACKNOWLEGEMENTS

To my supervisor Prof. K.M.Reineck, very many thanks for support and advice throughout the period during which this research was undertaken. Thanks are also due to Prof. F.W.Stephenson for his supervision during my year at Virginia Polytechnic Institute & State University, and to the other members of the research team there, in particular Bill McCall and Eric Li, with whom I had the privilege of working closely. Useful discussions were also held with Dr. J.A.Nossek concerning COFREC filtering. Much of the financial support I received was from the Council for Scientific and Industrial Research, without which this work would not have been possible.

Thankyou to my wife, Beryl, for her support and love, especially during the final stages of preparing this manuscript.

Finally, thankyou to God, who has created a magnificent universe full of mysteries to be discovered, and who involves Himself in His creation through Jesus Christ.

PREFACE

In 1980 I came into contact with some recent publications on Switched Capacitor (SC) filters while completing an undergraduate thesis project on low number of component network realizations employing the unsymmetrical lattice structure. Through working on this thesis project, my interest was aroused in circuit theory, and I became familiar with some of the analytical tools necessary for such research. In particular, it appeared that the analog to digital transformations and associated frequency warping in SC filters required some investigation.

In most publications, prewarping had been applied to the filter specifications before realization in SC form. However, the examples given were invariably piecewise-constant-magnitude responses, where the shape of the SC filter response in relation to that of a reference function was unimportant provided the pass-band and stop-band requirements were fulfilled. My aim was to investigate ways whereby close approximations to a reference filter response shape could be obtained, allowing the realization of general non-piecewise-constant-magnitude responses.

Prewarping by adjustment of the pole and zero locations is the primary contribution of this research, and has resulted in two publications. A paper entitled "A Novel Prewarping Technique for the Design of Wideband SC Filters" was presented at the 26th Midwest Symposium on Circuits and Systems, Puebla, Mexico in August 1983. In this paper I introduced three pole/zero prewarping approaches, giving examples of their application. The second publication, "A Pole/Zero Prewarping Procedure in SC Filter Design", was an extension of the first paper, and was intended for

wider readership. This appeared in the IEEE Transactions on Circuits and Systems in September 1984. In addition to giving the pole/zero prewarping expressions, I discussed methods for the error analysis, as presented in chapter 6.

A third paper has been accepted for presentation at the International Conference on Circuits and Systems, Beijing, China in June 1985. In this paper, entitled "High Frequency SC Filters Incorporating Surface Acoustic Wave Technology", I have discussed original ideas regarding the elimination of frequency warping effects by using "Complementary Frequency Conversion" (COFREC) filtering, as presented in chapter 4.

In this thesis I have studied the analog to digital mappings that occur when realizing filters in SC form, and have summarised existing methods of prewarping, showing the need for a general approach to this problem. A full description of pole/zero prewarping with its associated error analysis is included, and examples are given demonstrating its use. Regarding the concept of COFREC filtering, I have suggested a way in which it can be implemented using Surface Acoustic Wave devices, and have attempted to identify factors involved in their realization, giving possible limitations to their immediate use.

I have also included chapters on noise analysis and the use of interpolation and decimation in SC filters. Both aspects have received limited attention in literature, and while investigating the former I gained valuable practical experience in the construction and testing of these filters.

CONTENTS

Chapter 1

INTRODUCTION

In its relatively short history of some 12 years, the design of Switched Capacitor (SC) networks has developed into a mature discipline. During this time, different classes of SC filters have emerged together with a variety of analysis and design procedures. Areas of application include analog and digital data transmission, speech synthesis, interpolation/decimation, signal processing, programmable filters and adaptive equalisers.

Certain bounds relating to the realization and use of SC filters have been, and are still being researched. The non-linear warping of a filter frequency characteristic, found to be inherent in sampled signal systems, is one such bound. In cases where the sampling frequency is very much larger than the signal frequencies within the pass-band, this effect will be negligible. However, generally this condition is not always fulfilled, and therefore compensation must be applied in the form of prewarping, requiring the initial filter specifications to be adjusted to account for the effects of warping.

For piecewise-constant-magnitude transfer responses, prewarping is easily applied. The specified pass-band and stop-band edge frequencies are each adjusted so as to compensate exactly for the effect of warping. However, for transfer responses that can not be described in this way, other techniques must be applied.

A number of different prewarping methods have previously been applied for the design of SC filters. However, no general approach to the problem of prewarping exists, and evaluation and

optimization techniques in the application of prewarping, have so far not been formalized. As a result, an investigation into the whole question of prewarping as related to SC filter design was begun in 1981.

The objective of the study was to investigate methods whereby non-piecewise-constant-magnitude transfer responses could be effectively approximated using SC filters. For three distinct approaches, design equations were derived which involved the prewarping of the poles and zeros of a required transfer response. The efficiency of each approach was then evaluated by calculating the magnitude error contributed by each pole and zero when applied to the SC realization. Computer-simulated examples were used to demonstrate the advantages of each of the pole/zero prewarping techniques, showing that very good agreement between a required, and SC filter realized response is possible.

Another novel "prewarping" method was also studied and described, involving the elimination of warping effects in SC filters. This is achieved by using a pair of frequency conversion filters (a pre-filter and post-filter) to warp the signal, and thus leave the main filter specifications unaffected.

Realization of these "Complementary Frequency Conversion" (COFREC) filters is best implemented by Surface Acoustic Wave (SAW) devices. This requires close scrutiny of the design and technology approach best suited for this application, as well as an investigation of the limitations affecting its immediate application. Nevertheless, this novel concept involving COFREC filtering is considered to hold great promise.

In the first part of chapter 2, a brief outline of the main features relating to the development of SC filters is presented. Key references in each area are cited where appropriate, allowing this section to be used as a selective bibliography. The basic concept of resistor replacement by a switched capacitor is then introduced in the second part, and integrated SC filters are compared briefly with their RC active counterparts.

The sampled-data nature of SC networks is described in chapter 3. Mappings are compared for the four common analog to digital transformations (LDI, Bilinear, Forward-Difference "FD" and Backward-Difference "BD"), and the phenomenon of frequency warping in SC filters is specifically examined.

In chapter 4, classical prewarping methods are described, while the principles of COFREC pre- and post-filtering are studied in some detail. In addition, pole/zero prewarping is outlined briefly here before the equations used in its application and evaluation are derived more formally in chapters 5 & 6. A general second order transfer response expression is used to illustrate the derivation process, which involves a comparison of the desired and effective locations of the poles and zeros in the SC filter design.

Subsequently, graphical methods are presented which can assist in the evaluation and selection of the most suitable prewarping approach. These involve magnitude error plots shown for each pole and zero in the SC filter. Computer-simulated examples are then given in chapter 7 which demonstrate the application of pole/zero prewarping and the use of the evaluation expressions. Three examples are presented, the first of which compares pole/zero prewarping with classical prewarping, as applied to a

piecewise-constant-magnitude transfer response.

In the second example, a tenth-order speech synthesis filter is used to demonstrate the suitability of pole/zero prewarping as applied to a non-piecewise-constant-magnitude transfer response which extends over a relatively wide band. Special optimization techniques, based on the error analysis developed in chapter 6, are illustrated in both these examples, and very good agreement with the desired responses is shown to exist.

The third example also concerns a piecewise-constant-magnitude transfer response, used to compare the four analog to digital transformations discussed. Although pole/zero prewarping achieves comparable results for all four transformations, the difficulties experienced with FD and BD structures concerning prewarping, and the adverse effects on the filter performance are highlighted.

Practical experience in the use and testing of SC filters was gained at Virginia Polytechnic Institute & State University, Blacksburg, Va., USA. Chapters 8 and 9 contain a summary of joint research work undertaken here as a contract in the analysis, measurement and prediction of noise in SC circuits.

Prediction of the noise behaviour was achieved by various approaches, including spectral analysis, a z-domain transfer function method and SPICE computer simulation modelling. In addition, a new approach in the time-domain, using the TCAPS computer simulation program, was developed. This eliminated the need for lengthy analysis of the internal structure of an SC network, necessary when using transfer function computation and summing methods for each noise source in the frequency-domain.

When these prediction methods were applied to two filter examples, the results compared favourably with experimental tests performed on both discrete component and fabricated chip versions. The construction and testing of these filters comprised the author's main responsibility on the research team. Characterization tests were also conducted on the operational amplifiers (OAs) used, so as to provide data, consistent with the experimental filters, for inclusion in the prediction methods.

The choice of the sampling frequency within an SC filter is an important consideration, since it will affect the design and performance of the filter. Further, different sections within the same filter may have differing requirements for the sampling frequency. It may therefore be desirable to reduce (decimate) or increase (interpolate) this frequency to suit local needs within the filter. In chapter 10 the principles of interpolation and decimation are described with reference to their application in SC networks. It is shown how sample rate conversion within SC structures may be used to improve the design and performance of the filter. In particular, the anti-aliasing filter requirements may be relaxed by increasing the sampling frequency, while, in certain sections of a filter, a reduction in the sampling frequency will allow cheaper hardware and lower capacitor ratios to be used. Examples of SC interpolation and decimation filters are given, and the questions of both multi-stage interpolators/ decimators and interpolation/decimation by rational factors is addressed.

Chapter 2

INTRODUCTION TO SC NETWORKS

2.1 DEVELOPMENT OF SC NETWORK THEORY

The purpose of this chapter is to introduce the basic concepts of Switched Capacitor (SC) networks and some of the main aspects in their development. The references cited are intended as a selected bibliography rather than as a detailed literature survey.

In 1972 Fried [1] proposed the use of capacitors and switches in the design of analog sampled-data filters. However, it was not until 1977 that serious interest was being shown in such circuits [2,3]. By that time MOS technology had reached a point where implementation of very accurate capacitor ratios and high quality operational amplifiers were the order of the day. Before this, inaccuracies and problems with the implementation of RC active filters in integrated form, for the audio band, had contributed to the continued use of discrete designs.

With SC filters in MOS technology, it became possible to achieve high precision "analog" audio frequency filters, which could be married with digital and switching circuitry on a single chip [4,5,6]. Recently, attention has again been focussed on the design of integrated RC filters [7,8,9]. Together with SC circuits, these may further improve the realization of sampled-data and continuous time integrated filters especially in high frequency applications.

Except for the work of Fettweis [10,11,12], the design of SC filters was initially based on LC and RC active filter

equivalents. Switched capacitors were used to simulate the resistors in such circuits [2,3,13], and the integrators of ladder structures were replaced by SC integrators [4,14,15,16,17]. These ideas were then extended to the design of inductor, immitance and FDNR equivalents, in SC form, which meant direct substitution into circuits containing these elements [18,19,20,21,22,23,24]. A comparison of some of these approaches may be found in [25].

But SC filters were also designed independent of analog equivalent circuits. Laker [26] established a library of z-domain circuit elements for use in the analysis and synthesis of SC filters. Building blocks also emerged to allow the simple construction of higher order filters [27,28,29,30,31], as well as other classes of filters such as pseudo n-path [32,33,34,35] and wave-digital realizations [36,37,38].

In addition, the real time and mask programmability of SC filters was exploited from an early stage through variation of the sampling frequency and capacitor ratios [39,40,41,42]. Finally, various analysis techniques, particularly suited to SC networks, have been developed [43,44,45,46]. A comprehensive survey of analysis methods used to date may be found in [47].

As interest grew, factors of importance to SC structures became apparent. These included both theoretical considerations, common with other sampled-data networks, and technological considerations peculiar to SC circuits. In the design and realization of filters, special emphasis was placed on structures which were insensitive to, or could compensate for, some of these factors which might adversely influence the behaviour of the SC network. Some of the main areas of study are listed below along with key references where appropriate. For a more detailed account as related to the

design and development of SC filters Refs. [4,48,49,50] should be consulted.

2.2 THEORETICAL CONSIDERATIONS

(a) Frequency warping: The required characteristics of a sampled-data filter undergo frequency warping as a result of sampling. This is a non-linear function of the sampling to signal frequency ratio and is dependent on the analog to digital transformation employed in the filter realization. The nature of frequency warping and methods whereby it may be reduced constitute the main work of this thesis.

(b) Aliasing: Through sampling, replicas of the positive and negative frequency signal spectrum within an SC filter are found at integer multiples of the sampling frequency. Aliasing occurs when spectral components of the signal, or of unwanted noise, lie at frequencies larger than half the sampling frequency. The original signal spectrum may then be adversely affected through superposition of these aliased frequencies. This problem is addressed in chapter 10.

(c) Delay Errors: In some cases it may be impossible to exactly realize the required z-domain transfer response function in SC form. Delay errors are introduced in the network which result in distortion of the response. The most common example of this is the inability of SC structures to realize delay-free loops. These are necessary for the terminations of LDI-transformed ladder designs. Various ways have been described to reduce or eliminate such errors [51,52,53,54, 55,56].

2.3 DESIGN AND TECHNOLOGICAL CONSIDERATIONS

(a) Sensitivity to element variations: Variations in the element values of an SC filter may occur due to fabrication errors, temperature changes and parasitic influences. It is therefore desirable to design SC filters having low sensitivity to these variations. This may be accomplished by modelling the SC filter on low sensitivity LC and RC active filters. In addition, designs employing small capacitor ratios and spread help to reduce the effect of element value variations. [14,29,57,58,59]

(b) Circuit design and complexity: As in most synthesis procedures, design trade-offs are also expected here. These could involve factors such as: the number and type of the operational amplifiers and switches, the number and size of the capacitors, clocking scheme complexity, noise, power, bandwidth, sampling frequency and dynamic range.

It is not the purpose of this thesis to discuss these design issues specifically. However, some will be mentioned when they arise in the discussions on warping, noise and interpolation /decimation.

(c) Parasitic capacitance: Capacitors and switches fabricated in MOS technology also contain parasitic capacitances between earth and each of their nodes. The largest of these parasitic capacitances is between earth and the bottom plate of the capacitors. This can amount to as much as 20% of the capacitor value and is usually non-linear with respect to signal amplitude. This gives rise to both transfer response errors and harmonic distortion. Most circuits are therefore

designed using "parasitic insensitive" or "parasitic compensated" structures. These permit signal charge transfer to take place through the structure without any loss due to such parasitic capacitors. [4,60,61,62,63,64]

(d) Noise: Noise is generated within the operational amplifiers and switches of SC networks. Usually this will be sampled before appearing at the output. Prediction of the noise and methods for its reduction therefore need to take into account the sampled-data nature of SC networks. Chapters 8 and 9 will deal with these issues in some detail.

(e) Operational Amplifiers: In addition to considerations regarding noise generation within the OAs, other factors may need consideration, when designing SC filters, such as : gain-bandwidth (GB) product, slew rate, power consumption, physical size, offset voltage and size of the internal compensation capacitor. [3,50,65,66,67,68,69,70,71]

2.4 RESISTOR SIMULATION BY SWITCHED CAPACITORS

The principal motivation for the development of integrated SC filters was their superior performance and greatly reduced chip size when compared with integrated RC-active filter designs. In its simplest form an SC filter can be realized by replacing each of the resistors in an RC-active filter by their switched capacitor equivalents.

Consider a capacitor, earthed at one node and switched at the other between two voltages as shown in Fig. 2.1(a). Switching is controlled by two non-overlapping clock signals with frequency $F_s = (1/T)$.

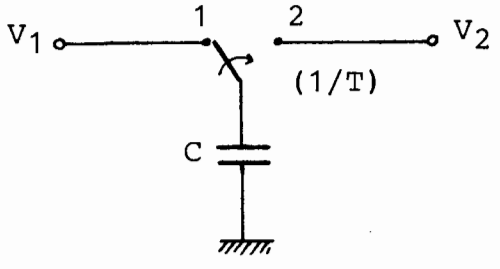

(a)

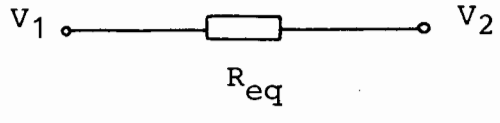

(b)

Fig. 2.1 Grounded switched capacitor (a) with its equivalent resistor circuit (b). $R_{eq}=(T/C)$. Switching is controlled by a non-overlapping clock of frequency $F_s=(1/T)$.

For the switch in position 2 the capacitor will carry a charge $Q_2 = CV_2$. When the switch changes to position 1 the charge on the capacitor is forced to be $Q_1 = CV_1$. This causes a charge $\Delta Q = C(V_1-V_2)$ to flow from V_1 to the capacitor. Likewise, when the switch reverts to position 2, the charge reverts to Q_2 and the extra charge ΔQ flows from the capacitor to V_2. Thus, during one clock cycle a charge $\Delta Q = C(V_1-V_2)$ flows from V_1 to V_2. This can be represented by an average current flow

$$I_{av} = \frac{\Delta Q}{\Delta t} = \frac{C(V_1 - V_2)}{T} \qquad ...(2.1)$$

Provided the clock cycle time is chosen sufficiently small, equation (2.1) remains true for V_1 and V_2 varying over time. If these represent signal voltages, the clock frequency must therefore be very much larger than the highest signal frequency. i.e.

$$F_s \gg f \qquad ...(2.2)$$

On examination, (2.1) is seen to obey Ohm's law, with the current being proportional to the potential difference. The constant of proportionality (C/T) can therefore be viewed as an equivalent conductance R_{eq}^{-1}. This is shown in Fig. 2.1(b) where the switched capacitor has been replaced with a resistor $R_{eq} = (T/C)$.

Using the switched-capacitor/resistor equivalence, RC-active filters may therefore be realized in analog sampled-data form using only capacitors, switches and operational amplifiers. The resulting filter is then characterized by capacitor ratios rather than resistor-capacitor time constants.

It is this fact that allows SC filters to be implemented in MOS technology with high precision. Capacitor ratios can be

fabricated with greater accuracy than resistor-capacitor products, since systematic tolerance errors in the values of two capacitors will track unlike those of a resistor and capacitor pair. Variations due to temperature and other effects follow this same principle leaving capacitor ratios largely unaffected while introducing errors into resistor-capacitor pair products.

Chapter 3

THE SAMPLED-DATA NATURE OF SC NETWORKS

3.1 ANALOG TO DIGITAL TRANSFORMATIONS

It has been shown how an SC integrator can be constructed using switched capacitors as resistor equivalents. This was based on the concept that charge transferred between the input and output nodes of a switched capacitor during each clock period simulate an average current flow of

$$I_{av} = \frac{V_1 - V_2}{(T/C)}$$

The resistor equivalence $R \equiv (T/C)$ is thus introduced as shown in Fig. 3.1.

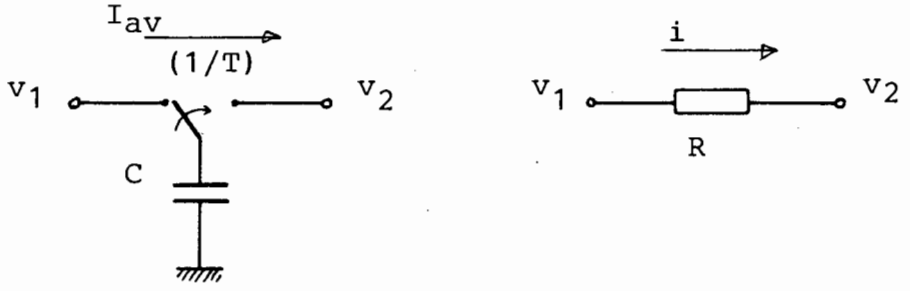

Fig. 3.1 Switched-Capacitor/Resistor equivalence

At dc the instantaneous current i in the resistor is equal to the average current, I_{av} . However, for signal frequencies above dc this is not the case and the discrepancy between the sampled current and the analog current increases as the signal to sampling frequency ratio increases. The effect of this is to cause a non-linear shift ("frequency warping") of the circuit frequency characteristics. The nature of this warping is dependent on the type of analog to digital transformation employed for SC. circuit realization.

Comparison of an SC integrator with its RC active equivalent can conveniently be used to demonstrate the effects just described. The circuit of Fig. 3.2(a) has the voltage transfer function

$$\frac{V_{out}}{V_{in}} = \frac{-1}{sRC_f} \qquad \ldots(3.1)$$

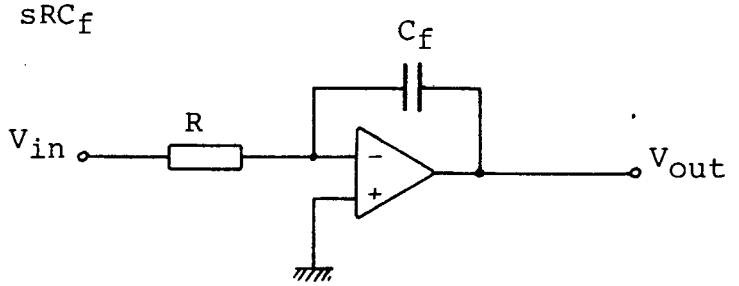

(a)

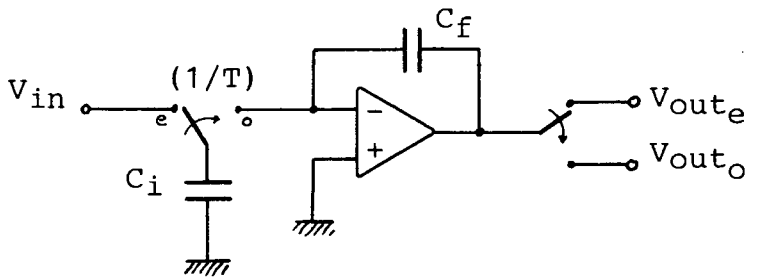

(b)

Fig. 3.2 (a) RC-active integrator.
(b) SC integrator.

For the circuit of Fig. 3.2(b) the laws of charge conservation are applied to obtain the voltage transfer function. During the "odd" clock phase (t_o) the input capacitor C_i is connected to the operational amplifier inverting input and the charge on the feedback capacitor C_f is given by

$$Q_{C_f}(t_o) = Q_{C_f}(t_o-T) + dQ(t_o)$$

where $Q_{C_f}(t_o-T)$ is the charge on C_f one cycle previously and $dQ(t_o)$ is the charge transferred from the input capacitor to the feedback capacitor during the clock phase t_o. This, in turn, is equal to the charge accumulated on the input capacitor during the

previous "even" phase $(t_o - T/2)$ when the input capacitor was connected to V_{in}. The inverting gain of the operational amplifier introduces a negative sign so that

$$Q_{C_f}(t_o) = Q_{C_f}(t_o - T) - Q_{C_i}(t_o - T/2)$$

Therefore, using the law relating voltage and charge on a capacitor

$$C_f[V_{out}(t_o) - V_{out}(t_o - T)] = -C_i V_{in}(t_o - T/2)$$

Taking the z-Transform of this difference equation yields an equation showing the delay terms z^{-1} and $z^{-\frac{1}{2}}$

$$C_f[V_{out} - V_{out}z^{-1}] = -C_i V_{in} z^{-\frac{1}{2}}$$

or

$$\frac{V_{out_o}}{V_{in}} = \frac{-C_i \; z^{-\frac{1}{2}}}{C_f \; 1 - z^{-1}} \qquad \ldots(3.2)$$

Similarly the output for the "even" phase is given by

$$\frac{V_{out_e}}{V_{in}} = \frac{-C_i \; z^{-1}}{C_f \; 1 - z^{-1}} \qquad \ldots(3.3)$$

The resistor/SC equivalence $R \equiv (T/C)$ can be used in comparing the voltage transfer expressions of the RC-active and SC integrators. This yields a mapping of the frequency variables s and z. For equations (3.1) and (3.2) one obtains

$$\frac{1}{s} \rightarrow T \frac{z^{-\frac{1}{2}}}{1 - z^{-1}} \qquad \ldots(3.4)$$

known as the Lossless Discrete Integrator (LDI) transformation [72,73]. In (3.5) the Forward-Difference (FD) transformation is given which results when using the output phasing of (3.3)

$$\frac{1}{s} \rightarrow T \frac{z^{-1}}{1 - z^{-1}} \qquad \ldots(3.5)$$

Other well known transformations used in the synthesis of SC networks are the Backward-Difference (BD) and the Bilinear (Bil) transformations given in equations (3.6) and (3.7) respectively. Possible realisations are shown in Figs. 3.3 and 3.4.

$$\frac{1}{s} \rightarrow T \frac{1}{1 - z^{-1}} \qquad \ldots(3.6)$$

$$\frac{1}{s} \rightarrow (T/2) \frac{1 + z^{-1}}{1 - z^{-1}} \qquad \ldots(3.7)$$

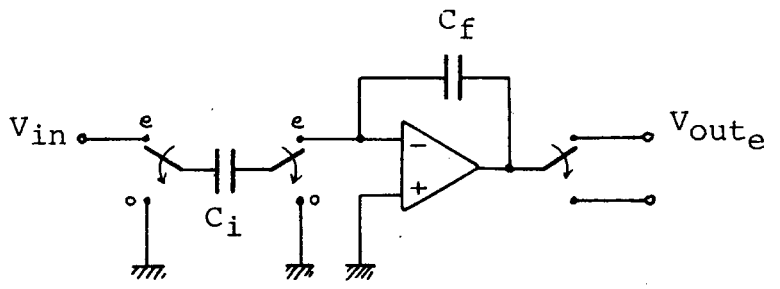

$$V_{out_e} = \frac{-C_i}{C_f} \frac{1}{(1 - z^{-1})} V_{in}$$

Fig. 3.3 SC integrator based on the Backward-Difference transformation.

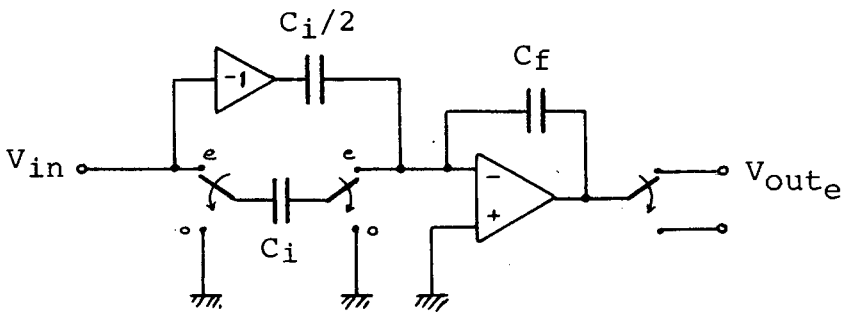

$$V_{out_e} = \frac{-C_i (1 + z^{-1})}{C_f (1 - z^{-1})} V_{in}$$

Fig. 3.4 SC integrator based on the Bilinear transformation.

It will be noticed in Figs. 3.2, 3.3 and 3.4 that the transformations realised are dependent on which phase of the bi-phase clock is used to sample the output; a fact used to advantage in cascaded and ladder SC filters where the input of one integrator samples the output of the previous integrator. For example, careful arrangement of the switch phasing in a ladder structure using the integrator of Fig. 3.3, ensures an LDI response for each integration except for the termination loops [4]. In addition, the circuit is insensitive to parasitic capacitances, unlike the integrator of Fig. 3.2.

3.2 TRANSFER RESPONSE WARPING

Equations (3.4)-(3.7) provide mappings of the complex frequency variables. These may be used to relate the transfer response expressions of an SC circuit with its analog equivalent. For example, the transfer response of a second order low-pass filter would be given by

$$H_{analog}(s) = \frac{b_0}{s^2 b_2 + s b_1 + b_0} \qquad ...(3.8)$$

With s replaced by $(z^{\frac{1}{2}} - z^{-\frac{1}{2}})/T$ the transfer response expression of an SC equivalent filter based on the LDI transformation is derived:

$$H_{SC}(z) = \frac{b_0}{(z^{\frac{1}{2}}-z^{-\frac{1}{2}})^2 b_2/T^2 + (z^{\frac{1}{2}}-z^{-\frac{1}{2}}) b_1/T + b_0} \qquad ...(3.9)$$

In order to obtain the response of this system to analog signals the relationship between the z-Transform and the Laplace-Transform must be considered.

$$z \equiv e^{sT} \qquad ...(3.10)$$

Equation (3.9) can therefore be re-written as

$$H_{SC}(sT) = \frac{b_0}{(e^{sT/2}-e^{-sT/2})^2 b_2/T^2+(e^{sT/2}-e^{-sT/2})b_1/T+b_0} \quad ...(3.11)$$

Of particular interest is the behaviour of the SC filter under continuous frequency excitation. i.e.

$$s = j\omega \quad ...(3.12)$$

and $$z = e^{j\omega T} \quad ...(3.13)$$

then

$$H_{analog}(j\omega) = \frac{b_0}{-\omega^2 b_2 + j\omega b_1 + b_0} \quad ...(3.14)$$

and

$$H_{SC}(j\omega T) = \frac{b_0}{-(\frac{2}{T})^2 \sin^2(\frac{\omega T}{2}) b_2 + j(\frac{2}{T})\sin(\frac{\omega T}{2}) b_1 + b_0} \quad ...(3.15)$$

Comparing equations (3.14) and (3.15) one can see that the response characteristic of the SC filter is identical to the equivalent analog filter response provided the frequency scale is warped according to the following relationship

$$\omega \rightarrow (2/T)\sin(\omega T/2) \quad ...(3.16)$$

Now setting $s = j\omega$ and $z = e^{j\omega T}$ in (3.4)-(3.7), results in the continuous frequency warping expressions for the four transformations discussed earlier.

LDI $\quad j\omega \rightarrow j(2/T)\sin(\omega T/2)$ $\quad ...(3.17)$

Bil $\quad j\omega \rightarrow j(2/T)\tan(\omega T/2)$ $\quad ...(3.18)$

FD $\quad j\omega \rightarrow j(2/T)\sin(\omega T/2)e^{j\omega T/2}$ $\quad ...(3.19)$

BD $\quad j\omega \rightarrow j(2/T)\sin(\omega T/2)e^{-j\omega T/2}$ $\quad ...(3.20)$

$$(2/T)\sin(\omega T/2) < \omega < (2/T)\tan(\omega T/2) \qquad \ldots(3.21)$$

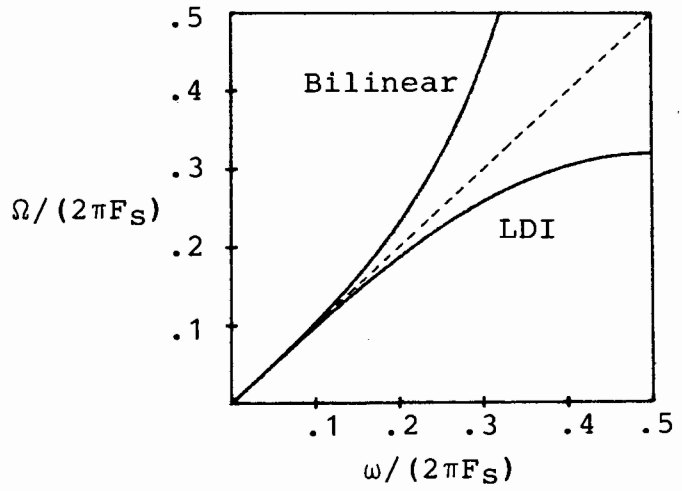

Fig. 3.5 Comparison of warping relations (3.17) and (3.18)

Expression (3.21) can be represented by plotting $\Omega=(2/T)\sin(\omega T/2)$ and $\Omega=(2/T)\tan(\omega T/2)$ against ω as shown in Fig. 3.5. From this it is seen that the the effective signal frequency within an LDI (Bil) structure is less (greater) than the actual signal frequency.

For the LDI and Bil transformations the continuous frequency variable $j\omega$ maps to a continuous frequency variable $j[f(\omega)]$, where $f(\omega)$ is a real quantity. This mapping ensures that, apart from a warping of the frequency axis, the magnitude transfer response shape is preserved. Together with condition (3.21) this results in the magnitude response characteristic being either "expanded" (for the LDI case) or "contracted" (for the Bil case) along the frequency axis while maintaining its shape. This can be seen in Fig. 3.6 for the case of a sixth order elliptic filter. Lee & Chang [54] have pointed out that this property makes the Bil transformation preferable "because the transition bands become narrower, thus enhancing the filtering function".

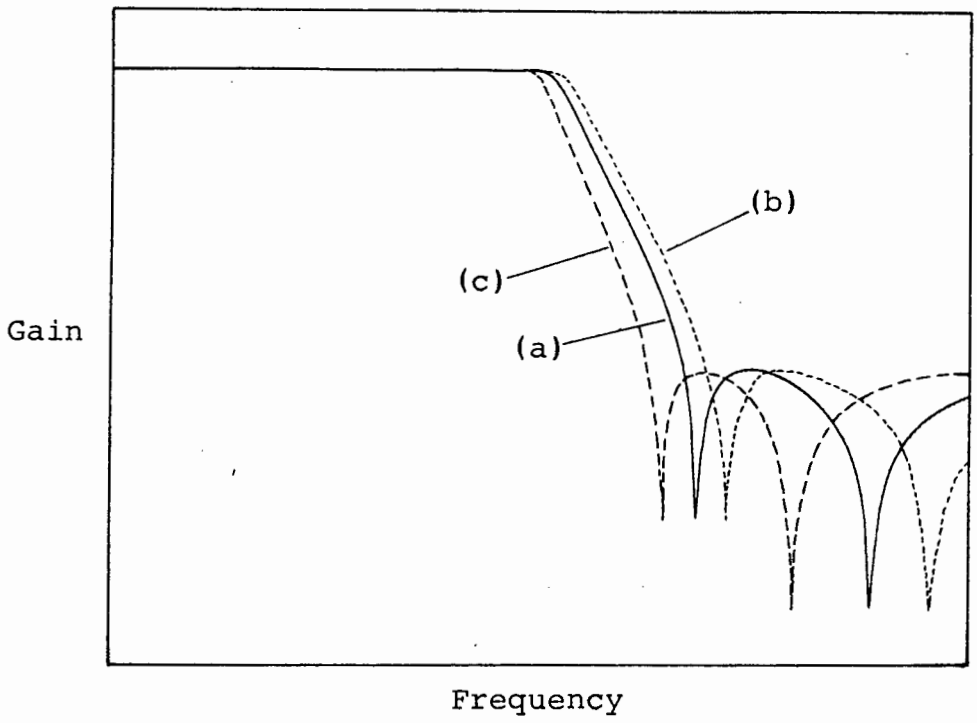

Fig. 3.6 Magnitude response of a sixth-order elliptic filter comparing analog (a), LDI (b) and Bil (c) realizations.

With the Forward-Difference and Backward-Difference transformations, however, the magnitude response shape is not preserved. The effective signal frequency $j[f(\omega)]$ within network realisations using these transformations no longer preserves $f(\omega)$ a real quantity. i.e. the effective signal frequency is no longer continuous in nature. The form of the transfer response is thus altered. Re-writing relationships (3.19) and (3.20) it can be shown that a real term has been introduced into the frequency variable.

$$\text{FD} \quad j\omega \rightarrow j(1/T)\sin(\omega T) - (2/T)\sin^2(\omega T/2) \qquad \ldots(3.22)$$

$$\text{BD} \quad j\omega \rightarrow j(1/T)\sin(\omega T) + (2/T)\sin^2(\omega T/2) \qquad \ldots(3.23)$$

Thus a purely imaginary frequency variable is mapped to a complex quantity. For the Forward-Difference and Backward-Difference transformations this becomes evident in the form of Q-enhancement and Q-degradation of the magnitude response, as shown in Fig. 3.7 for a second order example.

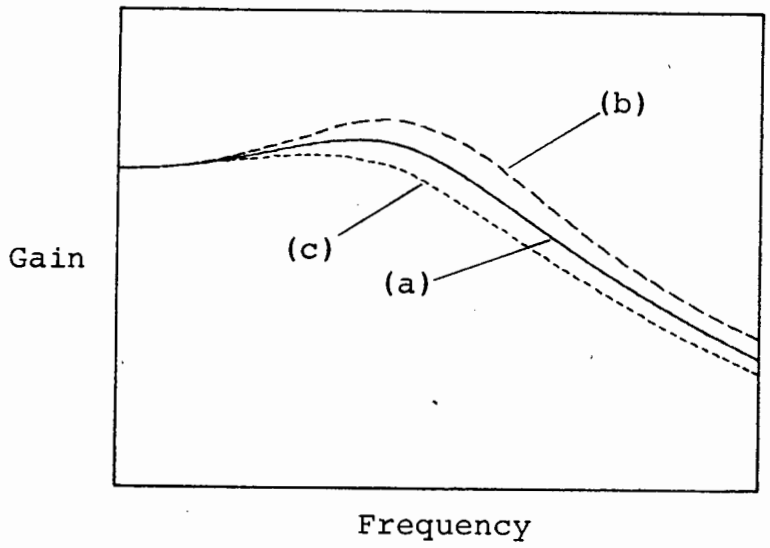

Fig. 3.7 Magnitude response of a second-order filter comparing analog (a), FD (b) and BD (c) realizations.

Due to the Q-enhancement experienced with Forward-Difference structures, certain restrictions apply to the pole locations. Condition (3.24) can be derived from the FD mapping (3.5). This ensures that the poles remain in the left-half-plane, and that stability of the system is maintained.

$$(F_s/f_{pole}) > 2\pi Q_{pole} \qquad \ldots(3.24)$$

3.3 COMPLEX FREQUENCY MAPPING

Expressions (3.4)-(3.7) provided for complex mapping relationships between the analog and digital frequency variables in the s-domain and z-domain. A graphic representation of this process is shown in Fig. 3.8 with the reverse mappings as follows

$$\text{LDI} \qquad z \rightarrow (1/2)[s^2T^2 + 2 \pm sT\sqrt{s^2T^2 + 4}\,] \qquad \ldots(3.25)$$

$$\text{Bil} \qquad z \rightarrow \frac{(2/T) + s}{(2/T) - s} \qquad \ldots(3.26)$$

$$\text{FD} \qquad z \rightarrow 1 + sT \qquad \ldots(3.27)$$

$$\text{BD} \qquad z \rightarrow \frac{1}{1 - sT} \qquad \ldots(3.28)$$

3.3.1 STABILITY CONDITION

Stable poles in the z-domain lie within the unit-circle. Thus the LDI, Bilinear and Backward-Difference transformations map stable poles in the s-domain to stable poles in the z-domain as shown by the shaded regions in Figs. 3.8(a)-(d). As already seen from condition (3.24), this is only true for restricted s-domain pole locations in the case of the Forward-Difference transformation. It should also be noted that the reverse LDI mapping is a double valued mapping such that z takes on two values for each s value. Thus, for every value within the unit-circle there exists one outside. In SC filter design the LDI transformation is therefore defined and used in such a way as to yield only the z-domain poles that lie within the unit-circle.

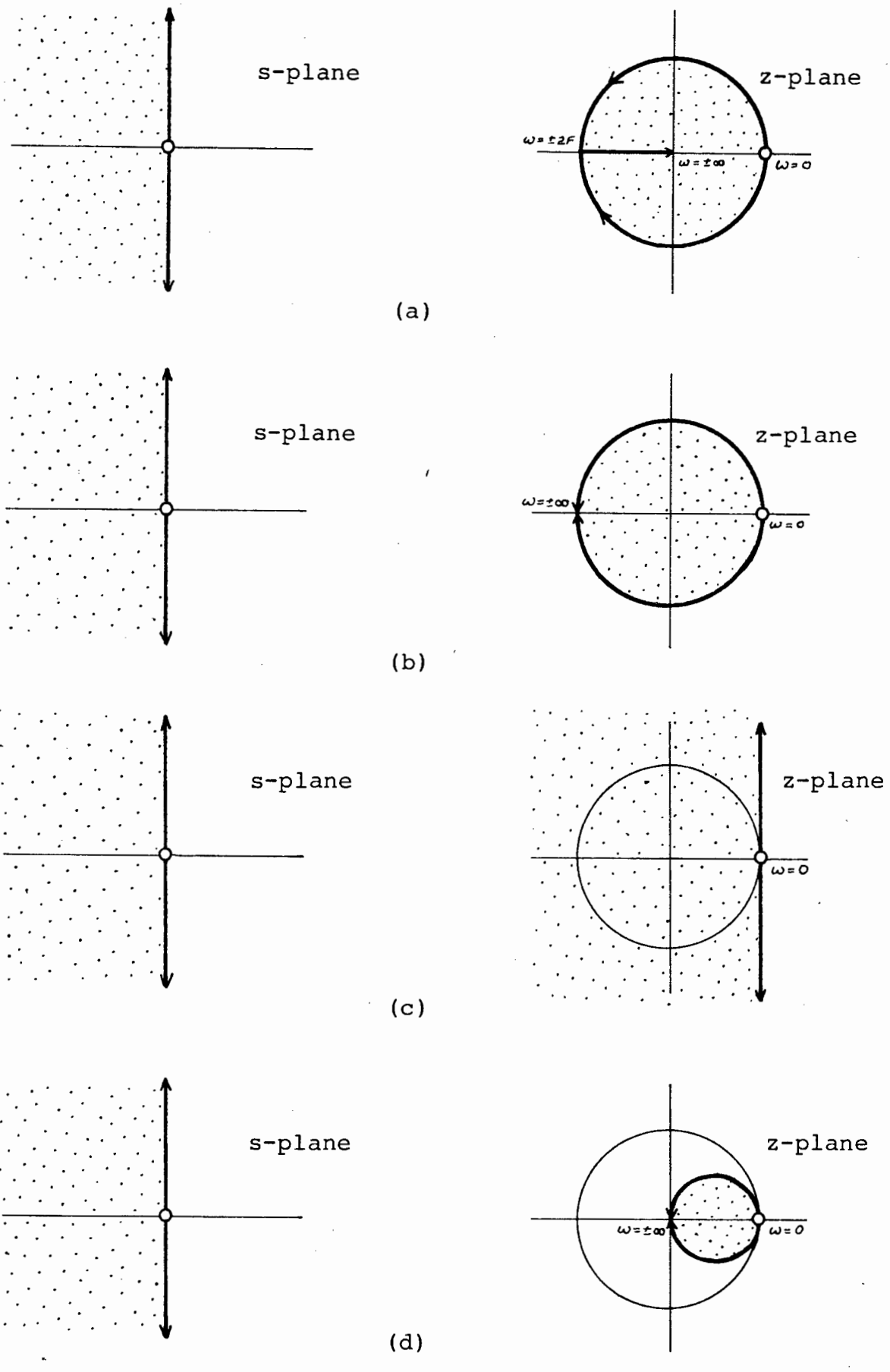

Fig. 3.8 Analog to digital mappings as defined in expressions (3.4)-(3.7). (a) LDI, (b) Bil, (c) FD and (d) BD.

3.3.2 TRANSFER RESPONSE UNDER CONTINUOUS FREQUENCY EXCITATION

As seen earlier, it is possible for the response shape of a filter to be preserved (apart from a frequency scale warping) after analog to digital transformation. The requirement that allows this is that continuous frequency signals applied to the SC filter should remain continuous upon transformation. The locus of continuous frequency signals in a digital filter is given by $z = e^{j\omega T}$. Thus the unit-circle in the z-domain should map to the $j\omega$ axis in the s-domain. Clearly, both the LDI and Bilinear transformations possess this property. In the case of the LDI transformation the unit-circle is mapped to the $j\omega$ axis between the points $j\omega = \pm j\pi F$ while, for the Bilinear transformation, it is mapped to the entire $j\omega$ axis.

It should also be noted that for any digital filter, continuous frequency signals are periodically mapped to the same points in the s-plane since the unit-circle in the z-plane is a periodic function of ω. The result of this can be seen in the frequency domain where positive and negative frequency replicas of the signal spectrum are repeated at integer multiples of the sampling frequency. This is dealt with in more detail in chapter 8 and chapter 10. For the remainder of this chapter it will be assumed that ω lies within the Nyquist domain ($-\pi F$; $+\pi F$).

3.4 S-PLANE DISTORTION MAPS

So far the problem of warping has been approached in two ways. Firstly, the effective signal frequency in an SC filter was compared with that in an equivalent analog filter. The second, and most usual approach, described the frequency mappings that take place between the s-domain and z-domain. Certain characteristics of these mappings were discussed briefly in relation to the filter response.

The first approach will now be extended to also include complex frequencies. In the relationships (3.4)-(3.7), s and z are replaced by the following identities.

$$s = (\sigma + j\omega) \qquad \ldots(3.29)$$

and $$z = \exp(\sigma T + j\omega T) \qquad \ldots(3.30)$$

The effective excitation frequency $s' = (\sigma' + j\omega')$ within an SC structure results as a function of the actual excitation frequency $s = (\sigma + j\omega)$. For the LDI case

$$s' = \frac{1}{T}[e^{\sigma T/2}e^{j\omega T/2} - e^{-\sigma T/2}e^{-j\omega T/2}]$$

$$= \frac{2}{T}[\cos(\omega T/2)\sinh(\sigma T/2) + j\sin(\omega T/2)\cosh(\sigma T/2)] \qquad \ldots(3.31)$$

LDI $$\sigma' = (\frac{2}{T})\cos(\omega T/2)\sinh(\sigma T/2) \qquad \ldots(3.32)$$

$$\omega' = (\frac{2}{T})\sin(\omega T/2)\cosh(\sigma T/2) \qquad \ldots(3.33)$$

Bil $$\sigma' = (\frac{2}{T})\frac{\sinh(\sigma T)}{\cos(\omega T) + \cosh(\sigma T)} \qquad \ldots(3.34)$$

$$\omega' = (\frac{2}{T})\frac{\sin(\omega T)}{\cos(\omega T) + \cosh(\sigma T)} \qquad \ldots(3.35)$$

FD $$\sigma' = (\frac{1}{T})[e^{\sigma T}\cos(\omega T)-1] \quad ...(3.36)$$

$$\omega' = (\frac{1}{T})e^{\sigma T}\sin(\omega T) \quad ...(3.37)$$

BD $$\sigma' = (\frac{1}{T})[1-e^{-\sigma T}\cos(\omega T)] \quad ...(3.38)$$

$$\omega' = (\frac{1}{T})e^{-\sigma T}\sin(\omega T) \quad ...(3.39)$$

The above expressions (3.32)-(3.39) summarise the effective warping of complex frequencies within SC structures. Graphical representation of this allows simple assessment of the four transformations in SC filter design. If the expressions are applied to all frequency points in the s-plane and the warped points plotted, a distorted s-plane results. A convenient way of depicting this is shown in Figs. 3.9-3.12, where a co-ordinate grid has been included for both the original and the distorted s-plane.

The poles and zeros of the analog version of a filter are plotted in the s-plane against the original co-ordinate grid. The complex frequencies at which these poles and zeros occur in an SC realization can then be read off the distorted grid.

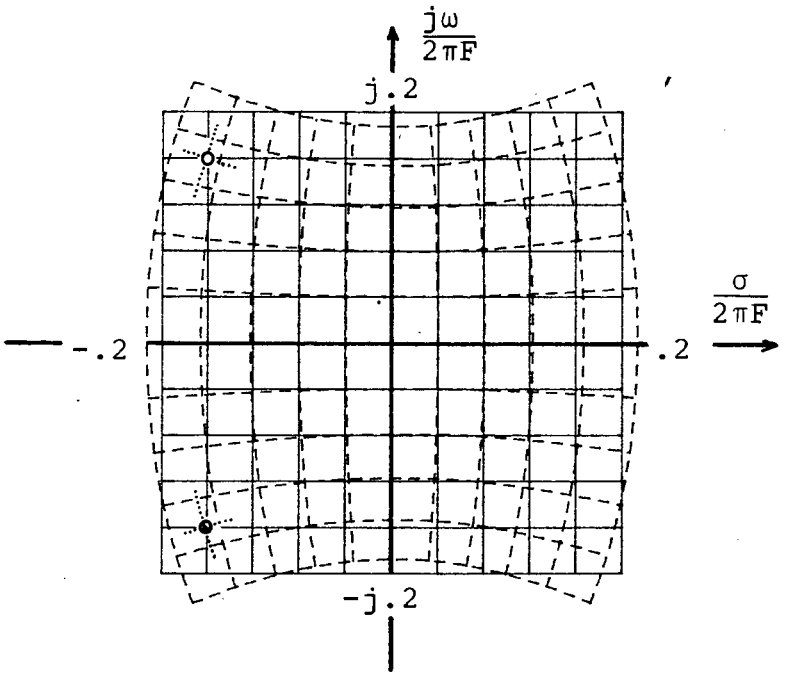

Fig. 3.9 Distortion of s-plane due to LDI mapping.

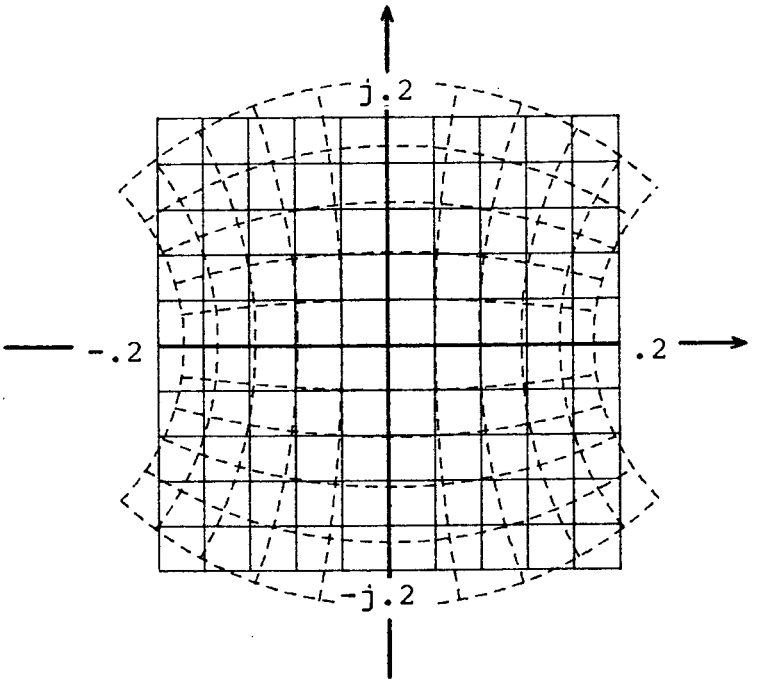

Fig. 3.10 Distortion of s-plane due to Bil mapping.

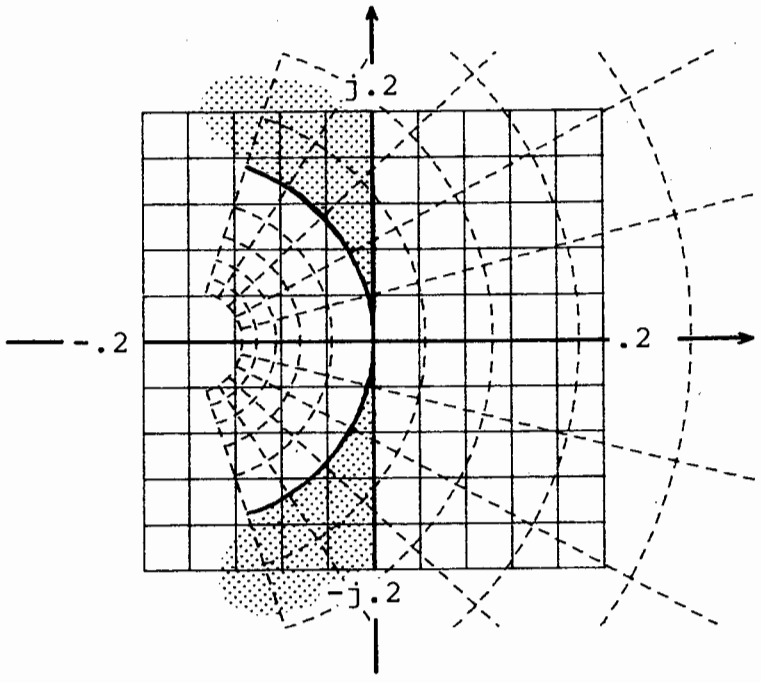

Fig. 3.11 Distortion of s-plane due to FD mapping.

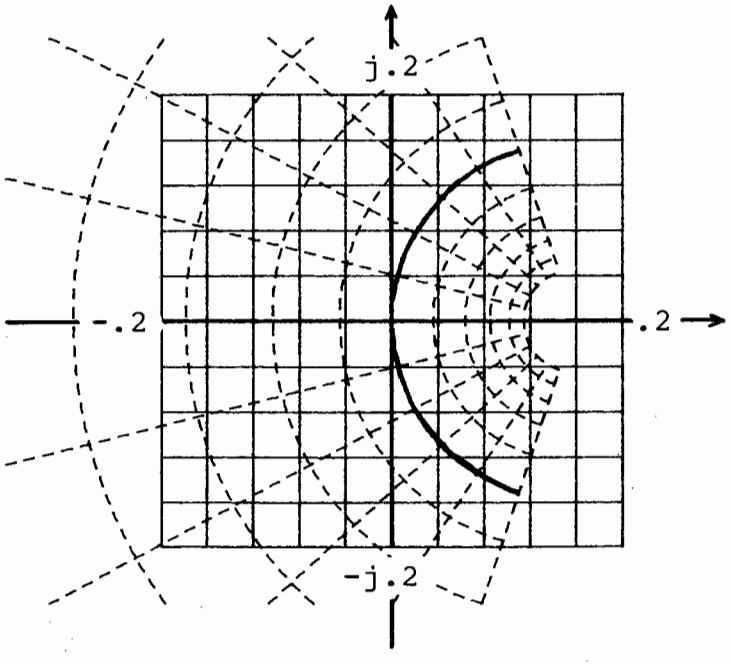

Fig. 3.12 Distortion of s-plane due to BD mapping.

Referring to Fig. 3.9, the analog version of a filter has poles located at

$$(\sigma/2\pi F_s) = -0.16 \quad \text{and} \quad (\omega/2\pi F_s) = \pm 0.16$$

The location of these poles within an equivalent LDI structure can then be read off the distorted grid as

$$(\sigma/2\pi F_s)' = -0.17 \quad \text{and} \quad (\omega/2\pi F_s)' = \pm 0.147$$

Due to the non-linearity of the transformations these maps cannot be used to evaluate the response of a filter, because the effective locations of the poles and zeros are dependent on the excitation frequency. They do however afford a convenient and simple insight into the nature of warping. For instance, it is immediately apparent that a filter with poles in the shaded region of Fig. 3.11 will yield an unstable SC structure, if based on the Forward-Difference transformation.

Also apparent is the significant improvement of the LDI and Bil transformations over the FD and BD transformations. This is seen when comparing the amount of distortion introduced by each transformation. As already discussed, the LDI and Bil transformations also approximate closer to the filter response shape by yielding common analog and SC $j\omega$ axes.

In Tables 3.1-3.3 the percentage shift in pole center frequency and Q due to warping is given for three values of pole Q. From this it can be seen that, for comparable shifts, the ratio of pole to sampling frequency is six times larger for the LDI and Bil transformations than for the FD and BD transformations. i.e. for comparable errors in the SC filter magnitude response, the available bandwidth in LDI and Bil structures is approximately six

times larger than in FD and BD structures.

Table 3.1 Pole center frequency and Q shift for Q=1.58

Q_p=1.58	LDI	Bil	FD	BD
F_s/f_p	1.258	1.258	8.388	8.388
f_p	+2.09%	-4.35%	+1.91%	-1.85%
Q_p	-5.03%	+9.09%	+14.3%	-20.8%

Table 3.2 Pole center frequency and Q shift for Q=0.7071

Q_p=0.71	LDI	Bil	FD	BD
F_s/f_p	1.258	1.258	8.388	8.388
f_p	-0.01%	+0.19%	+4.13%	-4.31%
Q_p	-2.74%	+4.87%	+3.91%	-4.56%

Table 3.3 Pole center frequency and Q shift for Q=0.53

Q_p=0.53	LDI	Bil	FD	BD
F_s/f_p	1.258	1.258	8.388	8.388
f_p	-2.12%	+4.07%	+5.45%	-5.87%
Q_p	+0.54%	-0.94%	-0.60%	+0.66%

Chapter 4

PREWARPING

4.1 NECESSITY FOR PREWARPING

In order to minimise warping effects it could be argued that the sampling frequency should be simply very much larger than the signal frequencies. There are however several reasons why this may be impracticable:

a) In order to accomodate the high sampling rate , the operational amplifiers (OAs) may require stringent frequency and speed characteristics. The extra cost of employing such high quality components may not be justified when, for the signal frequencies concerned, low cost devices would have sufficed. The "on" resistance of the switches would also have to be low in order to ensure fast charging times for the capacitors.

b) In the case of high frequency filters, upper limit hardware constraints may make it impossible to specify a high sampling to signal frequency ratio. Research work in this area continues with the highest switching frequencies to date reported to be in the MHz range [74,75]. It is predicted that even higher switching frequencies would facilitate SC filters to accomodate radio and video frequency applications [76,77,78].

c) The capacitor ratios of an SC integrator section are proportional to the sampling to pole frequency ratios, F_s/f_p. Maintaining a high value of F_s/f_p would therefore imply the

fabrication of large capacitor ratios [29]. With this however, the ratio accuracy would decrease [4] while the total capacitance area increases [3], resulting in a higher chip cost. The charging and discharging times of the larger capacitors would in turn limit the sampling frequency [2].

For further discussion concerning these questions References [49,50] should be consulted. It is now apparent that in most SC network designs some form of prewarping is desirable. Various approaches have been presented in literature with each being specific to the design procedure and the filter function.

4.2 PREWARPING APPROACHES IN SC FILTER DESIGN

4.2.1 PIECEWISE-CONSTANT-MAGNITUDE FILTER CHARACTERISTICS

By far the most common filter applications and examples used in SC literature are simple low-pass, high-pass and band-pass designs. The filter characteristics are then specified in terms of the pass-band edge frequency ω_p , the stop-band edge frequency ω_s , minimum stop-band attenuation and maximum pass-band ripple. Prewarping is effected merely by altering the specified edge frequencies in such a way as to compensate for the warping that will take place. Irrespective of the design procedure used thereafter, the response of the filter realised will fulfil the desired characteristics.

The prewarping equations for LDI and Bilinear structures correspond to the warping introduced as in expressions (3.17) and (3.18) i.e.

LDI $\Omega_p = \frac{2}{T} \sin(\omega_p T/2)$ ...(4.1)

Bil $\Omega_p = \frac{2}{T} \tan(\omega_p T/2)$ ...(4.2)

and likewise for the stop-band edge frequencies. Various examples may be found in the literature [13,27,28,30,52,65,79]. SC filters can be designed in this way and will then meet exactly (apart from perhaps certain non-ideal effects) the required characteristics. The actual response curve is less important, provided however, that the pass-band and stop-band requirements are fully met.

4.2.2 CAPACITOR RATIO ADJUSTMENT

Once an SC filter has been designed using simple resistor equivalence replacement $R \equiv (T/C)$, the effects of frequency warping can be reduced by adjusting the capacitor ratios. Brodersen, Gray & Hodges [4] achieve this for second order filters by comparing ω_0 and Q, as defined in the continuous frequency transfer response expressions of the SC and analog versions of the filter. Other authors [39,61,31] use a similar approach of matching these transfer response expressions. This matching will, however, only be exact at the particular frequency chosen (the pole frequency $\omega = \omega_0$ for a second order system).

4.2.3 SAMPLING FREQUENCY ADJUSTMENT

Modified capacitor ratios can also be achieved by adjusting the sampling frequency value $F_S=(1/T)$ used in the design equations [61,80]. Once again, non-linearity of the transformation dictates adjustment to take place at one specific frequency such as the pass-band edge ω_p.

In the design of ladder filters, Martin [61] uses this approach and adjusts the sampling period according to the following equation

$$T' = \frac{2}{\omega_p}\sin(\omega_p T/2) \qquad \ldots(4.3)$$

4.2.4 POLE AND ZERO LOCATION ADJUSTMENT

This method entails individual application of prewarping to each location of the poles and zeros of a required analog transfer response expression. In this way each such location can be prewarped for exact matching at its private centre frequency. i.e. that frequency at which maximum influence on the magnitude response occurs. By nature, this prewarping is not restricted to filters where the frequency characteristics are piecewise-constant in their magnitude response.

In literature so far, no formal description or evaluation of the method has been presented apart from publications by the Author [81,82,83]. This work therefore constitutes an attempt to set out modus operandi for its application. In the evaluation of the procedure, certain rules, guidelines, optimization methods and usage predictions for application of pole/zero prewarping, in the design of SC filters, are derived.

The method is most flexible and is particularly useful where filter requirements are given in terms of a frequency transfer response (either by way of pole and zero locations or as the quotient of two polynomials in s). Pole/zero prewarping will be dealt with in detail in the next chapter.

4.2.5 COMPLEMENTARY FREQUENCY CONVERSION (COFREC) FILTERING

4.2.5.1 PRINCIPLES OF OPERATION

In future, high frequency applications may require that filters use lower sampling to signal frequency ratios with the result that warping will increase. An attractive alternative to prewarping has been suggested by the Author in a recent publication [81]. The method involves the use of a pre-filter which performs a non-linear frequency shifting operation on the incoming signal in such a way that the resulting signal frequency spectrum relates to the warped filter characteristic in precisely the same way the original spectrum would have related to the desired filter characteristic. The reverse process would then have to be applied at the output.

If the warping of a filter characteristic is represented by the transfer response mapping of $H(\omega) \rightarrow H'(\Omega)$, then the operation of the COFREC filters in relation to the SC filter would be as shown in Fig. 4.1(a). The equivalent ideal analog filter is depicted in Fig. 4.1(b).

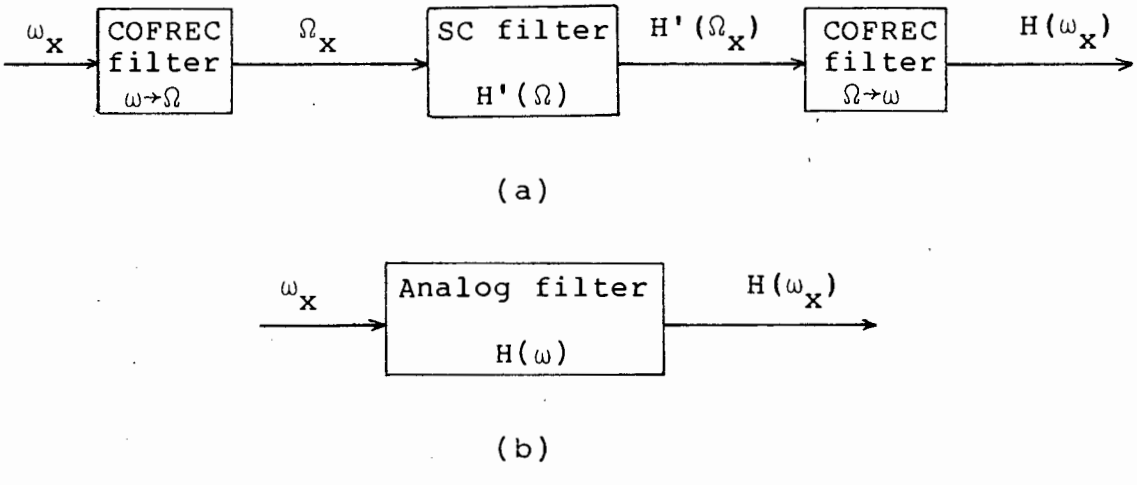

Fig. 4.1 Equivalence between an analog filter and an SC filter containing COFREC filters.

With the relationships introduced in (3.17) and (3.18), the COFREC filters would exhibit the following characteristics in their pass-bands.

LDI pre-filter $\Omega = \frac{2}{T} \sin(\omega T/2)$ ...(4.4)

LDI post-filter $\omega = \frac{2}{T} \sin^{-1}(\Omega T/2)$ ...(4.5)

Bil pre-filter $\Omega = \frac{2}{T} \tan(\omega T/2)$ ...(4.6)

Bil post-filter $\omega = \frac{2}{T} \tan^{-1}(\Omega T/2)$ ...(4.7)

4.2.5.2 SURFACE ACOUSTIC WAVE (SAW) COFREC FILTERS

An investigation into the feasability and ways of implementing such filters has recently begun. One approach, presently under investigstion, would be by way of Surface Acoustic Wave (SAW), Fast Fourier Transform (FFT) devices suggesting a basic layout as shown in Fig. 4.2. In order to achieve continuous operation two parallel routes are used where τ is the SAW FFT period.

Frequency warping presents a special problem for filters that use the sampling frequency (1/T) as a programming parameter. Since prewarping expressions assume a fixed value of sampling frequency, they can not be applied here. In literature, this problem has so far not been addressed.

The COFREC filter depicted in Fig. 4.2 performs frequency warping for a fixed sampling frequency. This is defined by the physical layout of the inverse FFT SAW device. Using techniques based on the concepts of variable frequency SAW filters, variable slope chirp filters and SAW frequency hop synthesisers, it would be possible to perform the warping operation for variable T and so allow for SC filters with variable sampling frequency. In this

way, a solution is arrived at for immediate implementation of high frequency programmable SC filters exhibiting none of the warping effects normally associated with low sampling to signal frequency ratios.

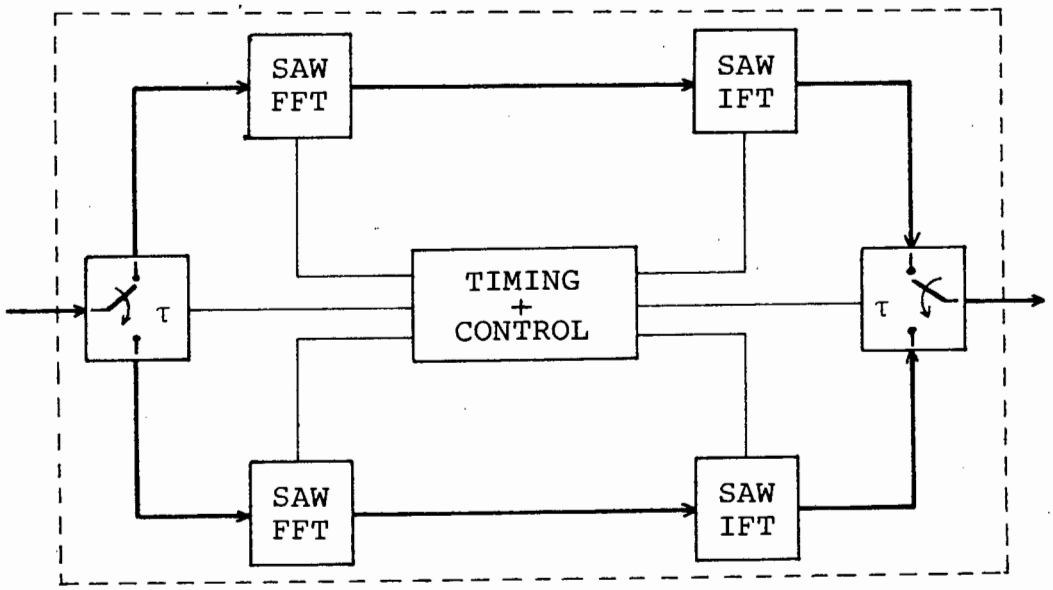

Fig. 4.2 Block diagram of a COFREC filter using SAW devices.

In the studies and investigations associated with the implementation of SAW COFREC filters the following points require special attention.

(a) Modulation techniques: SAW filters are able only to realize band-pass functions. The pass-band will therefore be situated around a multiple of the SC filter sampling frequency. As a result, the required warping characteristics given in equations (4.4)-(4.7) must be applied symmetrically about a new origin located at the pass-band center frequency. This arrangement also allows for the possibility of performing the pre- and post-filtering at frequencies higher than the SC filter sampling frequency. In

this way, the size and the fractional bandwidth requirement of the SAW devices would be reduced.

The signal at the output of the pre-filter will be a band-pass signal centered at a multiple of the SC filter sampling frequency. If a pseudo n-path SC filter structure is used for the main filter, decimation to the base-band would then not be necessary.

(b) SAW COFREC filter design: Various approaches to the design of SAW FFT devices are possible - a study of which may be found in [84]. The particular design chosen depends, among other things, on the required fractional bandwidth and the FFT period. These, in turn, will be influenced by factors such as: the signal bandwidth, the SC filter sampling frequency, the desired modulation arrangement and the SAW filter center frequency. If necessary, the design must also allow for variable SC filter sampling frequency using methods based on the concepts of variable frequency SAW filters, variable slope chirp filters and SAW frequency hop synthesisers.

(c) Technology to be used: In choosing a technology for the implementation of SAW filters, various factors require special attention. These include consideration of the required fractional bandwidth and electro/mechanical coupling constant, the temperature coefficient, and matching requirements for the electrical circuit. Principles governing the influence a specific technology has on these factors are well established [eg. 85,86] and may be applied in the design of the SAW devices, used in the COFREC filters.

These devices may be fabricated independently of the SC filter chip and control circuitry, in the technology most suited to each specific design. Using a hybrid approach, it would then be possible to implement an SC filter and associated COFREC filters in a single package.

Alternatively, thin-film technology could be used for the SAW devices, where, a piezoelectric layer is deposited onto a non-piezoelectric substrate [87,88]. The interdigital transducers being located at the interface between the two layers. This technique has been applied successfully in other SAW applications, where both high temperature stability and high electro/mechanical coupling is achieved.

With monolithic piezoelectric crystal devices, these advantages can not be gained, as the above two characteristics are usually mutually exclusive. For the two most common crystal types, ST-X Quartz or Y-Z $LiNbO_3$, either high temperature stability, at the expense of electro/mechanical coupling, is obtained for the former or the opposite effect for the latter.

Another advantage of using thin-film technology is that, using a silicon substrate [89,90], it would be possible to fabricate the SC filter with associated SAW COFREC filtering and control circuitry on a single chip.

4.2.5.3 LIMITATIONS AND ASSESSMENT

Although the concept of exact compensation for the effects of frequency warping by way of COFREC filters appears to be very attractive, certain limitations are evident.

(a) Complexity: The rationale behind using COFREC filtering techniques is that programmable sampled-data filters may be designed to meet a required transfer response precisely without concern for the frequency warping effects normally associated with such filters. However, the complexity involved in the design and realization of the COFREC filters may, to a certain extent, limit its immediate widespread application.

For the realization of certain transfer responses, there may exist more efficient and appropriate solutions for the type of filter used. For example, when designing high frequency narrowband SC filters it may be more convenient to decimate to a lower frequency before filtering rather than attempt precision filtering at the higher frequency.

(b) Size of the SAW COFREC filters: Integration of SC filters in MOS technology allows for implementation of programmable "analog" filters on a single chip. If SAW COFREC filtering is to be included in the design too, the chip size will increase by at least an order of magnitude. The precise amount will depend on the center frequency and bandwidth of the SAW devices, with size generally being inversely proportional to the center frequency.

Recent advances made in the design of miniature SAW devices may help to overcome this problem. In a recent publication,

Hikita et. al. [91] described techniques for the design of miniature narrow-band SAW filters for use with VHF frequencies.

(c) Signal loss: The COFREC filter suggested in the block diagram of Fig. 4.2 would involve a total of four SAW devices inserted into the signal path of the SC filter (taking into account both the pre- and post-COFREC filters). As SAW devices are characterized by a high insertion loss, the overall loss is expected to be high and as a result the dynamic range will be significantly reduced. This limitation may require a search for other approaches for the design and implementation of COFREC filters.

(d) Delay: The absolute group delay of signals passing through an SC filter and associated SAW COFREC filters will be quite substantial. This is primarily due to the large delay in SAW devices and may, in certain telecommunications applications, be prohibitive so as to require corrective action.

Investigations associated with this novel concept of complementary frequency conversion filtering are seen to hold great promise. A paper on this work has been accepted for presentation by the author at the International Conference on Circuits and Systems in Beijing, China, June 1985.

Chapter 5

POLE/ZERO PREWARPING

5.1 EFFECTIVE POLE AND ZERO LOCATIONS

In section 3.4 of chapter 3 it was observed that the effective pole and zero locations, representing the characteristics of an SC filter, are a function of the signal frequency within the filter. (i.e. the characteristics exhibit a non-linear shift with frequency.)

In order to obtain exact compensation for this effect it is therefore required to prewarp the filter specifications in a nonlinear way. i.e. by a different amount, depending on the input frequency. Except in the case of an adaptive filter, subject only to signals of a single continuous frequency, this is clearly not possible. If, however a filter is described only by its general pass-band and stop-band requirements, as mentioned earlier, exact "nonlinear" prewarping is possible using equation (4.1) or (4.2). In this case each specified frequency is prewarped so as to fulfil the requirement at that particular frequency.

"Pole/zero prewarping" addresses the problem of how to prewarp a filter characteristic that can not be described by pass-band and stop-band regions. Instead, the requirements may be given in terms of a transfer response expression. The expression is factored into simple and conjugate pair poles and zeros with prewarping being applied individually to each of these.

The choice of a suitable method for this prewarping will depend on the characteristic of the filter in question and the application

requirements. A first approach would be to prewarp each pole and zero in a way such that its effective location coincides with the desired location for the frequency at which it has most influence on the transfer response. This frequency corresponds to the centre frequency of the pole or zero in question.

The effective shift of each pole and zero from its desired location at frequencies other than its private centre frequency introduces error into the transfer response. However, since each pole and zero most critically affects the transfer response at its private centre frequency, the resulting distortion in the magnitude transfer response is minimised. Variations on this approach, hereafter referred to as "Center Frequency" (CF) prewarping, may be used to further minimise the distortion. Two such alternatives, described below, are "Selectivity" (S) and "Complex Mapping" (CM) prewarping.

The drawback with pole/zero prewarping, where each pole and zero is prewarped by a different amount, is that the unique relationship between the original locations of the poles and zeros is altered. This relationship, in turn, determines the precise shape of the transfer response. In chapter 6 this issue is discussed in further detail.

5.2 DEVELOPMENT OF THE PROCEDURE

Consider a general second order transfer response function

$$T(s) = H \frac{s^2 + s2\sigma_z + \omega_{0z}^2}{s^2 + s2\sigma_p + \omega_{0p}^2} \qquad ...(5.1)$$

with

$$H = \frac{\omega_{0p}^2}{\omega_{0z}^2} \qquad ...(5.2)$$

such that

$$T(s) = \frac{s^2/\omega_{0z}^2 + s2\sigma_z/\omega_{0z}^2 + 1}{s^2/\omega_{0p}^2 + s2\sigma_p/\omega_{0p}^2 + 1} \qquad ...(5.3)$$

and

$$T(j\omega) = \frac{1 - \omega^2/\omega_{0z}^2 + j\omega 2\sigma_z/\omega_{0z}^2}{1 - \omega^2/\omega_{0p}^2 + j\omega 2\sigma_p/\omega_{0p}^2} \qquad ...(5.4)$$

To represent the implementation of this as an SC structure requires application of the LDI or Bilinear (Bil) transformations as given by their respective frequency warping expressions

LDI $\qquad s \rightarrow (1/T)(z^{\frac{1}{2}} - z^{-\frac{1}{2}}) \qquad ...(5.5)$

$$\omega \rightarrow (2/T)\sin(\omega T/2) \qquad ...(5.6)$$

Bil $\qquad s \rightarrow (2/T)(1 - z^{-1})/(1 + z^{-1}) \qquad ...(5.7)$

$$\omega \rightarrow (2/T)\tan(\omega T/2) \qquad ...(5.8)$$

The effective SC LDI-implemented transfer response expression given by $T_{SC}(j\omega)$ in (5.9) is derived by substituting (5.6) into (5.4).

$$T_{SC}(j\omega) = \frac{1-(\frac{2}{T})^2\sin^2(\frac{\omega T}{2})/\omega_{0z}^2+j(\frac{2}{T})\sin(\frac{\omega T}{2})2\sigma_z/\omega_{0z}^2}{1-(\frac{2}{T})^2\sin^2(\frac{\omega T}{2})/\omega_{0p}^2+j(\frac{2}{T})\sin(\frac{\omega T}{2})2\sigma_p/\omega_{0p}^2} \qquad ...(5.9)$$

For the sake of brevity, only the influence of poles on $T_{SC}(j\omega)$ will be evaluated. This is given by the denominator of (5.9) $D_{SC}(j\omega)$. Results for the influence of the zero are analogous. Accordingly, the subscripts p and z will be omitted. i.e.

$$D_{SC}(j\omega) = 1-(\frac{2}{T})^2\sin^2(\frac{\omega T}{2})/\omega_0^2+j(\frac{2}{T})\sin(\frac{\omega T}{2})2\sigma/\omega_0^2 \qquad ...(5.10)$$

Methods whereby ω_0 and σ may be adjusted, giving a prewarped version of (5.10), are examined below. Expressions for the adjustment of the pole selectivity, given by $Q = \omega_0/(2\sigma)$, will also be included.

5.2.1 "CENTER FREQUENCY" (CF) PREWARPING

The first pole/zero prewarping approach to be described achieves exact correspondence, at the pole center frequency, between the denominator of (5.4) and the prewarped version of (5.10). i.e. the poles are shifted in a way that their effective locations, in the SC-implemented filter, coincide with the desired locations when the signal frequency $\omega = \omega_0$. This may be achieved by adjusting the pole locations according to expressions (5.11) (or (5.12) in the case of a Bilinear structure).

LDI $\quad \sigma' = \sigma \ \mathrm{sinc}(\omega_0 T/2)$ ...(5.11a)

$\omega_0' = \omega_0 \ \mathrm{sinc}(\omega_0 T/2)$ ...(5.11b)

$Q' = Q$ ...(5.11c)

Bil $\quad \sigma' = \sigma \ \mathrm{tanc}(\omega_0 T/2)$ ...(5.12a)

$\omega_0' = \omega_0 \ \mathrm{tanc}(\omega_0 T/2)$ ...(5.12b)

$Q' = Q$ ...(5.12c)

where

$$\mathrm{sinc}(x) = \sin(x)/x \qquad ...(5.13)$$

$$\mathrm{tanc}(x) = \tan(x)/x \qquad ...(5.14)$$

The effective pole contribution of the SC implemented version after this prewarping is given by $D'_{SC}(j\omega)$. This is obtained by substituting (5.11a) and (5.11b) into (5.10).

$$D'_{SC}(j\omega)=1-\sin^2(\frac{\omega T}{2})/\sin^2(\frac{\omega_0 T}{2})+j(2\sigma/\omega_0)\sin(\frac{\omega T}{2})/\sin(\frac{\omega_0 T}{2}) \quad ...(5.15)$$

At the pole centre frequency ω_0 cancellation occurs so that

$$D'_{SC}(j\omega_0) = j2\sigma/\omega_0 \quad ...(5.16)$$

Comparing (5.16) with the denominator of (5.4), it can be seen that exact correspondence between the desired pole influence and the effective pole influence will occur at its center frequency.

5.2.2 "SELECTIVITY" (S) PREWARPING

In section 5.1 above it was observed that, while the effective location of a pole within an SC filter may coincide with the desired location at the prewarping frequency, error is introduced in the transfer response at all other frequencies. Thus, using CF-prewarping, exact correspondence between the desired and effective pole location is achieved at its center frequency. However, if other poles are present, they will introduce error at this frequency, since they will have been prewarped at their own private center frequencies.

A variation of CF-prewarping may be used so as to adjust the selectivity of each pole in addition to its center frequency. The advantage obtained is that, rather than achieve exact correspondence between the desired and the effective pole location at its center frequency, a certain amount of error is introduced so as to compensate for the influence of other poles.

Selection of the precise expressions, whereby this may be achieved, is arbitrary, since the overall effect within a filter is subject to the filter characteristics themselves. The prewarping expressions of (5.17) (or (5.18) in the Bilinear case) are suggested as one approach that was seen to reduce the error in the vicinity of each pole frequency as required.

LDI $$\sigma' = \sigma \, \mathrm{sinc}^{-1}(\omega_0 T/2) \qquad \ldots(5.17a)$$

$$\omega_p' = \omega_p \, \mathrm{sinc}(\omega_0 T/2) \qquad \ldots(5.17b)$$

$$(Q')^2 = (Q^2 - 1/4)\mathrm{sinc}^4(\omega_0 T/2) + 1/4 \qquad \ldots(5.17c)$$

Bil $$\sigma' = \sigma \, \mathrm{tanc}^{-1}(\omega_0 T/2) \qquad \ldots(5.18a)$$

$$\omega_p' = \omega_p \, \mathrm{tanc}(\omega_0 T/2) \qquad \ldots(5.18b)$$

$$(Q')^2 = (Q^2 - 1/4)\mathrm{tanc}^4(\omega_0 T/2) + 1/4 \qquad \ldots(5.18c)$$

where ω_p is the imaginary part of the pole. i.e.

$$\omega_p^2 = \omega_0^2 - \sigma^2 \qquad \ldots(5.19)$$

and sinc(x) and tanc(x) are defined as in (5.13) and (5.14).

Unlike with CF-prewarping, no simple reduction of $D_{sc}'(j\omega_0)$ occurs at the pole center frequency. However, correspondence between the effective and the desired pole location does occur in the vicinity of this frequency as seen in the error polts in chapter 6. The effect of S-prewarping in comparison to CF-prewarping is assessed on the basis of these plots.

5.2.3 "COMPLEX MAPPING" (CM) PREWARPING

In this approach the pole and zero locations are made to coincide with the complex frequency mappings of (5.5) and (5.7). i.e. the locations follow the complex frequency warping shown in Figs. 3.9 and 3.10. The prewarping expressions of (5.22) and (5.23) are obtained by substituting (5.20) and (5.21) into (5.5) and (5.7).

$$s = (\sigma + j\omega_p) \qquad \ldots(5.20)$$

$$z = \exp(\sigma T + j\omega_p T) \qquad \ldots(5.21)$$

This yields

LDI

$$\sigma' = \frac{2}{T}\cos(\omega_p T/2)\sinh(\sigma T/2) \qquad \ldots(5.22a)$$

$$\omega_p' = \frac{2}{T}\sin(\omega_p T/2)\cosh(\sigma T/2) \qquad \ldots(5.22b)$$

$$(Q')^2 = (1/4)\left[1 + \frac{\tan^2(\omega_p T/2)}{\tanh^2(\sigma T/2)}\right] \qquad \ldots(5.22c)$$

Bil

$$\sigma' = (2/T)\frac{\sinh(\sigma T)}{\cos(\omega_p T) + \cosh(\sigma T)} \qquad \ldots(5.23a)$$

$$\omega_p' = (2/T)\frac{\sin(\omega_p T)}{\cos(\omega_p T) + \cosh(\sigma T)} \qquad \ldots(5.23b)$$

$$(Q')^2 = (1/4)\left[1 + \frac{\sin^2(\omega_p T)}{\sinh^2(\sigma T)}\right] \qquad \ldots(5.23c)$$

As with S-prewarping, an evaluation of this approach will be found in chapter 6.

5.3 CONCLUSION

Expressions for prewarping the poles and zeros of a required filter characteristic have been derived by the Author and are presented above. The need for these arose out of the lack of any formal description or evaluation in literature of prewarping methods for use in non-piecewise-constant-magnitude filter characteristics.

It was clear at the beginning of the study that the results obtained from the use of pole/zero prewarping would depend to some degree on the particular configuration of the poles and zeros in the required filter. It was therefore necessary to investigate various approaches to pole/zero prewarping. Each of these holds certain advantages for particular filter applications.

Three approaches are given which may be used selectively to achieve the most accurate approximation to the desired magnitude response. Techniques for this selection, and the application of pole/zero prewarping generally, follow from the analysis contained in chapter 6. These principles are then demonstrated by way of examples in chapter 7.

The concept of pole/zero prewarping was reported independently in a paper by Brugger & Hosticka [92]. The purpose of this paper was to enable the design of SC networks based on the Backward-Difference transformation. Only one approach was given however with no formal evaluation as to its effectiveness or extension for use with other analog to digital transformations.

Using the inverse matched-z transformation, the authors derive expressions for the prewarping of simple and complex conjugate pair poles and zeros. The results correspond to those of

CM-prewarping. They are shown to yield an accurate approximation of a 3rd order Chebyshev low-pass filter. A sampling to pass-band frequency ratio of 16 is used and a pass-band ripple of 1dB specified. This involves a Q of 2 for the conjugate pole pair.

Problems will arise, however, when using the Backward-Difference transformation for high Q poles and low sampling to pole frequency ratios. The prewarped version of an elliptic filter in [92] is shown to require the realisation of right-half plane zeros. In order to prevent poles lying in the right-half plane where prewarping has been applied, requires that the original pole and zero locations obey condition (5.24). This condition may be derived from equation (3.38).

$$e^{\sigma T}\cos(\omega_p T) > 1 \qquad \ldots(5.24)$$

No such restriction applies in the case of the LDI and Bil transformations. They also yield closer approximations to the required magnitude transfer response as discussed in chapter 3. In chapter 7 the third order Chebyshev filter example of Brugger & Hosticka is extended to include the LDI, Bil and FD transformations. The results using these transformations are then compared with those achieved using the BD transformation.

Chapter 6

ERROR ANALYSIS

6.1 THE NEED FOR EVALUATION OF P/Z PREWARPING

Examples demonstrating the effectiveness of pole/zero prewarping are contained in chapter 7. However, a more general approach to evaluating pole/zero prewarping is necessary if it is to be used in SC filter design. The error introduced into the magnitude response by each pole and zero at frequencies other than their private center frequencies requires special attention. This error is dependent on the sampling to pole (or zero) frequency ratio, the selectivity of the pole (or zero) and the signal frequency. An overall evaluation of pole/zero prewarping and the three particular methods described ("Center Frequency" CF, "Selectivity" S and "Complex Mapping" CM prewarping) must account for this dependency. This is made possible by using the graphical representation developed below. It allows assessment as to:

a) The suitability of pole/zero prewarping for various filter characteristics.

b) Comparison of the effects CF-, S- and CM-prewarping have on the SC filter response.

c) Optimization of the prewarping for a particular design. This includes: (i) the choice and combination of the three methods within the filter, (ii) the tuning of pole and zero locations, (iii) the introduction of additional poles or zeros into the filtering function.

Error analysis forms the basis of these optimization procedures in a way that complete computer aided design is possible.

d) Prediction of the amount of deviation remaining in the completed design.

6.2 ERROR EXPRESSION DEVELOPMENT

If $|H(j\omega)|$ is the required magnitude transfer response of a filter and $|H'_{SC}(j\omega)|$ that of the SC implementation after pole/zero prewarping then, for any particular frequency, the error measured in dB between the two is given by

$$E(j\omega) = 20 \log_{10} \left[\frac{|H'_{SC}(j\omega)|}{|H(j\omega)|} \right] \qquad ...(6.1)$$

In terms of the pole and zero factors this can be written as a sum of errors

$$E(j\omega) = \sum_{i}^{m} (e_{pi}) + \sum_{k}^{n} (e_{zk}) \qquad ...(6.2)$$

where n and m refer to the orders of the numerator and denominator of the transfer response and e_{pi} and e_{zk} are the error contributions in dB due to $pole_i$ and $zero_k$.

Consider a complex pole pair $(s^2 + s2\sigma + \omega_0^2)$. Its contribution to the magnitude squared transfer response $|H(j\omega)|^2$ is given as

$$|P(j\omega)|^2 = [(1 - \omega^2/\omega_0^2)^2 - 4\sigma^2\omega^2/\omega_0^4]^{-1} \qquad ...(6.3)$$

The contribution of the pole/zero prewarped version, implemented in SC form and based on the LDI transformation can now be derived. This is obtained by substituting the LDI warping expression (5.6) into (6.3). CF-prewarping is applied to σ and ω_0 by substituting equations (5.11) into (6.3). The result is given by $|P'_{SC}(j\omega)|$ in (6.4).

$$|P'_{SC}(j\omega)| = \left[\left[1- \frac{\sin^2(\frac{\omega T}{2})}{\sin^2(\frac{\omega_0 T}{2})}\right]^2 + \frac{\sin^2(\frac{\omega T}{2})}{Q^2\sin^2(\frac{\omega_0 T}{2})}\right]^{-1} \qquad ...(6.4)$$

Substitution of (6.3) and (6.4) into (6.1) then yields the error contribution $e_{pc}(f/F_s;f_0/F_s;Q)$, in the final SC realization, due to a complex pole pair. This is given in (6.5).

$$e_{pc} = 10\ \log_{10}\left[\frac{[1-(f/f_0)^2]^2 + (f/f_0/Q)^2}{\left[1- \frac{\sin^2(\pi f/F_s)}{\sin^2(\pi f_0/F_s)}\right]^2 + \frac{\sin^2(\pi f/F_s)}{Q^2\sin^2(\pi f_0/F_s)}}\right] \qquad ...(6.5)$$

where $Q = \omega_0/(2\sigma)$. Likewise, the contribution $e_{pr}(f/F_s;f_0/F_s)$ of a real pole $(s + \omega_0)$ to the error in the final SC realization, after CF-prewarping, can be derived as given in (6.6).

$$e_{pr} = 10\ \log_{10}\left[\frac{1 + (f/f_0)^2}{\left[1 + \frac{\sin^2(\pi f/F_s)}{\sin^2(\pi f_0/F_s)}\right]}\right] \qquad ...(6.6)$$

A similar procedure is followed to obtain corresponding expressions for S- and CM-prewarping and for the Bilinear transformation. These are contained in Appendix 1. Error expressions for the Forward-Difference and Backward-Difference transformations using CM-prewarping are seen to be identical to those obtained for the LDI transformation. In order to assess pole/zero prewarping using the Backward-Difference transformation

as described by Brugger & Hosticka [92], it was necessary to consider and derive error expressions for these transformations.

The error contribution of a zero to the magnitude transfer response may be determined by the inverse contribution of a pole at the same location. Therefore, all the expressions given in Appendix 1 apply equally to the error contribution of a zero e_z provided they are taken as the negative inverse. i.e. for a pole and zero at the same location

$$e_z \equiv -e_p \qquad \ldots(6.7)$$

For a qualititive assessment of the three approaches concerning pole/zero prewarping, it is convenient to look at the error plots of the expressions, given in Appendix 1, for various values of Q as shown in Figs. 6.1 and 6.2. Enlarged versions of these plots may be found in Appendix 2.

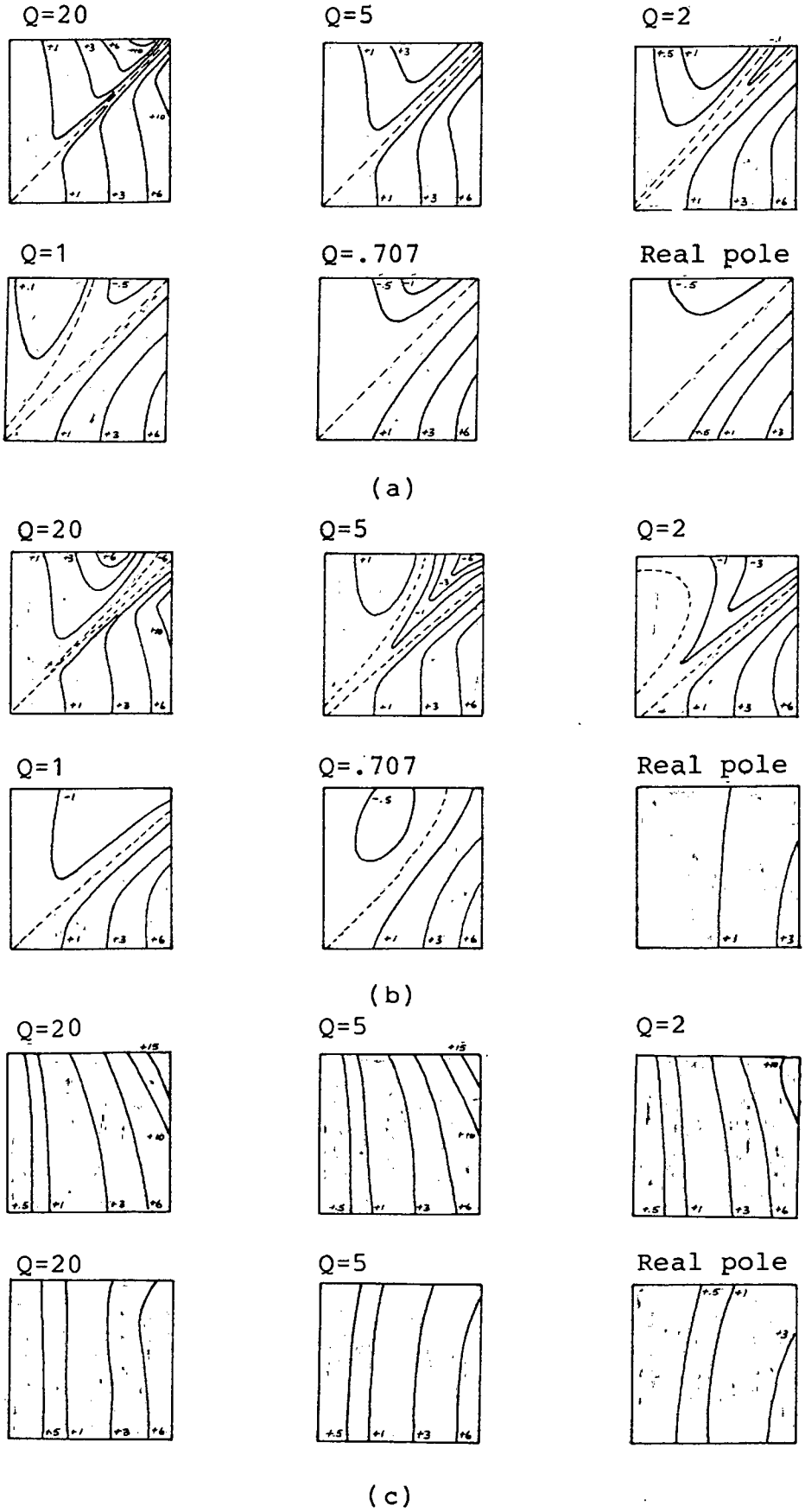

Fig. 6.1 Error in dB evaluated for each pole in an LDI-implemented SC filter using (a) CF-prewarping, (b) S-prewarping and (c) CM-prewarping. Positive regions in red. Vertical axis: pole freq. Horizontal axis: signal freq.

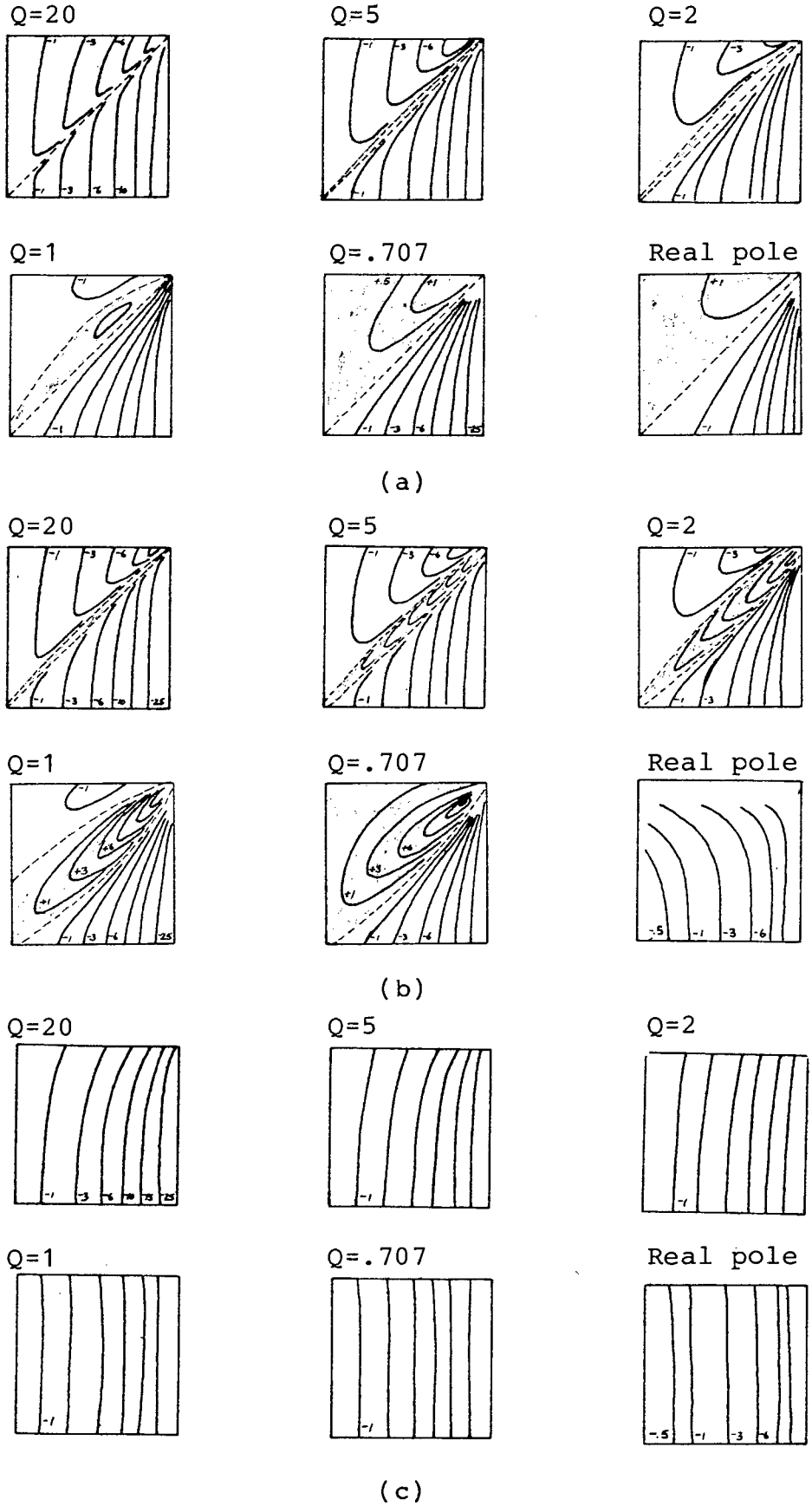

Fig. 6.2 Error in dB evaluated for each pole in a Bil-implemented SC filter using (a) CF-prewarping, (b) S-prewarping and (c) CM-prewarping. Positive regions in red. Vertical axis: pole freq. Horizontal axis: signal freq.

6.3 ASSESSMENT

The plots of Figs. 6.1 and 6.2 may be used to estimate the error contribution due to each pole and zero in an SC filter, thus giving a general picture of the effectiveness of each prewarping approach, for both the LDI and Bil transformations. For a more precise assessment, or for the application of optimization techniques such as those demonstrated in sections 7.2 and 7.3, an approach based on the original expressions, contained in Appendix 1, is more suitable. Accordingly, only general observations emerging from the plots are mentioned here.

Expression (6.7) implies that, for filters containing zeros, a certain amount of error cancellation may take place. Thus, maximum error cancellation would generally be encountered in filters containing an equal number of poles and zeros. For complete cancellation these should occur in pairs with identical locations, so that

$$\sum_{i}^{m} (e_{pi}) + \sum_{k}^{n} (e_{zk}) = 0 \qquad \ldots(6.8)$$

Since this requirement is unreasonable for any practical filter an alternative is to specify that the error contribution be independent of the pole (or zero) location. i.e.

$$\partial e/\partial f_0 = 0 \qquad \ldots(6.9)$$

and

$$\partial e/\partial Q = 0 \qquad \ldots(6.10)$$

For cases where $n < m$ conditions (6.9) and (6.10) would still prove to be advantageous, ensuring minimum distortion of the magnitude response. i.e. $E(j\omega)$ then is a smoothly increasing function of frequency. This rather ideal situation of error characteristic is shown in Fig. 6.3.

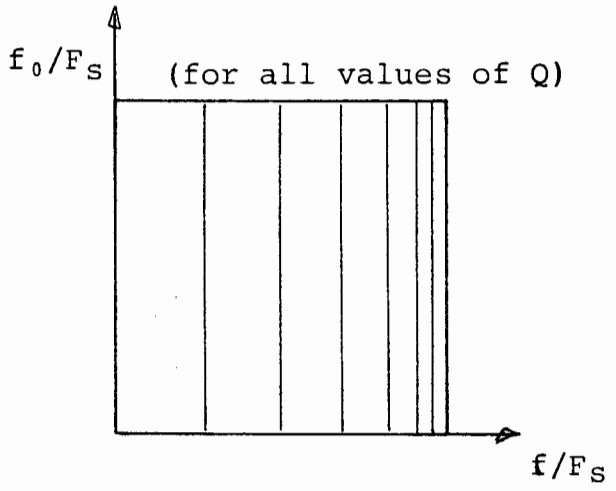

Fig. 6.3 Ideal pole error contribution showing independence of the pole location. (spacing and values of the contours unimportant)

It is apparent from Figs. 6.1 and 6.2, that CM-prewarping best approximates this ideal and can therefore be said to yield the best filter magnitude approximation. CF- and S-prewarping are, however, useful in reducing the total error in the vicinity of the pole and zero frequencies, should such be necessary. This is also evident from Figs. 6.1 and 6.2 where the error contribution reaches a minimum in the neighbourhood of $f=f_0$. The usefulness of this type of characteristic will be demonstrated in section 7.3, where S-prewarping is seen to have a greater effect than CF-prewarping in this regard.

In section 7.3, it is also demonstrated how a very good filter approximation may be achieved with the addition of an extra section cascaded with the prewarped filter, thus introducing additional poles into the response function. This is possible in the case of LDI structures, since the overall error to be compensated for, by the additional section, will generally be positive as seen in Fig. 6.1. If Bilinear structures are used, however, the general error trend is seen to be negative, requiring additional zeros for such compensation to be effective. Addition

of these may be possible without increasing the order of the original filter.

It can also be observed from Figs. 6.1 and 6.2 that the LDI transformation will generally exhibit less overall distortion of the magnitude response, since the contour gradients of the Bil error plots are steeper and show greater directional variation than those of the LDI plots.

It should be noted that the error expressions developed are based on the assumption that the LDI (or Bilinear) transformed response $H_{SC}(z)$ of equation (6.11), can be realised exactly in SC form. In cases where this is not possible the distortion errors incurred would have to be evaluated separately.

$$H_{SC}(z) = H(s)\Big|_{s=\frac{1}{T}\frac{z^{-\frac{1}{2}}}{1-z^{-1}}} \qquad \ldots(6.11)$$

Chapter 7

COMPUTER-SIMULATED VERIFICATION OF P/Z PREWARPING

7.1 SIMULATION METHODS USED

A Hewlett-Packard HP-85 computer was used to simulate the use of pole/zero prewarping. Three examples are given which illustrate some of the techniques available in its application. In each case results obtained when using different prewarping approaches are compared. For the simulation, the filter transfer characteristics were described by the pole and zero locations. The magnitude of the function was then evaluated for continuous frequency signals. Simulation of the SC version of the filter was accomplished by modifying the signal frequency variable according to the warping relationships introduced in (3.17) and (3.18). Accordingly, these were given as

$$\text{LDI} \qquad j\omega \rightarrow j(2/T)\sin(\omega T/2) \qquad \ldots(7.1)$$

$$\text{Bil} \qquad j\omega \rightarrow j(2/T)\tan(\omega T/2) \qquad \ldots(7.2)$$

Thus, for a reference filter given by T(s) in terms of a continuous frequency magnitude response

$$|T(\omega)| = \left|T(s)\right|_{s=j\omega} \qquad \ldots(7.3)$$

the SC LDI-implemented version of the filter (without prewarping) is given by

$$T_{SC}(z) = T(s)\Big|_{s=\frac{1}{T}\frac{z^{-\frac{1}{2}}}{1-z^{-1}}} \qquad \ldots(7.4)$$

with continuous frequency magnitude response

$$|T_{SC}(\omega)| = \left|T_{SC}(z)\right|_{z=e^{j\omega T}} = \left|T(\omega)\right|_{\omega \to \frac{2}{T}\sin(\frac{\omega T}{2})} \quad \ldots(7.5)$$

and similarly for the Bil transformation. This method assumes that the transformed function $T_{SC}(z)$ can be realised exactly in SC form. In addition, all non-idealities (present in real SC structures) were ignored in the simulations. For the purposes of assessing the effectiveness of pole/zero prewarping these assumptions are valid.

7.2 SIXTH ORDER ELLIPTIC LOW-PASS FILTER (LDI TRANSFORMED)

In this example pole/zero prewarping can be compared with classical prewarping as applied to a piecewise-constant-magnitude function. The required characteristics are

$$f_p/F_s = 0.1111 \qquad A_{min} = 47 \text{ dB}$$
$$\Omega_s = 1.34 \qquad A_{max} = 0.24 \text{ dB}$$

These are satisfied by filter parameters CC62050 found in Zverev [93,pp248-249]. For classical prewarping, equation (4.1) is applied to the pass-band and stop-band edge frequencies giving modified requirements

$$(f_p/F_s)' = 0.1089 \qquad A'_{min} = A_{min}$$
$$\Omega'_s = 1.3183 \qquad A'_{max} = A_{max}$$

These are satisfied by filter parameters CC62052. After denormalisation to a pass-band edge frequency of 1 kHz and sampling frequency of 9 kHz the pole and zero locations for the reference filter CC62050 and the classically prewarped filter CC62052 are then as shown in Table 7.1 .

By contrast, pole/zero prewarping is applied to the parameters of the reference filter CC62050 and therefore look-up tables for the classically prewarped characteristics are not required. Prewarped pole and zero locations using CF- and CM-prewarping, as described in chapter 5, are given in Table 7.2 .

Table 7.1 Pole and zero locations given by center frequency ω_0 and Q for the 6th order elliptic filters CC62050 and CC62052.

	Reference filter (CC62050)		Classically prewarped filter (CC62052)
zeros	8594.05	ω_0	8169.28
	inf.	Q	inf.
	11146.86	ω_0	10517.26
	inf.	Q	inf.
poles	3569.41	ω_0	3558.28
	0.6401	Q	0.6422
	5525.12	ω_0	5451.75
	1.8460	Q	1.8916
	6473.98	ω_0	6337.01
	7.9955	Q	8.3731

Table 7.2 Pole and zero locations given by center frequency ω_0 and Q for the 6th order filter CC62050 after application of CF- and CM-prewarping.

	CF-prewarping		CM-prewarping
zeros	8271.24	ω_0	8271.24
	inf.	Q	inf.
	10447.94	ω_0	10447.94
	inf.	Q	inf.
poles	3546.06	ω_0	3574.59
	0.6401	Q	0.6434
	5438.77	ω_0	5451.46
	1.8460	Q	1.9017
	6335.30	ω_0	6336.39
	7.9955	Q	8.3576

The effects of the different approaches are shown in Fig. 7.1 . In the pass-band region, the trace of the classically prewarped SC filter is almost identical to that of the reference filter. This is to be expected since classical prewarping ensures the preservation of the equiripple properties. Within this region, where $F_S/f > 9$, warping has little effect on the positions of the ripple peaks and troughs.

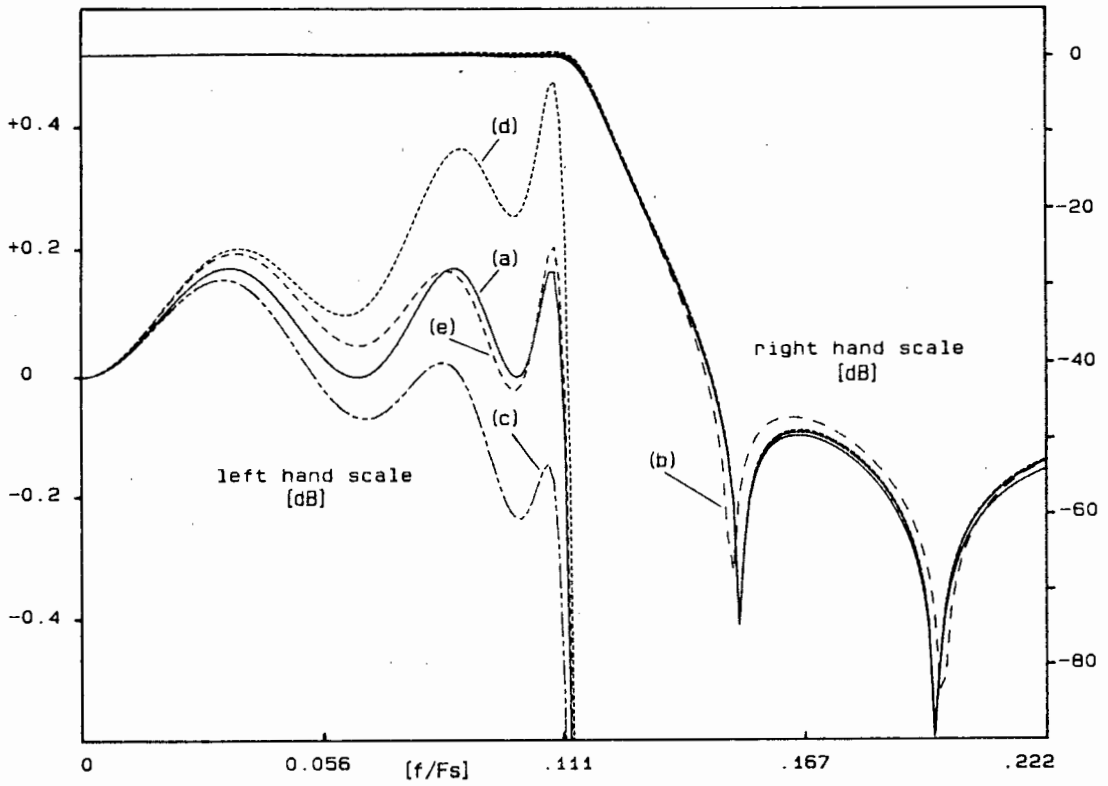

Fig. 7.1 Comparison of different prewarping methods in the LDI realisation of a 6th order elliptic SC filter. (a) Reference filter. (b) Classical prewarping. (c) CF-prewarping. (d) CM-prewarping. (e) Combination of CF- and CM-prewarping.

In the stop-band region of the classically prewarped filter, deviations are evident, resulting from the choice of a different

elliptic function. Here, exact correspondence of the zero locations with those of the reference filter is not important, provided the filter pass-band and stop-band characteristics are fulfilled.

Pole/zero prewarping aims at minimising errors throughout the frequency band. This is seen from the close agreement of traces (c) and (d) when compared with the reference filter for both the pass-band and stop-band regions. Unfortunately however, these filters no longer exhibit elliptic properties, resulting in substantial deviation from the equiripple trace in the pass-band.

CM-prewarping shows a net positive deviation while CF-prewarping shows a net negative deviation. Examination of Figs. 6.1 confirms that these trends are correct. In Fig. 6.1(a) the poles are seen to contribute either negative or very small positive error in the vicinity of their center frequencies. Added to this the negative error contributions of the infinite Q zeros results in a net negative error. In Fig. 6.1(c) all the pole error contributions are seen to be positive. The presence of the zeros results only in a reduction of this positive error.

Reduction of the pass-band deviation is possible by combining the use of CF- and CM-prewarping for the poles. In this way the stop-band accuracy is preserved while optimising the pass-band accuracy. Deviation within the pass-band was plotted for the eight possible combinations of these approaches. This is shown in Fig. 7.2 from which it can be seen that combining the effects of the methods in the order CM-CF-CM achieves the least amount of deviation. This involves using CM-prewarping on poles 1 & 3 (Q_1 = 0.6401 & Q_3 = 7.9955) and CF-prewarping on the remaining pole (Q_2 = 1.8460).

The pole and zero locations of this filter, for a combination of pole/zero prewarping approaches, are indicated by the dashed boxes in Table 7.2 . In Fig. 7.1 the result of using this technique is shown by trace (e). Maximum deviation from the equiripple case has been reduced to below 0.05 dB .

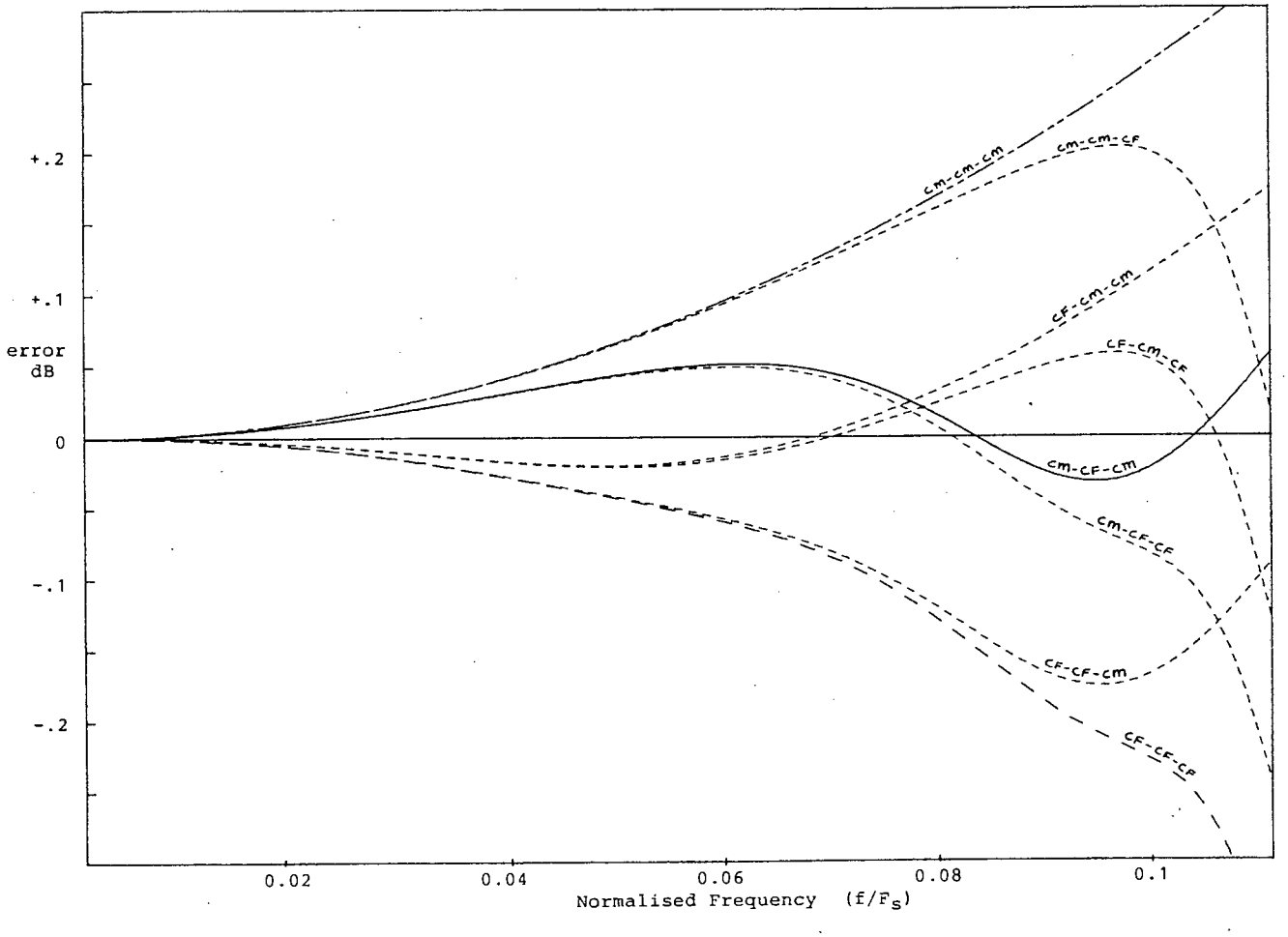

Fig. 7.2 Pass-band error of the 6th order filter for different combinations of pole/zero prewarping.

7.3 TENTH ORDER SPEECH SYNTHESIS FILTER

The magnitude response of a speech synthesis filter will usually describe an irregular curve extending over a bandwidth of two or three decades. Prewarping applied prior to realization in SC form should therefore yield an accurate approximation of the curve over this entire band. Pole/zero prewarping is seen to be ideally suited in such cases.

The specifications can often be given in terms of the frequency and selectivity of localised resonance peaks (or nulls). Clearly, a first approach would be to prewarp each of these specified resonance frequencies in the same way that the pass-band and stop-band edge frequencies of a piecewise-constant-magnitude filter are prewarped. This technique has been described as CF-prewarping, where the center frequency only is adjusted leaving selectivity unaffected.

The specifications of speech synthesis filters are not usually very rigid. The errors remaining after application of CF-prewarping may therefore be quite acceptable. The expressions derived in chapter 6 may be used to estimate the errors that would occur. Increased accuracy, if required, is possible using S- and CM-prewarping in conjunction with other techniques shown in this example.

The formant structure of phoneme /IY/ may be simulated using a 10th order filter [94]. Pole and zero locations for this filter are contained in Table 7.3 .

Table 7.3 Pole and zero locations for a 10th order filter in terms of center frequency and Q.

	ω_0	Q
zeros	11781.0	inf.
	37699.1	inf.
poles	1696.5	4.5
	14388.5	22.9
	18912.4	25.1
	21991.1	20.0
	28274.3	16.0

7.3.1 REALIZATION USING "CENTER FREQUENCY" (CF) PREWARPING

Application of CF-prewarping, as described by expressions (5.11), results in the prewarped specifications of Table 7.4. Sampling frequency is 16 kHz.

Table 7.4 Pole and zero locations for the 10th order filter after applying CF-prewarping.

	ω_0	Q
zeros	11516.7	inf.
	29564.1	inf.
poles	1695.7	4.5
	13908.5	22.9
	17830.5	25.1
	20300.6	20.0
	24736.3	16.0

In Fig. 7.3 the result of using these prewarped specifications in an SC realized filter is compared with the reference filter. Although the transfer response shape follows that of the reference filter, the error steadily increases with frequency throughout the band. In addition, the effective selectivity of the resonance peaks is seen to be slightly reduced.

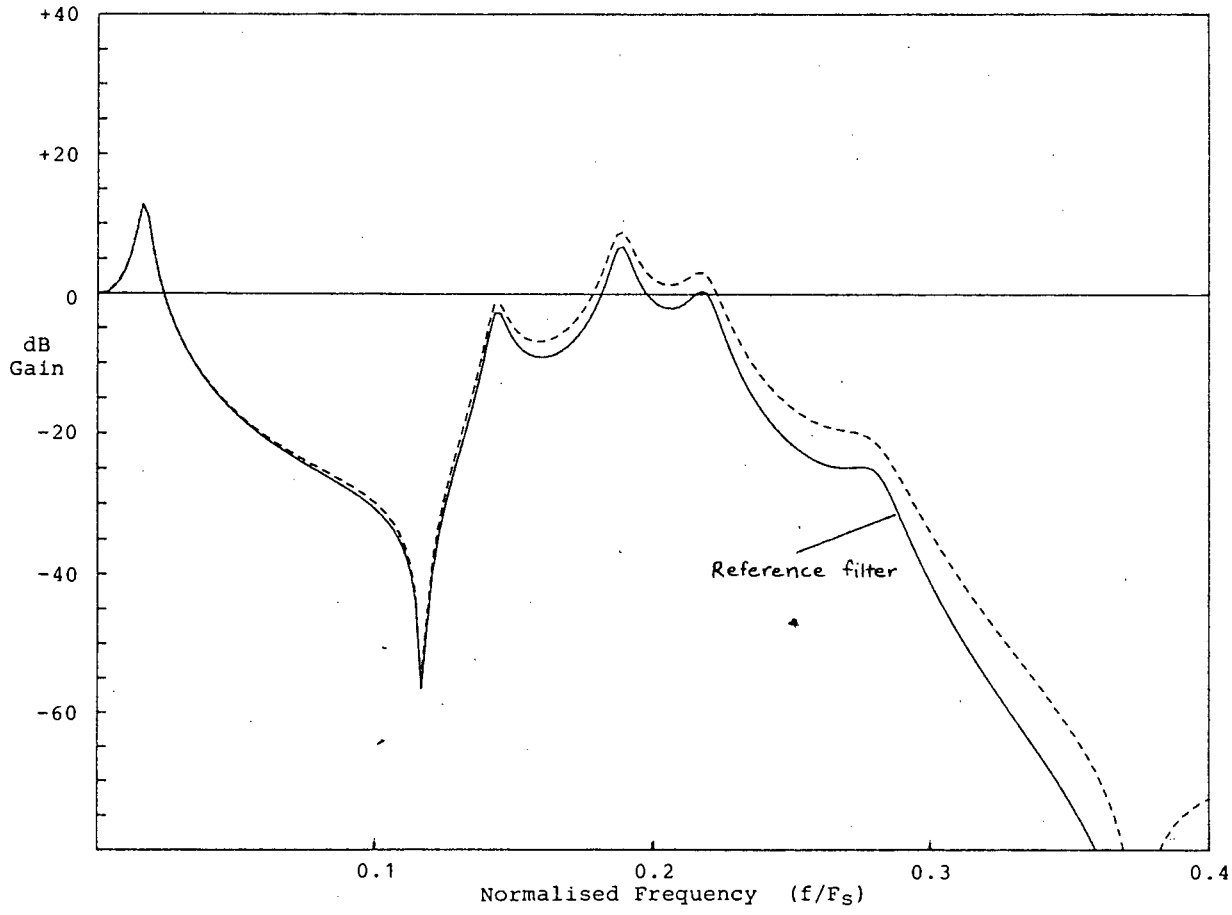

Fig. 7.3 Magnitude response of the 10th order SC filter using CF-prewarping.

7.3.2 REALIZATION USING "SELECTIVITY" (S) PREWARPING

In most applications that employ the LDI transformation there will be a net positive error as seen in Figs. 6.1 . Assuming this to be the case, it is also evident from the figures that S-prewarping is more effective than CF-prewarping in reducing the error in the vicinity of the pole and zero center frequencies. The pole and zero locations using S-prewarping (expressions (5.17)) are shown in Table 7.5 with the SC realization depicted in Fig. 7.4 .

The disadvantage of reducing the error only in the vicinity of the pole and zero center frequencies is clearly seen. The selectivities are further reduced resulting in increased distortion of the magnitude response. Since, in speech synthesis filters it is the shape of the magnitude response that is important, alternative techniques at reducing the errors must be sought.

Table 7.5 Pole and zero locations for the 10th order filter after applying S-prewarping.

	ω_0	Q
zeros	11516.7	inf.
	29564.1	inf.
poles	1695.7	4.5
	13909.0	21.4
	17831.4	22.3
	20302.9	17.0
	24744.8	12.3

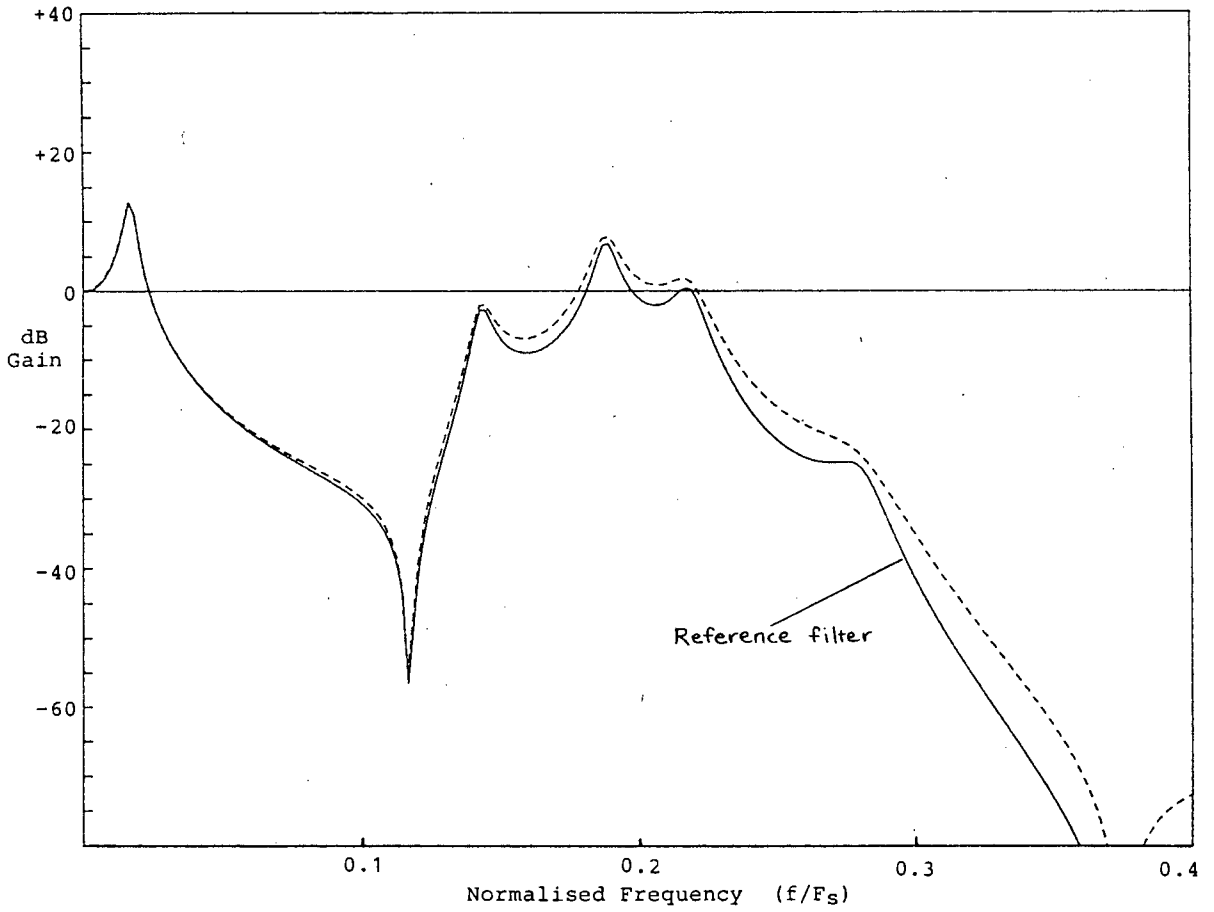

Fig. 7.4 Magnitude response of the 10th order SC filter using S-prewarping.

7.3.3 REALIZATION USING "COMPLEX MAPPING" (CM) PREWARPING

In Table 7.6 the pole and zero locations resulting from the application of CM-prewarping (expressions (5.22)) are given. The SC realization of these specifications is depicted in Fig. 7.5 . Once again the error is seen to be a steadily increasing function of frequency. There is little distortion of the magnitude response shape with only a slight increase in the effective pole selectivities.

Table 7.6 Pole and zero locations for the 10th order filter after applying CM-prewarping.

	ω_0	Q
zeros	11516.7	inf.
	29564.1	inf.
poles	1685.2	4.5
	13906.1	24.6
	17828.6	28.5
	20298.2	23.9
	24737.0	22.1

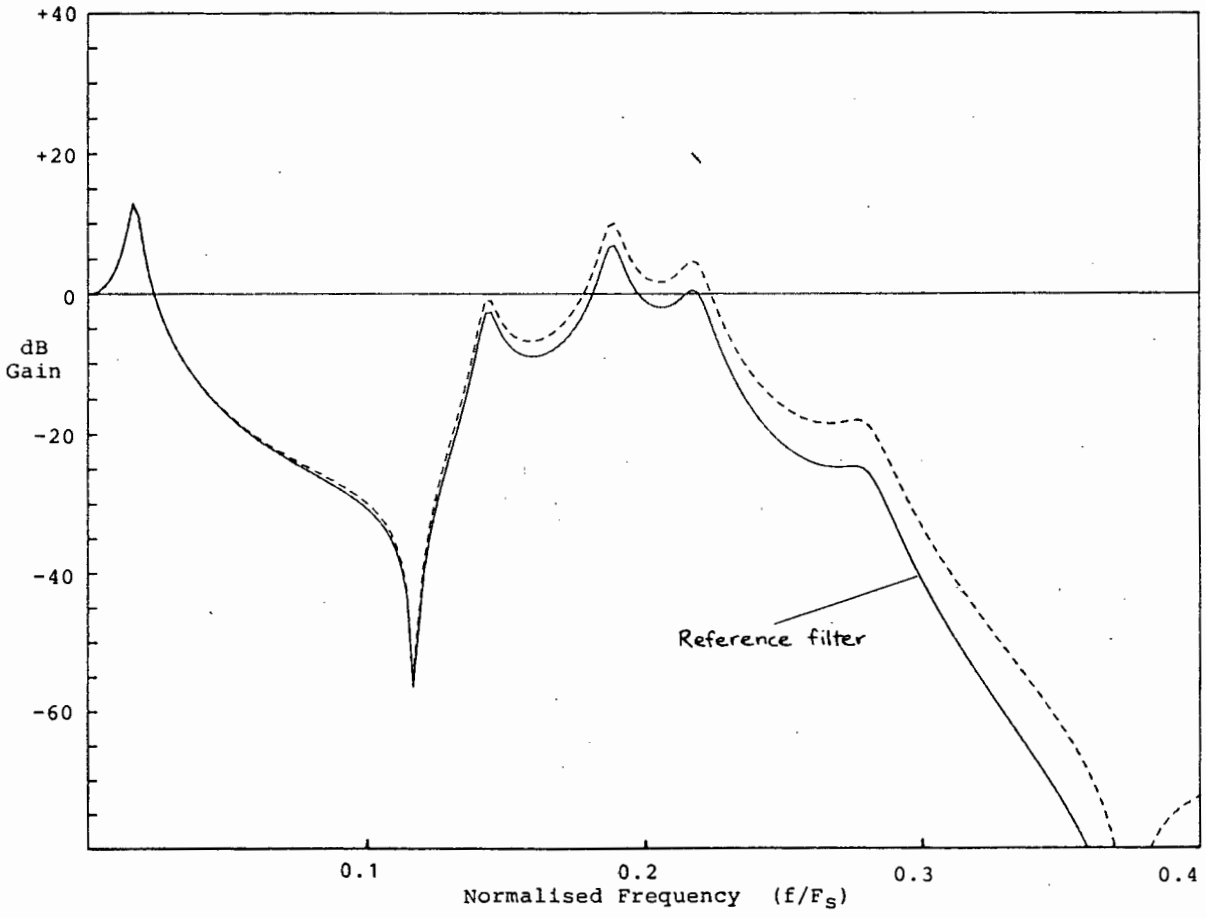

Fig. 7.5 Magnitude response of the 10th order SC filter using CM-prewarping.

Reduction of the error throughout the band is possible by increasing the order of the filter. This is achieved by using an additional cascaded first order section. The location of the extra pole is calculated by specifying its contribution $|P(\omega_x)|$ to the magnitude response at a particular frequency ω_x. The value of this contribution is chosen equal, but opposite in sign, to the error at ω_x thus yielding exact correspondence with the reference filter at this frequency.

The error is obtained using the expressions developed in chapter 6. For a frequency 3.6 kHz in the mid-band region of the filter this is calculated as +4.4265 dB. For a pole at σ the contribution is given by

$$|P(\omega)|^2 = \left[(4/T^2/\sigma^2)\sin^2(\omega T/2) + 1\right]^{-1} \qquad ...(7.6)$$

Using (7.6) and setting $P(\omega_x) = -4.4265$ dB provides the required first order pole (s + 15616.16). The result of including this extra pole in the SC realization is shown in Fig. 7.6 . As expected, exact correspondence between this filter and the reference filter is seen to occur at ω_x = 3.6 kHz.

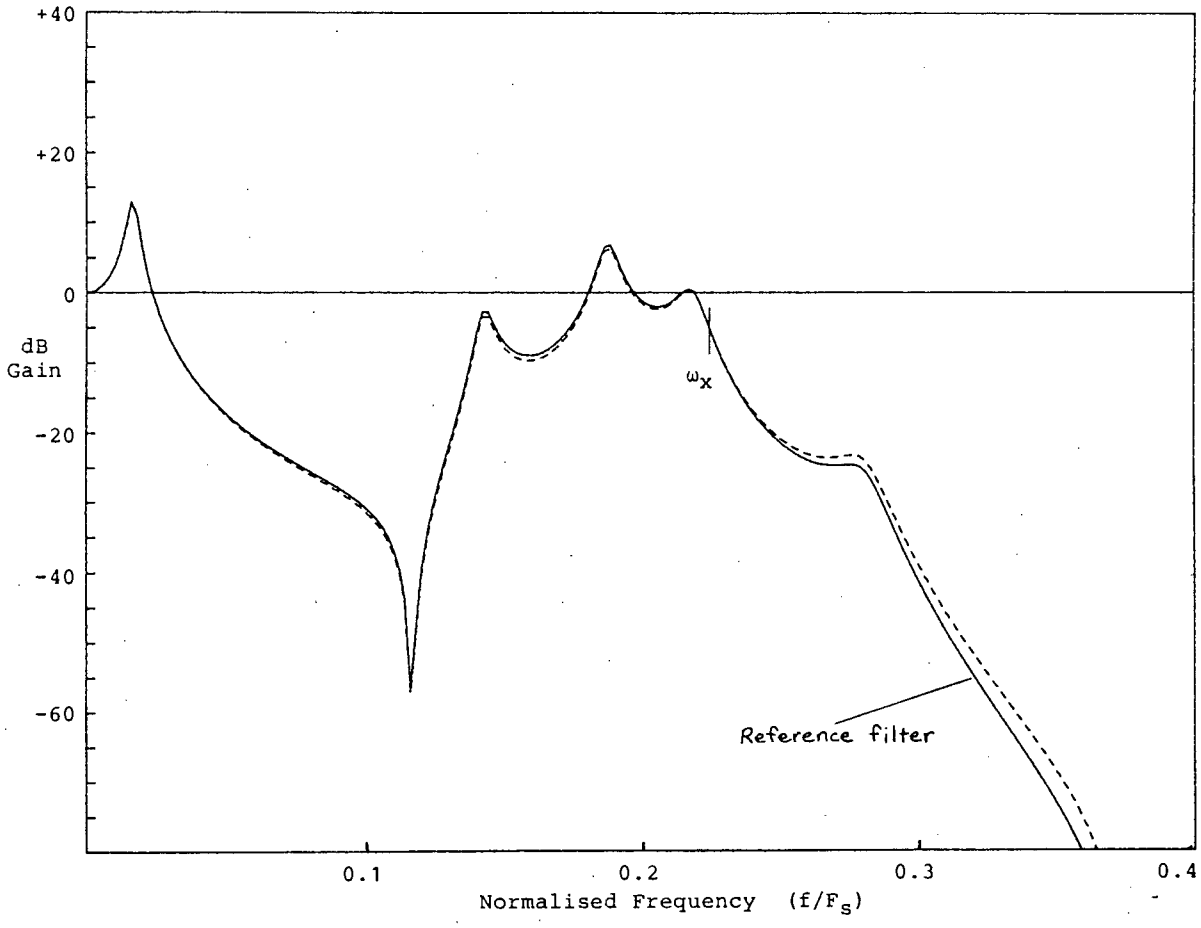

Fig. 7.6 Magnitude response of the 10th order SC filter using CM-prewarping and an extra pole located at σ = -15616.16 .

The accuracy of the SC filter realization can be further improved by increasing the order of the additional cascaded section. If a second order section is used, two frequencies must be chosen at which the additional contribution to the magnitude response is specified. This is given in (7.7).

$$|P(\omega)|^2 = \left[\left[1 - \frac{(\frac{2}{T})^2 \sin^2(\frac{\omega T}{2})}{\omega_0^2}\right]^2 + \frac{4\sigma^2}{\omega_0^4}(\frac{2}{T})^2 \sin^2(\frac{\omega T}{2})\right]^{-1} \quad \ldots(7.7)$$

Equation (7.7) can be re-written in terms of σ^2 where ω is the frequency at which the magnitude contribution $|P|^2$ is specified.

$$4\sigma^2 = \left[\frac{\omega_0^4(1-|P|^2)}{|P|^2(\frac{2}{T})^2\sin^2(\frac{\omega T}{2})}\right] + 2\omega_0^2 - (\frac{2}{T})^2\sin^2(\frac{\omega T}{2}) \qquad ...(7.8)$$

The error at $\omega_x = 2\pi$ 2.8 kHz is +2.662 dB and at $\omega_y = 2\pi$ 4.2 kHz +6.057 dB. Setting P_x = -2.662 dB and P_y = -6.057 dB, equation (7.8) can be solved for ω_0 and σ so that, for the additional second order cascaded section, ω_0 = 18229 and Q = 0.6797 . The effect of including such a second order section is seen in the very good agreement demonstrated in Fig. 7.7 .

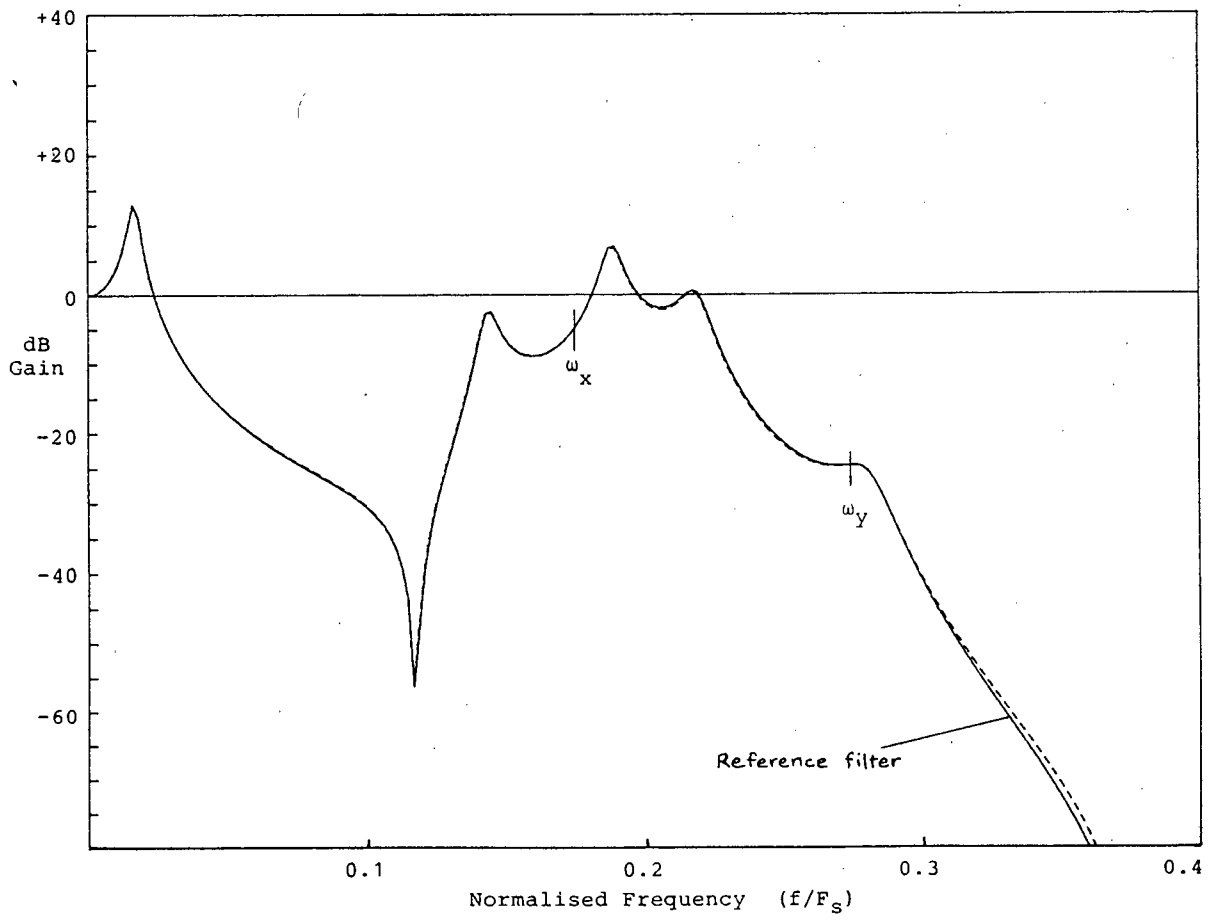

Fig. 7.7 Magnitude response of the 10th order SC filter using CM-prewarping and an extra pole pair with ω_0 = 18229 and Q = 0.6797 .

7.4 THIRD ORDER CHEBYSHEV LOW-PASS FILTER

The third example is taken from a paper by Brugger & Hosticka [92]. Here the authors develop pole/zero prewarping expressions for application in Backward-Difference SC realizations. These expressions correspond to CM-prewarping as derived in chapter 5 for the LDI and Bilinear transformations.

In the paper the magnitude responses for the reference filter and BD-prewarped transfer function are compared prior to realization. The effect of the prewarping on the original function is thus shown. This procedure will be extended to include LDI, Bilinear and Forward-Difference prewarping. In addition, the simulated responses, after SC realization are compared.

The prewarping expressions for the four transformations are given in (7.9)-(7.12). Note that these are given in terms of the co-ordinates of the poles and zeros in the s-plane. σ should therefore be replaced with $-\sigma$ in (7.12) to give the equations of Brugger & Hosticka, which are written in terms of the denominator polynomial coefficients.

LDI $$\sigma' = (2/T)\cos(\omega_p T/2)\sinh(\sigma T/2) \qquad \ldots(7.9a)$$

$$\omega_p' = (2/T)\sin(\omega_p T/2)\cosh(\sigma T/2) \qquad \ldots(7.9b)$$

Bil $$\sigma' = \left(\frac{2}{T}\right)\frac{\sinh(\sigma T)}{\cos(\omega_p T) + \cosh(\sigma T)} \qquad \ldots(7.10a)$$

$$\omega_p' = \left(\frac{2}{T}\right)\frac{\sin(\omega_p T)}{\cos(\omega_p T) + \cosh(\sigma T)} \qquad \ldots(7.10b)$$

FD $$\sigma' = (1/T)[e^{\sigma T}\cos(\omega_p T) - 1] \qquad \ldots(7.11a)$$

$$\omega_p' = (1/T)e^{\sigma T}\sin(\omega_p T) \qquad \ldots(7.11b)$$

BD $\quad \sigma' = (1/T)[1 - e^{-\sigma T}\cos(\omega_p T)]$ ...(7.12a)

$$\omega_p' = (1/T)e^{-\sigma T}\sin(\omega_p T) \qquad ...(7.12b)$$

The denominator polynomial of the filter is

$$(s + \sigma_1)[s^2 + (\omega_0/Q)s + \omega_0^2]$$

$$= (s + 3103.894)[s^2 + 3103.894s + (6264.307)^2] \qquad ...(7.13)$$

This has a pass-band ripple of 1dB and cut-off frequency of 1kHz. In Table 7.7 the prewarped characteristics for the four transformations are listed with $\omega_0^2 = \sigma^2+\omega_p^2$ and $Q=\omega_0/2/\sigma$.

Table 7.7 Reference and prewarped characteristics of the third order Chebyshev low-pass filter.

	Ref.	LDI	Bil	FD	BD
σ_1	3103.9	3108.8	3094.2	2821.4	3425.4
ω_0	6264.3	6229.3	6335.3	5934.4	6538.8
Q	2.018	2.043	1.970	1.182	8.682

In Fig. 7.8 the simulated SC realizations of these characteristics are shown for each transformation. The responses of the FD and BD realizations are identical to that of the LDI realization. This is to be expected since the CM-prewarping error contribution expressions for these transformations are identical, as noted in chapter 6.

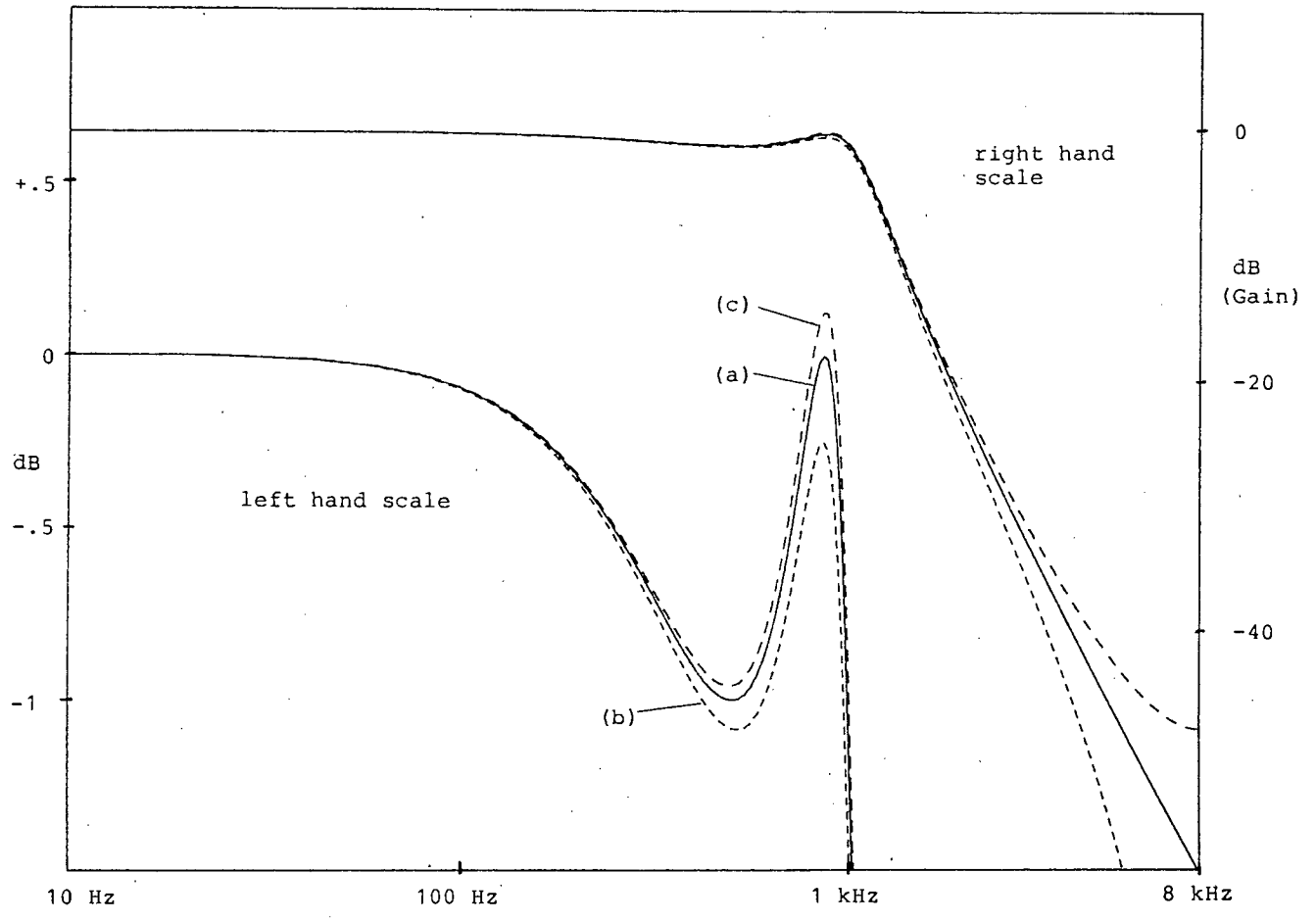

Fig. 7.8 Simulated SC realization response of the 3rd order Chebyshev filter using different analog to digital transformations and associated prewarping. (a) Reference filter. (b) Bilinear transformed filter. (c) LDI, Forward-Difference and Backward-Difference transformed filters.

Although the FD and BD transformations with associated prewarping yield identical results to the LDI transformation, there is a substantial difference in the prewarping effect that these two transformations have on the response function. This is evident on inspection of Table 7.7 . In order to see this more clearly the analog realization responses of these prewarped filter characteristics are depicted in Fig. 7.9 .

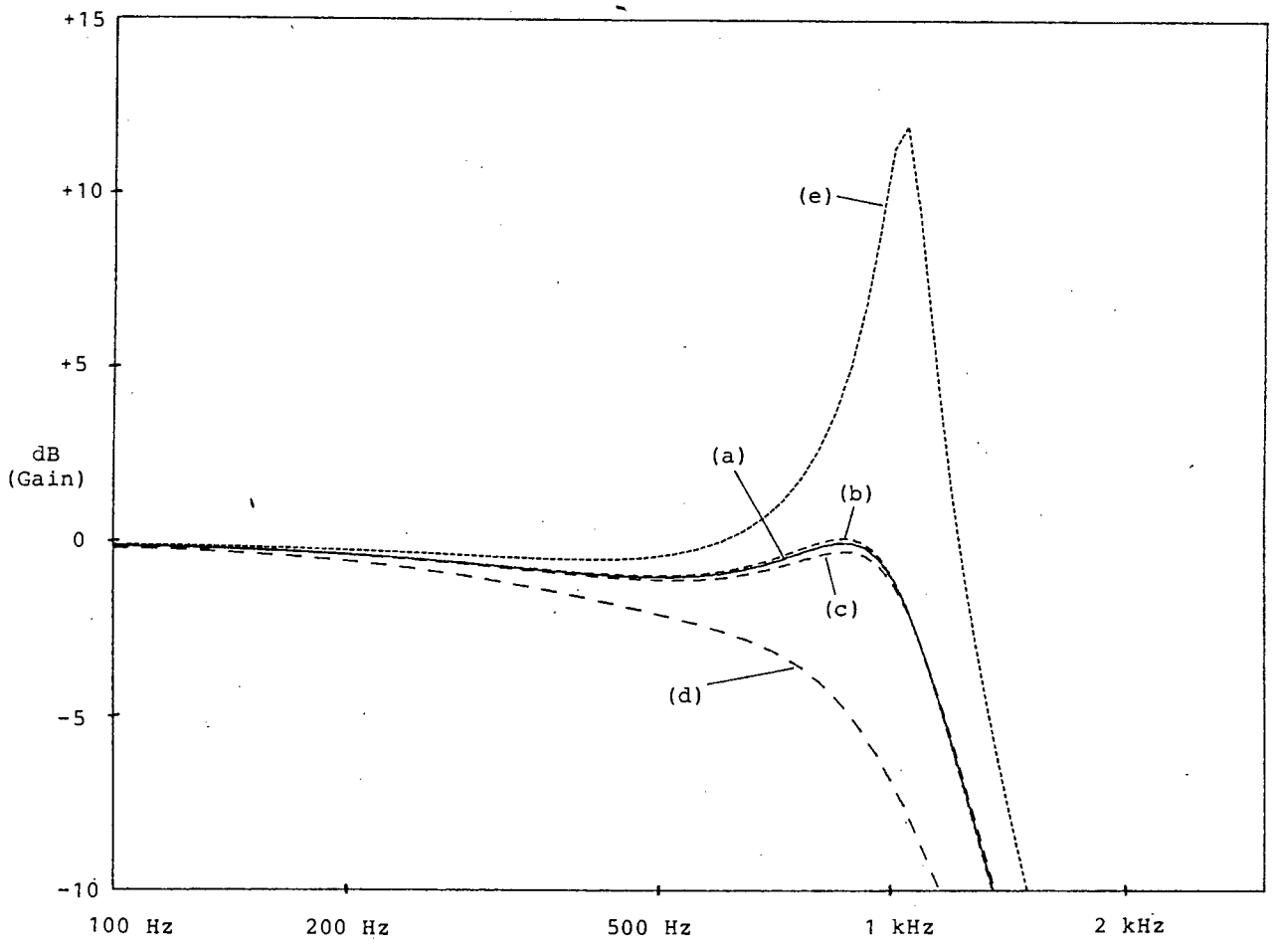

Fig. 7.9 Analog transfer responses of the prewarped filter characteristics given in Table 7.7 . (a) Reference filter. (b) LDI, (c) Bil, (d) FD and (e) BD prewarped characteristics.

7.5 CONCLUSION

Three examples have been given to illustrate the use of pole/zero prewarping. Close approximations of the required responses are seen to be possible. The first example allows comparison of pole/zero prewarping with classical prewarping as applied to a piecewise-constant-magnitude function. Although pole/zero prewarping yields comparable results, it would not normally be used in such cases. Prewarping the pass-band and stop-band edge frequencies in the classical way prior to selection of the filter parameters is both simple and reliable. If filter look-up tables are used, these parameters will usually be the element values of a standard structure, thus eliminating the need for circuit synthesis.

By contrast, pole/zero prewarping requires knowlege of the transfer response function. After the poles and zeros of this function have been prewarped, the circuit must then be synthesised. If the filter is being designed on the basis of an existing analog structure, care should be taken in this process to preserve any optimal characteristics governed by the relationships between the original element values. In addition, the pole/zero prewarping process may require optimization techniques to reduce the errors to within specified limits. This would not be necessary in the case of classical prewarping.

In the second example the filter characteristics are described by the pole and zero locations of the transfer response function. The magnitude response of this filter traces an irregular curve extending over a wide band. Pole/zero prewarping is shown to achieve very good results in this case. It is in such examples that pole/zero prewarping used in conjunction with the error

expressions developed in chapter 6, is ideally suited.

The third example was used to compare the effects of CM-prewarping for the four analog to digital transformations. The filter used is that given by Brugger and Hosticka [92] to demonstrate the prewarping of a Backward-Difference transformed function. This is here extended to include the LDI, Bilinear and Forward-Difference transformations. As can be seen in Fig. 7.9 , FD and BD prewarping alter the filter characteristics by a large amount unlike LDI and Bil prewarping. For FD and BD prewarping the possibility also exists that the form of the denominator and numerator polynomials will be changed. Complex poles and zeros may be shifted onto the imaginary axis or into the right-half-plane when using BD prewarping. Zeros on the imaginary axis will be shifted into the left-half-plane when using FD prewarping and into the right-half-plane when using BD prewarping.

The implication of this (apart from the possibility of unrealizable requirements resulting) is that, where the filter is modelled on an existing analog circuit, the topology may have to be changed and the circuit re-designed. In situations where this is not necessary, the large change in filter characteristics may still mean that optimal circuit properties such as component spread and sensitivity to component values are degraded. Based on these considerations, the LDI and Bil transformations are to be preferred.

Techniques are applied whereby the accuracy of an approximation can be increased. In the case of the sixth order filter the combination of two approaches to pole/zero prewarping was used. For the tenth order filter an additional cascaded section was used.

In the examples it has been shown how the error diagrams developed in chapter 6 may be used to predict the general effect of each pole/zero prewarping method. Further, the error contribution expressions of chapter 6 were effectively used for the error reduction. Such techniques could therefore well be incorporated in an interactive Computer Aided Design program. However, the development of such a program was not considered part of the scope of this thesis.

Chapter 8

NOISE IN SC NETWORKS

The generation of noise at the output of SC networks differs from that in RC-active networks due to their sampled-data nature. In most cases the noise bandwidth within these circuits is very much larger than the sampling frequency. This causes the aliasing of high frequency noise components into the filter base-band region. As a result, SC networks generally exhibit higher noise levels than their RC-active equivalents [95]. It is therefore important to understand the mechanisms whereby the noise is generated. This aids the development of methods to reduce noise and of predicting its level for specific filter designs. Several authors [96,44,97,98,99] have described methods for evaluating noise in SC and other sampled-data networks, while "Correlated Double Sampling" [100] and "Chopper Stabilization" are two methods that have been used by Young & Hodges [65] and Hsieh et. al. [101] for the reduction of noise.

This chapter is a summary of joint research undertaken as a contract at Virginia Polytechnic Institute and State University (VPI&SU), Blacksburg, USA [102,103,104]. Its scope covered the analysis, modelling, simulation and experimental measurement of noise within SC networks. The aim of the research was to develop strategies for predicting this noise. The author's principal responsibility with the research team was the laboratory and application work. This was used to supply data for the theoretical models and to test their validity. Both fabricated and discrete component structures were used for these tests.

8.1 NOISE SOURCES IN SC NETWORKS

Noise generated in SC networks is assumed to have two primary sources [97,105]:

(i) the operational amplifiers (OAs).

(ii) the "on" resistance of the MOS switches.

(the thermal noise contribution of the "off" resistance can usually be neglected because its power spectrum is concentrated at very low frequencies.)

All sources are assumed to be uncorrelated and their power spectral densities evaluated separately at the output. In addition, researchers to date have assumed a large degree of undersampling due to the noise source bandwidths being very much larger than the sampling frequency. This allows the assumption of separability to be extended to the undersampled version of each noise source where applicable. This large degree of undersampling is true for most SC networks because the noise bandwidths are determined by the RC time constants within the circuit and the OAs. These time constants are, in turn, small compared to the sampling period to ensure complete charge transfer each cycle.

8.2 DIRECT NOISE AND SAMPLED AND HELD NOISE

In order to obtain the contribution of each noise source at the output, the transfer function from this source to the output must be evaluated [44]. For sources which have a direct path to the

output during one or more time slots per sampling period the output contribution is evaluated in the classical manner for that time slot(s). This is termed "Direct Noise". In most cases however, a noise signal will be sampled and held for one or more time intervals before reaching the output. This "Sampled and Held Noise" will be subject to the undersampling effect mentioned above and must be evaluated using sampled-data techniques. A convenient approach used by Fischer [99] to model these two types of noise is to designate two outputs for each OA appearing in the network:

(i) a continuous noise output for noise signals which are not sampled by the following stage.

(ii) a sampled output for noise signals which are sampled by the following stage.

8.3 UNDERSAMPLING

"Undersampling" occurs when the noise bandwidth is greater than half the sampling frequency. The noise spectrum sidebands, centered around integer multiples of the sampling frequency, are then superimposed over the fundamental spectrum. The number of sidebands that are "folded" onto the frequency range $0 < f < F_s/2$ is referred to as the ratio of undersampling, k^2 ,where according to [99]

$$k = \sqrt{2BW_n/F_s - 1} \qquad \ldots(8.1)$$

BW_n is the bandwidth of the noise spectrum prior to sampling and F_s is the sampling frequency. This is shown in Fig. 8.1 where $BW_n = 1.5F_s$ giving a ratio of under undersampling $k^2 = 2$.

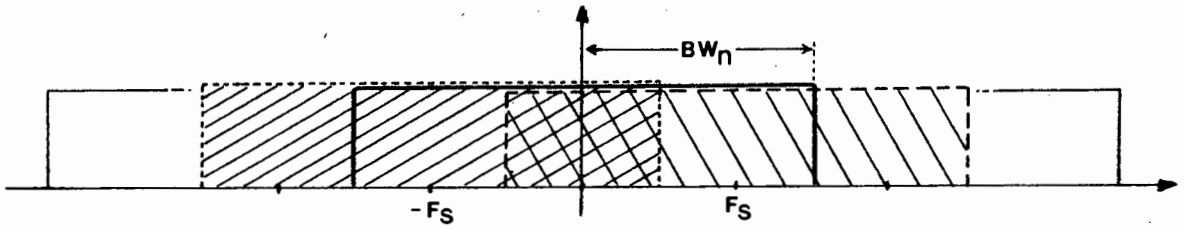

Fig. 8.1 Effect of sampling a signal at $F_S = (2/3)BW_n$

If the average power transmitted through the sampled system is held constant irrespective of the sampling frequency and sample duration, an upper limit on the sum of all the superimposed sidebands with the fundamental will be given by

$$S_t \leqslant (S_{neq} + k^2 S_{neq}) = S_{neq}(2BW_n/F_S) \qquad ...(8.2)$$

where S_{neq} is the power spectral density of an equivalent bandlimited white noise source containing the same total power within BW_n as the original noise spectrum.

In addition to the undersampling, the noise voltage signal is contained within a $\tau_H \text{sinc}(\omega\tau_H/2) = (2/\omega)\sin(\omega\tau_H/2)$ envelope due to the holding time τ_H of each sample. This envelope effectively bandlimits the sample and hold noise so that the undersampled noise is subject to negligible further undersampling in subsequent stages (i.e. anti-aliasing filtering between stages is inherently provided [99]). Finally, the noise must be multiplied by the transfer function that it sees to the output $|H(\omega)|^2$ and the effect of finite sampling on the power transmission must be included (multiplication by F_S^2).

This model of noise transmitted to the output of an SC network is represented in the block diagram of Fig. 8.2.

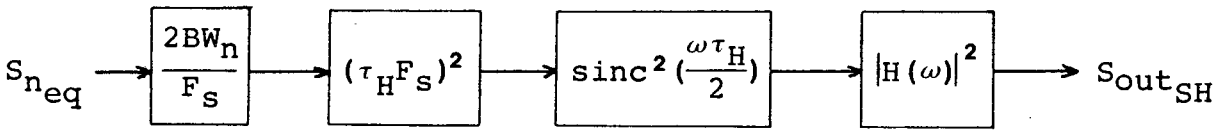

Fig. 8.2 Transfer path of sampled-and-held noise through an SC network.

By comparison, the transfer path of direct noise is shown in the diagram of Fig. 8.3.

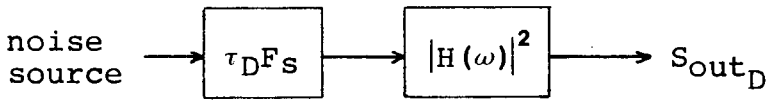

Fig. 8.3 Transfer path of direct noise through an SC network

Gobet and Knob [106] have shown that the inclusion of the roll-off characteristic of the white noise adds an extra multiplying factor. For their derivation, this is assumed to be a first order low-pass characteristic. If S_{n_0} is the spectral density of the source at dc and BW_n the cut-off frequency, then the output spectral density is given by

$$S_t = S_{no}\left(\frac{2BW_n}{F_s}\right)(\tau_H F_s)^2 \text{sinc}^2\left(\frac{\omega\tau_H}{2}\right)|H(\omega)|^2 \frac{\sinh\left(\frac{2\pi BW_n}{F_s}\right)}{\left[\cosh\left(\frac{2\pi BW_n}{F_s}\right) - \cos\left(\frac{\omega}{F_s}\right)\right]} \quad \ldots(8.3)$$

In the usual range of undersampling where $BW_n/F_s > 1$ the extra multiplying factor

$$\frac{\sinh(2\pi BW_n/F_s)}{\cosh(2\pi BW_n/F_s) - \cos(\omega/F_s)}$$

is approximately equal to 1. Equation (8.3) then corresponds directly to the transfer path shown in Fig. 8.2.

8.4 SWITCH RESISTANCE NOISE

Referring to Fig. 8.4(a), the thermal noise power spectral density generated within a MOS switch is given by

$$S_n = 2k\theta R_{on} \quad V^2/Hz \qquad ...(8.4)$$

where $k = 1.38 \times 10^{-23}$ Boltzman's constant

θ = absolute temperature in Kelvin

R_{on} = "on" resistance of the MOS switch

S_n is assumed to be a double-sided spectrum of uniform density extending over the bandwidth $-BW_n < f < BW_n$. In terms of noise voltage, the expression will be

$$\overline{e_n}^2 = 4k\theta R_{on} BW_n \quad V^2 \qquad ...(8.5)$$

The bandwidth is governed by the time constant of the switch resistance in conjunction with its associated capacitor. i.e.

$$BW_n = (R_{on}C)^{-1} \qquad ...(8.6)$$

Assuming typical values in use (capacitors in the range 1-100 pF and switch "on" resistance in the kilo-ohm range) this bandwidth is expected to be in the range 10-100 MHz. Equation (8.5) becomes

$$\overline{e_n}^2 = 4k\theta/C \qquad V^2 \qquad \ldots(8.7)$$

A continuous time equivalent circuit incorporating such a voltage source in series with a noisless resistor and ideal switch can therefore be used as shown in Fig. 8.4(b).

In order to include the effect of sampling at frequency $F_S = 1/T$, the spectrum in (8.4) is convolved with the squared Fourier transform of the sampling function. As described in section 8.3, this gives, for undersampled band-limited white noise

$$S_{n_S} = (1/T^2)S_n(2BW_n/F_S)$$

$$= 4k\theta(T/C)F_S^2 \qquad \ldots(8.8)$$

The Fourier transform of a uniform pulse of duration τ_H is

$$\tau_H \text{sinc}(\omega\tau_H/2) = (2/\omega)\sin(\omega\tau_H/2)$$

Holding each sample for this duration therefore results in an output spectrum

$$S_{n_{SH}} = S_{n_S}\tau_H^2\text{sinc}^2(\omega\tau_H/2)$$

$$= 4k\theta(T/C)(\tau_H F_S)^2\text{sinc}^2(\omega\tau_H/2) \qquad \ldots(8.9)$$

From this it will be observed that, for a switched capacitor, the thermal noise generated within the finite "on" resistance is independent of the resistance value. It is in fact determined by an equivalent resistance $R_{eq} = (T/C)$. This property enables the use of classical noise simulation methods, where the noise is modelled by replacing each switched capacitor with its noisy equivalent resistance.

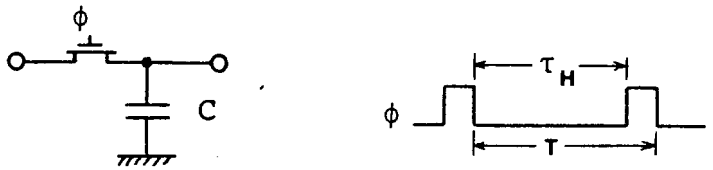

(a)

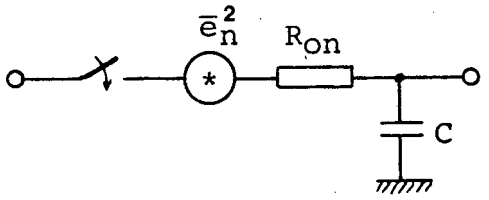

(b)

Fig. 8.4 (a) Capacitor in association with a single MOS switch controlled according to timing ϕ .
(b) Continuous time equivalent noise model with ideal switching.

8.5 MOS OPERATIONAL AMPLIFIER NOISE

A detailed noise model of an OA is described later. For the purposes of SC noise analysis, however, it is sufficient to lump all noise sources into a single noise voltage source. This is placed in series with the non-inverting input of the OA as shown in Fig. 8.5. The nature of this noise voltage is determined by the two predominant types of noise generated within an OA.

(i) Broad-band white noise.

(ii) 1/f flicker noise.

$\overline{e_n}^2$ is therefore given as [44]

$$\overline{e_n}^2(f) = \overline{e_{nw}}^2(1+f_p/f) \qquad ...(8.10)$$

The white noise rms voltage is defined by means of an equivalent resistance R_{eqw}. i.e.

$$\overline{e_{nw}}^2 = 4k\theta R_{eqw} \quad V^2/Hz \qquad ...(8.11)$$

The 1/f noise corner frequency is given by f_p as shown in Fig. 8.6. The bandwidth of the white noise is assumed approximately equal to the unity gain bandwidth (gain-bandwidth product) of the OA [95].

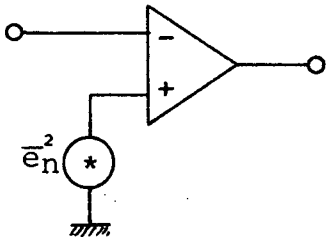

Fig. 8.5 Simplified OA noise model.

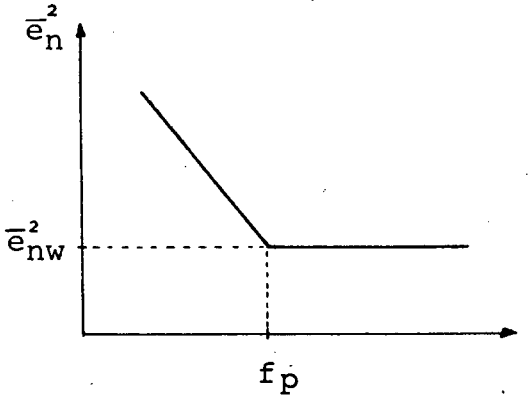

Fig. 8.6 Equivalent input noise of a MOS OA showing 1/f and broad-band components.

8.6 LOW NOISE SC NETWORKS

Knowlege of noise generation within SC networks allows certain reductions in this noise to be effected when designing a particular circuit. In addition to the usual low noise fabrication and design considerations such as gain optimisation [27,55] the following factors bear special relevance to SC networks.

1) Switch resistance noise is inversely proportional to C as seen in equation (8.5). Increasing the capacitor values will therefore cause a reduction in noise. This increase is achieved by uniform scaling in order to preserve the capacitor ratio relationships. It will, however, result in a larger chip and thus higher cost.

2) Use of low noise OAs. In most SC networks the OAs contribute a significant proportion of the noise. This should be reduced as far as possible. In particular the 1/f noise corner frequency should be less than the Nyquist frequency, $F_S/2$, to prevent aliasing of this component.

3) Reduce the OA gain-bandwidth product. Although this will reduce the noise bandwidth and hence the ratio of undersampling, care should be taken that the high frequency response of the network is not degraded.

4) Use of special circuit techniques such as "Correlated Double Sampling" [100] and "Chopper Stabilization" [101] for the reduction of low frequency noise.

8.7 PREDICTING NOISE IN SC NETWORKS

In this section a brief overview of the computer simulation and theoretical analysis in the research contract is presented. The chief responsibility for these sections lay with other members of the team. For a more detailed discussion and description of the mathematical procedures see [102,103,104].

The calculation of noise in the frequency domain at the output of an SC network may be accomplished analytically by:

a) including appropriate noise sources throughout the network.
b) computing the sampled-data transfer function from each source to the output.
c) summing at the output the contributions from each source multiplied by their respective transfer functions.

The main disadvantage of such a method is the complexity involved in computing all the transfer functions for high order SC networks. Existing simulation programs such as DIANA are capable of computing these transfer functions. However, at the time of investigation, the inclusion of noise sources within the network description was not possible on the version of DIANA available.

An alternative route was therefore developed [102,107] which does not entail analysis of the internal structure of the network. Involved is a time domain simulation of the network including all internal noise sources, for which the SC simulation program TCAPS was applied. The method can be summarised as follows:

(i) Include appropriate time-domain noise sources throughout the network.

(ii) Use TCAPS to simulate the time-domain output signal of the network driven by its internal noise sources.

(iii) Apply a suitable windowing function or autoregressive (AR) technique to obtain a spectral estimation of the output noise power.

Development of the procedure involved:

(a) The generation of un-correlated time samples of both white noise and 1/f noise to be used as input files for each noise source.

(b) The testing of various windowed periodogram and AR spectral estimation algorithms for use on the output time signal.

Initially, simulation runs were done on the Gobet and Knob integrator [97]. The results showed that the time-domain method can accurately predict the noise behaviour of this network. The most successful spectral estimation technique being the Yule-Walker AR algorithm.

Next, the simulation method was applied to a General Electric (GE) prototype Biquad filter chip and its scaled discrete component equivalent version. The Yule-Walker and Burg AR algorithms failed to predict the noise characteristic correctly, since the algorithms' validity depends on the noise signals being stationary in nature. This is not the case for noise frequencies very much larger than the sampling frequency. The circuit must therefore be treated as a time-variant network.

An alternative AR algorithm, the Autocorrelation method, which does not depend on the assumption of stationary signals, yielded the correct noise characteristic shape. The windowed periodogram method also gave the correct noise characteristic shape. However, there was a large discrepancy in the noise levels predicted by the two methods.

Due to the time limitations of the research contract it was decided not to pursue the time-domain spectral estimation technique any further. Instead SPICE modelling [99] was used successfully to simulate the noise behaviour of the GE Biquad. This was then extended to the EG & G Reticon R5609 7th order filter chip and its scaled discrete component equivalent version.

A parallel check was carried out in the frequency domain using transfer function computation and source contribution summing, by way of the z-domain analysis after Laker [26].

Finally, exact stochastic analysis of a periodically shunted capacitor and an SC integrator was undertaken. This also involved a check on the analysis of Gobet and Knob [95,97,106,108]. Their analysis however, is valid only for white noise sources and assumes the network to be time-invariant. In order to account for the time-varying properties of SC networks and to allow for noise inputs of a more general nature, it was found that a procedure similar to that of Liou and Kuo [44] was more suitable. In both cases, theoretical results compared favourably with experimental measurements.

Chapter 9

EXPERIMENTAL SC NOISE TESTS

Laboratory tests were conducted in conjunction with the simulated and theoretical work. These served two purposes:

(i) To supply data of the OA characteristics for use in the simulated and theoretical noise models.

(ii) To verify the noise behaviour of various circuits as predicted by simulation and theory.

OA characterisation tests were conducted on the Harris HA-4605 quad OA and an isolated OA on a prototype General Electric CMOS SC filter chip. These yielded values for:

(i) Gain Bandwidth Product and open loop gain.

(ii) Equivalent input noise voltage.

(iii) Equivalent input noise current.

Verification tests were conducted on filters in both fabricated and scaled discrete component form:

(i) An SC Biquad filter section.

(ii) A 7th order elliptic filter.

The Biquad and 7th order fabricated versions were supplied by General Electric, Lynchburg, USA and EG & G Reticon, USA respectively. No isolated OA was available on the Reticon chip for characterisation tests. In the absence of this data, values representing the OA characteristics were assumed to be similar to those of the GE chip OA.

9.1 EXPERIMENTAL DETAILS

With the exception of tests on the Reticon chip, which was mounted on a printed circuit board, all the other tested circuits were mounted on unmetallised board using i.c. sockets and wire-wrap connections. This was found to eliminate irregular noise characteristics and instability above 2 MHz which had been encountered previously when the test set-ups were mounted on a breadboard. 60 Hz mains frequency interference caused a problem in some cases. However, measurements were checked using batteries where necessary. The following equipment and conditions pertain to all tests:

- Spectrum Analyzers: Tektronix 7L5 module in a 7603 frame.
  Hewlett Packard 3580A
- Power Supply : Tektronix PS 503A
  Batteries
- Custom built two phase clock signal generator with adjustable duty cycle and phase.
- Clock standard signal generator : Hewlett Packard 3310A
- Ambient temperature $21^{o}C$.
- 100 μF power supply de-coupling.

For the discrete component filters, Harris HA-4605 quad OA packages were used. Only one OA per package was utilized, the other three pairs of inputs being grounded. The Harris HI-201 quad CMOS device was used for the switches while all the capacitors were NPO ceramic and the resistors carbon film. Unless otherwise stated, all the capacitors and resistors were measured to within 1% of the required value.

Operation of the 7th order filter was tested and compared with simulated results using DIANA This was done for the output of each OA as construction progressed systematically through the leap-frog structure.

9.2 OPERATIONAL AMPLIFIER CHARACTERISATION TESTS

9.2.1 OPERATIONAL AMPLIFIER NOISE MODEL

Models used to represent and measure the noise generated within an OA take on a number of forms in the literature. Most authors give circuits of varying complexity similar to that shown in Fig. 9.1.

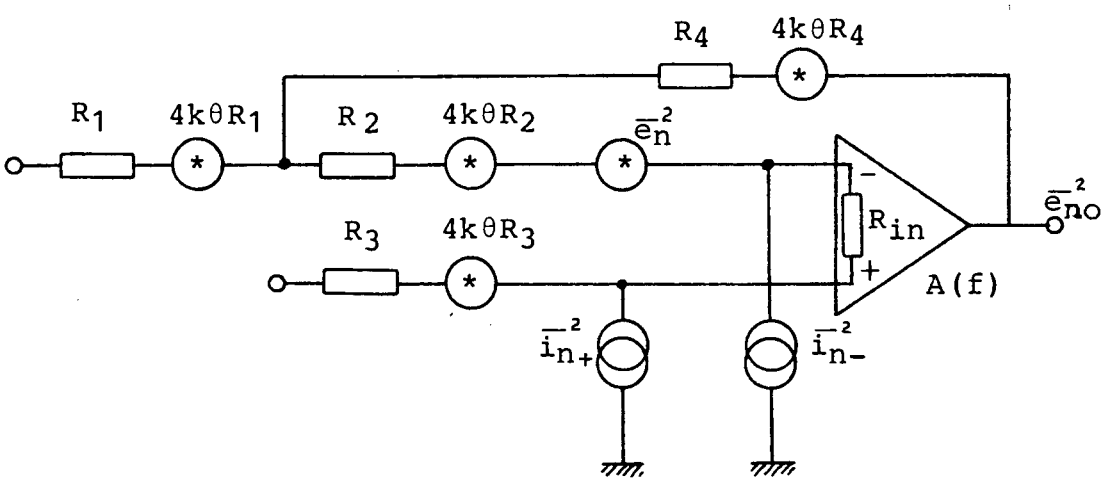

Fig. 9.1 Operational Amplifier noise model including associated resistances and thermal noise sources.

The contribution of each source to the total output noise is dependent on the associated circuitry and an appropriate OA model. Hence, resistances R_1, R_2, R_3 and R_4 are included with their thermal noise contributions, $4k\theta R$, represented by a noise voltage source in series with each.

Calculation of the total output noise first requires analysis of the above circuit. Comparing a number of publications [109,110, 111,112,113,114,115], it became apparent that the transfer expressions of the various sources are characterized in a multitude of ways. Three references [111,112,113], where full noise models are given together with measurement procedures, also lack consistency of the circuit nodal analysis. This was confirmed when attempts were made to evaluate equivalent input noise current using the methods and expressions of these authors.

Assuming all sources uncorrelated, analysis of the circuit in Fig. 9.1 gives the total output noise $\overline{e_{no}}^2$ as shown in equation (9.1).

$$\overline{e_{no}}^2 = \left[\overline{e_n}^2 + \overline{i_{n-}}^2(R_2+R_1//R_4)^2 + \overline{i_{n+}}^2R_3^2 + 4k\theta(R_2+R_3)\right] A_{CL+}^2 + 4k\theta R_1 A_{CL-}^2 + 4k\theta R_4 \qquad ...(9.1)$$

where $R_1//R_4 = R_1R_4/(R_1 + R_4)$. A_{CL+} and A_{CL-} are the closed loop non-inverting and inverting gains respectively as given in equations (9.2) and (9.3).

$$A_{CL+}(f) = \frac{1/\beta}{1 + \frac{1/\beta}{A(f)}\left[1 + \frac{R_2 + R_3}{R_{in}}\right] + \frac{R_4/R_{in}}{A(f)}} \qquad ...(9.2)$$

$$A_{CL-}(f) = \frac{-R_4/R_1}{1 + \frac{1/\beta}{A(f)}\left[1 + \frac{R_2 + R_3}{R_{in}}\right] + \frac{R_4/R_{in}}{A(f)}} \qquad ...(9.3)$$

$(1/\beta) = (R_1 + R_4)/R_1$ is the feedback attenuation. The OA is assumed to have finite input resistance R_{in} with an open loop gain charactertistic described by the single pole model

$$A(f) = \frac{A_0}{\left[1 + \frac{A_0 f}{f_{GB}}\right]} \qquad \ldots(9.4)$$

where A_0 is the open loop gain at dc.

f_{GB} is the unity gain frequency.

The GE OA employs a FET at the input which makes R_{in} of the order $10^{10}\,\Omega$. The input resistance of the Harris HA-4605 OA according to the data sheet is 500 kΩ .

For comparison with equation (9.1) the expressions of Whitehead [111], Bernardi [112] and Ryan & Scranton [113] are given in (9.5), (9.6) and (9.7) respectively. In all three cases $R_2 = 0$.

$$\overline{e_{no}}^2 = \left[\overline{e_n}^2 + \overline{i_{n-}}^2 (R_3 + R_1 // R_4)^2 + 4k\theta(R_3 + R_1 // R_4)\right] A_{CL+}^2 \qquad \ldots(9.5)$$

$$\overline{e_{no}}^2 = \left[\overline{e_n}^2 + \overline{i_{n-}}^2 (R_1 // R_4)^2 + \overline{i_{n+}}^2 R_3^2 + 4k\theta(R_1 + R_3)\right] A_{CL-}^2 \qquad \ldots(9.6)$$

$$\overline{e_{no}}^2 = \left[\overline{e_n}^2 + \overline{i_{n+}}^2 R_3^2 + 4k\theta R_3\right] A_{CL+}^2 + 4k\theta R_1 A_{CL-}^2 + \overline{i_{n-}}^2 R_4^2 + 4k\theta R_4 \qquad \ldots(9.7)$$

9.2.2 GAIN-BANDWIDTH PRODUCT

Three methods for obtaining the GB product (unity gain frequency) were used. The first two utilized the circuit of Fig. 9.2 while the third used that of Fig. 9.3.

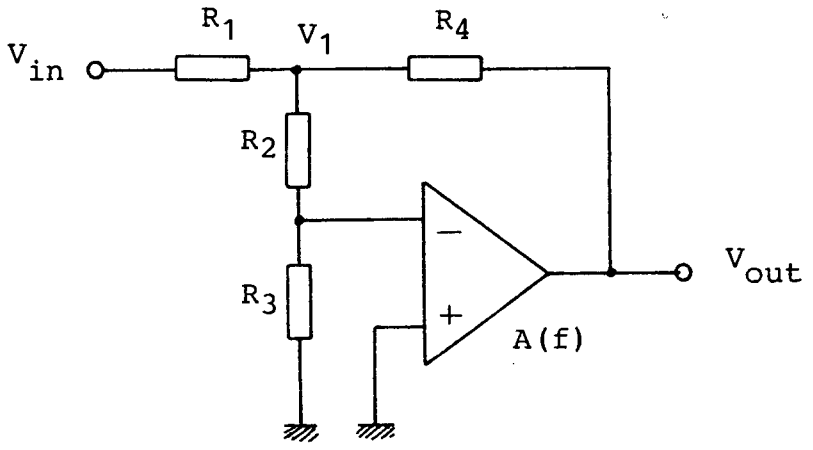

Fig. 9.2 Gain-bandwidth product test circuit No. 1
$R_1 = R_2 = R_4 = 47\ k\Omega$, $R_3 = 47\Omega$

Method 1 : The open loop gain A(f) of the OA in the circuit of Fig. 9.2 can be derived as

$$A(f) = -\left[1 + \frac{R_2}{R_3}\right] \frac{V_{out}}{V_1}(f) \qquad \ldots(9.8)$$

Assuming the single pole model for the OA, the unity gain frequency is given by $f_{GB} = (A_0 \times f_{3dB})$. f_{3dB} is the frequency at which A(f) falls to 3dB below the dc gain A_0. V_{in} was driven by a sinusoidal signal to obtain values for A_0 and f_{3dB} from which f_{GB} is calculated.

Method 2 : Again assuming the single pole model it suffices to obtain co-ordinates of one point in the linear roll-off region of the OA open loop gain characteristic A(f). The unity gain point can then be extrapolated along a line of -20 dB/decade such that

$$f_{GB} = f \times A(f) \qquad \ldots(9.9)$$

In practise this was found to be valid and consistent for the region 100 Hz < f < 60 kHz. V_{in} was driven by a sinusoidal signal to obtain values for A(f) within this range using equation (9.8). (9.9) can then be used to calculate f_{GB} .

Method 3 : Referring to the circuit of Fig. 9.3 , $V_{out} = -v^-$ at the unity gain frequency. Using high impedance FET input probes this point was observed on an oscilliscope. By driving V_{in} with a sinusoidal signal the frequency at which $V_{out} = -v^-$ could be determined.

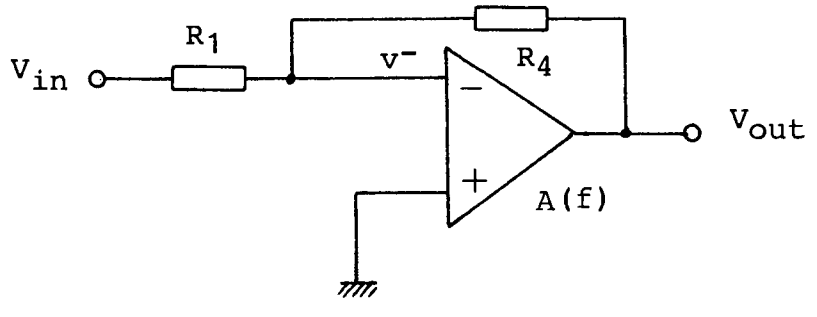

Fig. 9.3 Gain-bandwidth product test circuit No. 2
$R_1 = R_4 = 10\ k\Omega$

9.2.3 EQUIVALENT INPUT NOISE VOLTAGE TEST

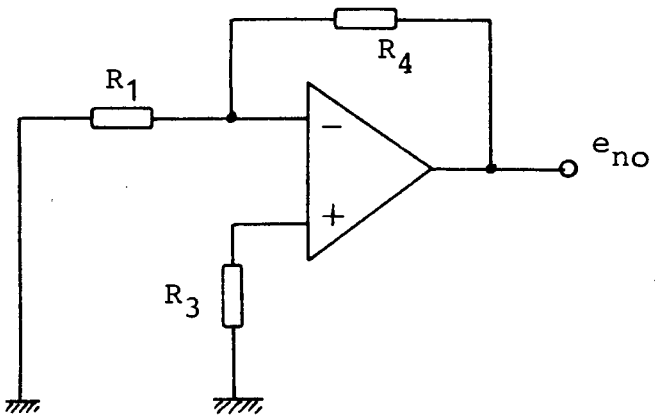

Fig. 9.4 Equivalent input noise voltage test circuit.
$R_1 = R_3 = 10\Omega$, $R_4 = 10\ k\Omega$

In the circuit of Fig. 9.4 the contribution of current noise to the total output noise can be neglected due to the low value of resistors R_1 and R_3 . Equation (9.1) therefore yields

$$\overline{e}_n^2 = \frac{\overline{e}_{no}^2 R_4^2}{A_{CL-}^2(f)\left[R_1+R_4\right]^2} - 4k\theta(R_3+R_1//R_4) \qquad ...(9.10)$$

$\overline{e}_{no}^2$ and $A_{CL-}(f)$ were measured using a spectrum analyser for frequencies 20 Hz to 5 MHz. The system noise was sufficiently low compared with $\overline{e}_{no}^2$ to be neglected. Values of $\overline{e}_n^2$ were obtained using (9.10) for the Harris 4605 and GE chip OAs.

9.2.4 EQUIVALENT INPUT NOISE CURRENT TEST

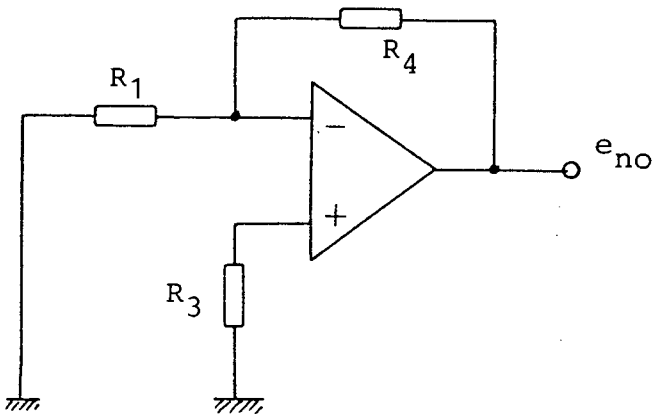

Fig. 9.5 Equivalent input noise current test circuit.
$R_1 = R_3 = 480\ k\Omega$, $R_4 = 4.7\ M\Omega$

If the input resistances R_1 and R_3 in the circuit of Fig. 9.5 are set very large (500 kΩ) the contribution of the current and thermal noise dominates the output noise spectrum. Assuming $\overline{i}_{n+}^2 = \overline{i}_{n-}^2 = \overline{i}_n^2$, equation (9.1) becomes

$$\overline{i}_n^2 = \frac{\left[\dfrac{\overline{e}_{no}^2 R_4^2}{A_{CL-}^2(f)\left[R_1+R_4\right]^2} - 4k\theta\left[R_3+R_1//R_4\right]\right]}{R_3^2 + \left[R_1//R_4\right]^2} \qquad \ldots(9.11)$$

Again $\overline{e}_{no}^2$ and $A_{CL-}(f)$ were measured for frequencies from 20 Hz to 5 MHz. Using (9.11) values of $\overline{i}_n^2$ were obtained for the Harris 4605 and GE chip OAs.

9.2.5 RESULTS

The graphs depicted in Figs. 9.6 and 9.7 show the equivalent input noise voltage and noise current for the Harris 4605 and GE chip OAs as measured in the above tests. Using the results obtained, the OAs may be characterised according to Table 9.1 .

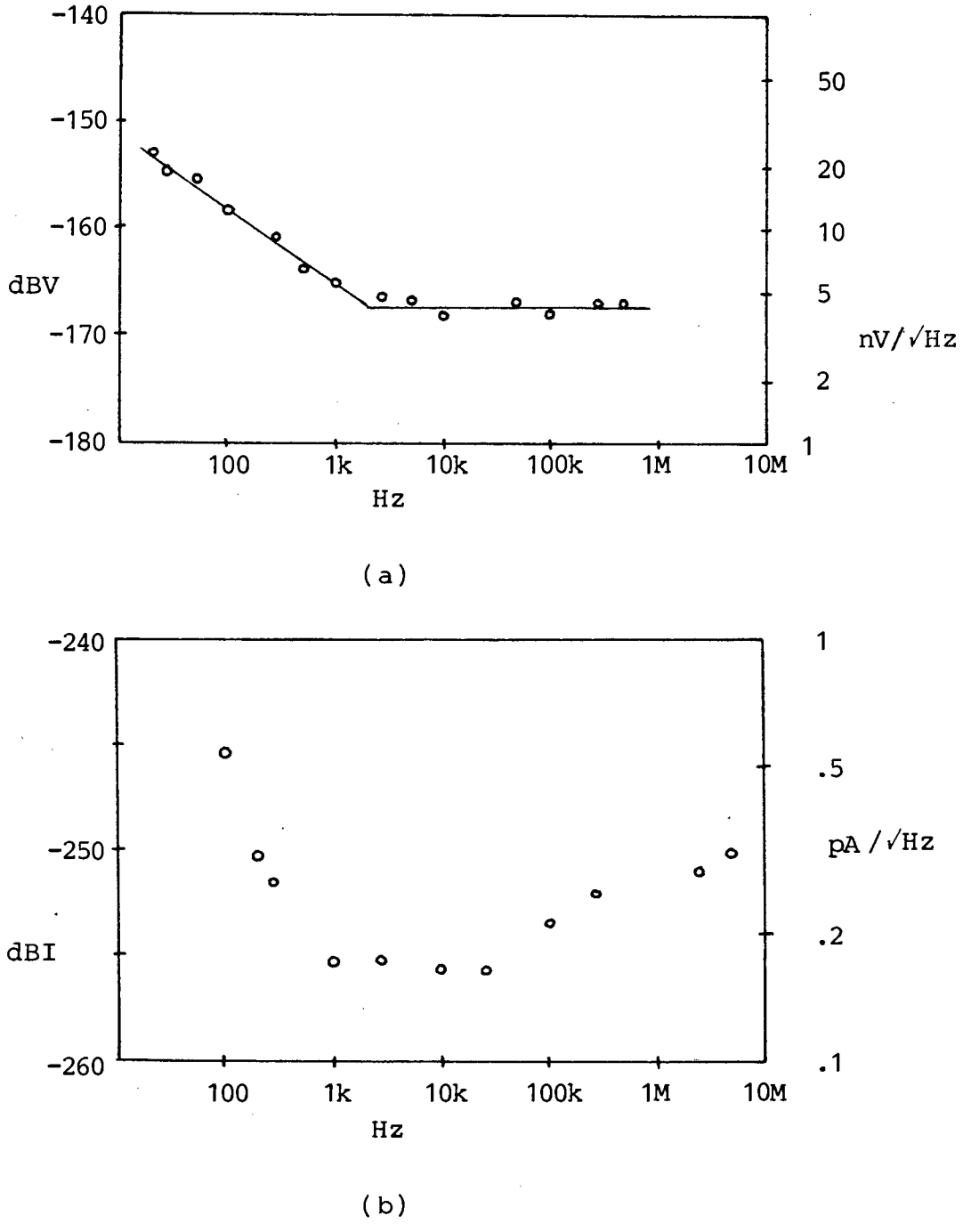

Fig. 9.6 Equivalent input noise voltage (a) and noise current (b) for the Harris 4605 OA.

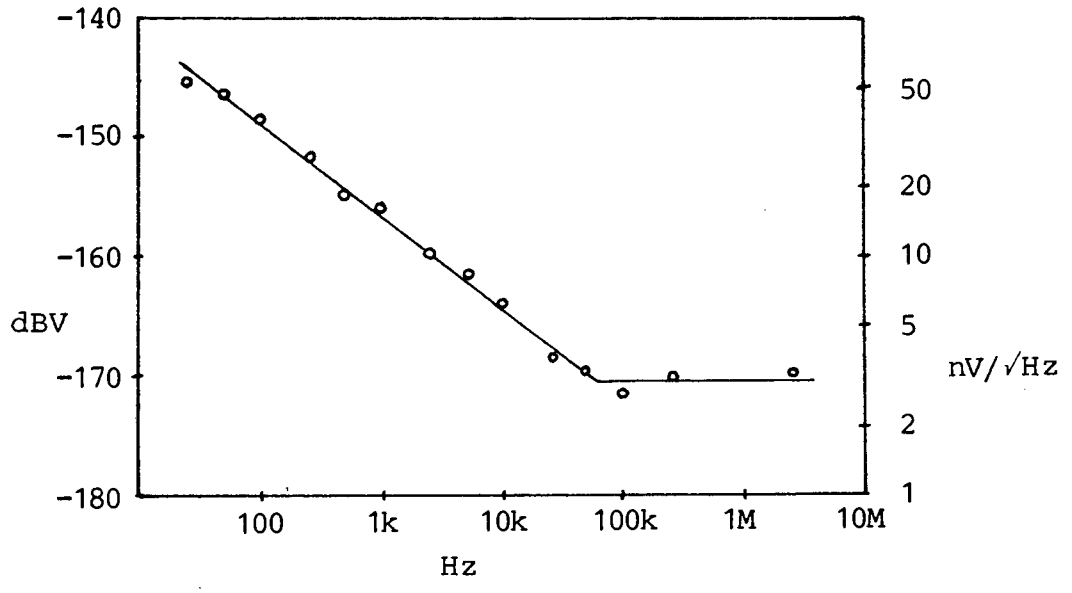

(a)

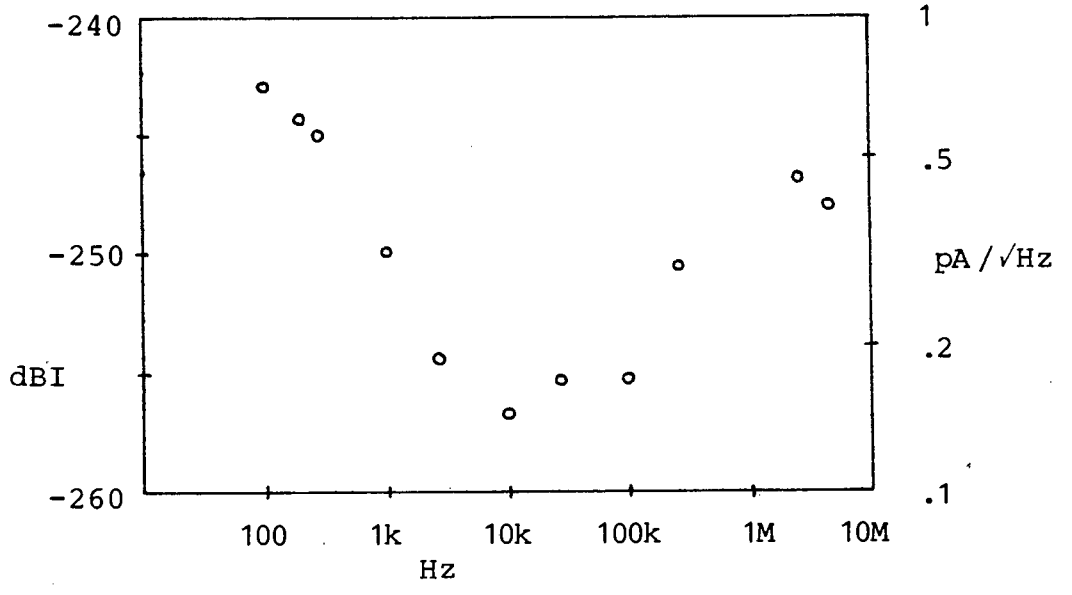

(b)

Fig. 9.7 Equivalent input noise voltage (a) and noise current (b) for the GE chip OA.

Table 9.1 Operational Amplifier Characteristics Summary

	Harris 4605	GE chip
Open loop gain A_0	$3x10^5$	$1.26x10^3$
Unity-gain frequency f_{GB}	9.2 MHz	8.55 MHz
Noise bandwidth BW_n	9.2 MHz	8.55 MHz
Input resistance R_{in}	500 kΩ	10^{10} Ω
Equiv. input white noise voltage	4.47 nV/$\sqrt{Hz}$	3.16 nV/$\sqrt{Hz}$
1/f noise voltage corner freq.	2 kHz	80 kHz
Equiv. input white noise current	0.18 pA/$\sqrt{Hz}$	0.14 pA/$\sqrt{Hz}$
1/f noise current corner freq.	700 Hz	2 kHz

9.3 FILTER VERIFICATION TESTS

9.3.1 BIQUADRATIC FILTER

Fig. 9.8 shows the schematic diagram for the Biquad filter with capacitor values as given in Table 9.2 . The centre frequency is at 1 kHz with a clock frequency of 50 kHz . Switch resistance R_{on} was 5.8 kΩ and 100 Ω respectively for the chip and discrete component versions. The measured noise level was found to be identical for both outputs V_1 and V_2 . Spectrum analyser traces of the output noise measured at V_1 are given in Figs. 9.9 and 9.10.

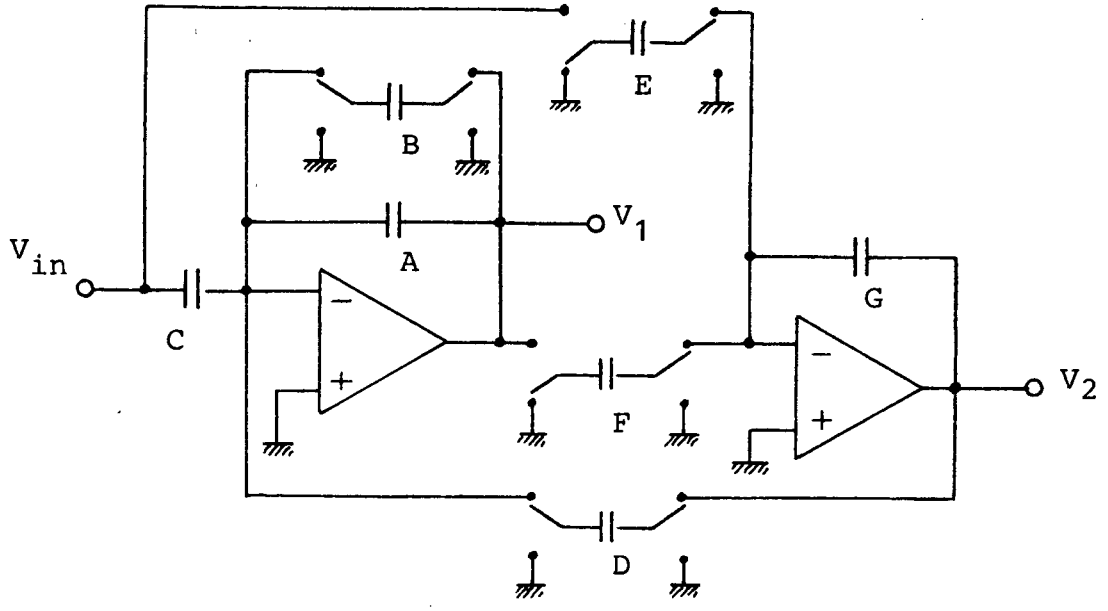

Fig. 9.8 Biquad SC Filter Schematic

Table 9.2 Capacitor values in pF for the Biquad Filters.

Capacitor	GE chip	Scaled discrete component version (measured to 0.5%)
A	49.5	9900
B	1.0	200
C	50.25	10050
D	6.25	1250
E	6.25	1250
F	6.25	1250
G	49.5	9900

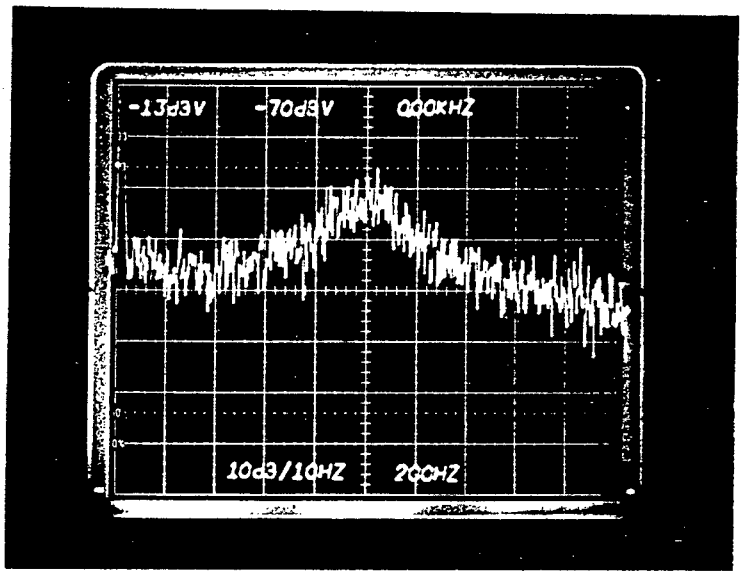

Fig. 9.9 Output Noise Spectrum of the GE chip Biquad filter.

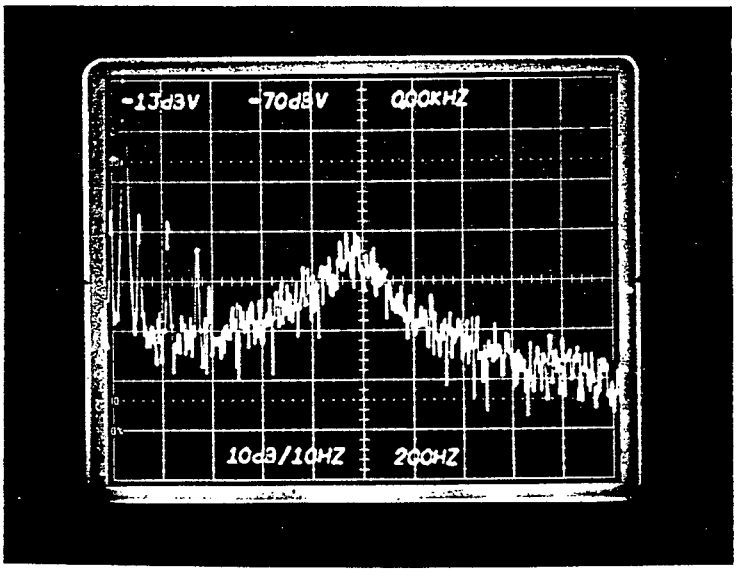

Fig. 9.10 Output noise spectrum of the discrete component Biquad filter.

The shape of the output noise spectrum shows good agreement with the simulated results. Table 9.3 compares the level of the noise peak at 1 kHz for the two simulation methods and the laboratory tests.

Table 9.3 Biquad peak output noise level at 1 kHz
Relative contributions of OA and Switch noise are shown. Values given in dB($V/\sqrt{Hz}$).

		GE chip	Discrete component version
SPICE Simulation	OA	-128	-121
	Switch	-112	-134
	Total	-112	-121
z-Domain transfer function method	OA	-116	-111
	Switch	-105	-125
	Total	-105	-111
Laboratory tests	Total	-102	-114

9.3.2 7th ORDER ELLIPTIC FILTER

The Reticon 7th order filter chip design characteristics were based on tables by Zverev [93] with $n = 7$, $\rho = 8\%$ and $\theta = 33^{\circ}$. The 3dB bandwidth is denormalized to 1 kHz with a clock frequency of 50 kHz. In Fig. 9.11 the schematic diagram is shown. Capacitor values are shown in Table 9.4 while in Figs. 9.12 and 9.13 the spectrum analyser traces of output noise for the chip and discrete component filters are presented.

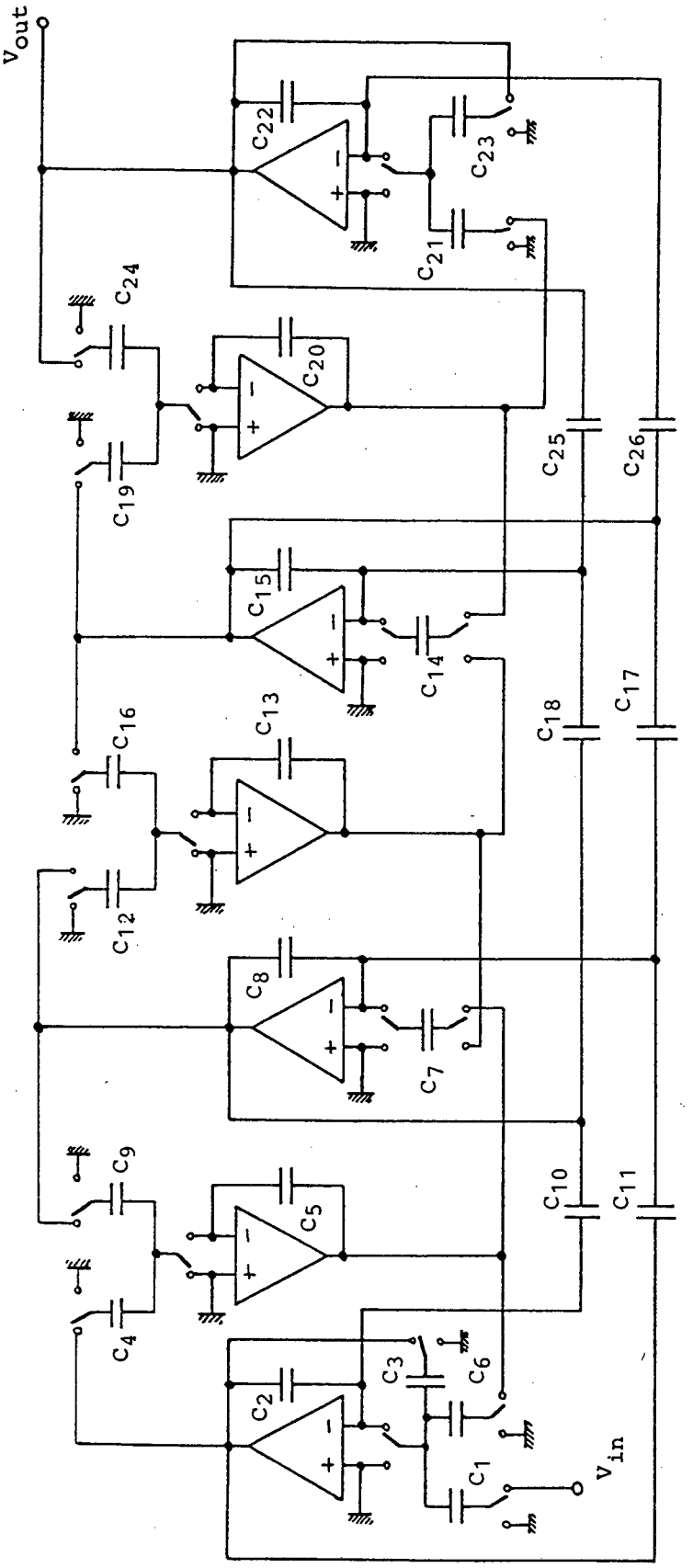

Fig. 9.11 7th Order Elliptic SC Filter Schematic

Table 9.4 Capacitor values for the 7th order filters

Capacitor	Design values	Chip values	Scaled discrete component version (measured to 0.6%)
C1	1.414Co	3.50	525
C2	8.183Co	20.25	3038
C3,C4	Co	2.48	371.3
C5	11.933Co	29.54	4431
C6,C7	Co	2.48	371.3
C8	16.779Co	41.53	6230
C9	Co	2.48	371.3
C10,C11	0.404Co	1.00	150
C12	Co	2.48	371.3
C13	11.669Co	28.88	4333
C14	Co	2.48	371.3
C15	17.153Co	42.46	6369
C16	Co	2.48	371.3
C17,C18	1.832Co	4.53	680.2
C19	Co	2.48	371.3
C20	10.650Co	26.36	3954
C21	1.414Co	3.50	525
C22	8.285Co	20.51	3076
C23	Co	2.48	371.3
C24	0.707Co	1.75	262.5
C25	0.967Co	2.39	359
C26	1.934Co	4.79	718.1

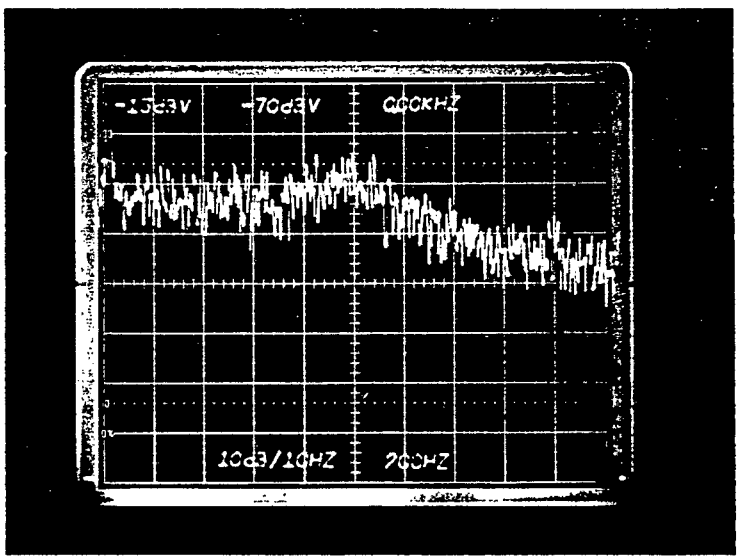

Fig. 9.12 Output Noise Spectrum of the Reticon Chip 7th order elliptic filter.

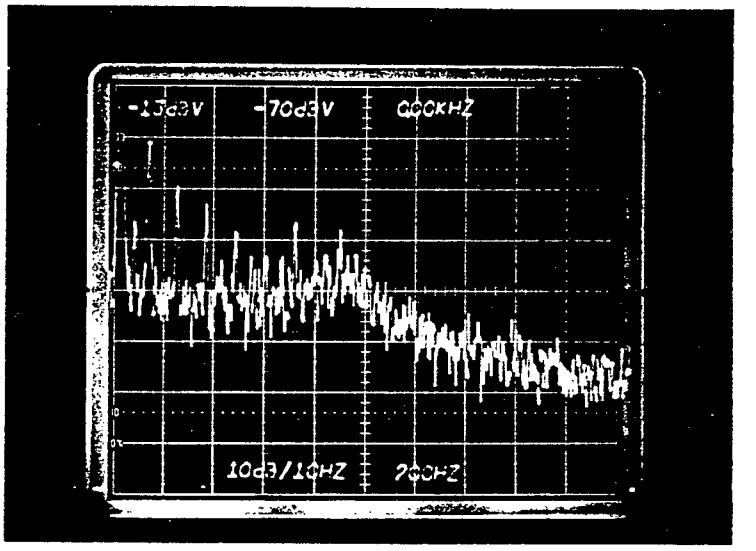

Fig. 9.13 Output noise spectrum of the discrete component 7th order filter.

The shape of the output noise spectrum shows good agreement with the simulated results. Table 9.5 compares the level of the noise peak at 1 kHz for the two simulation methods and the laboratory tests.

Table 9.5 7th order filter peak output noise level at 1 kHz. Relative contributions of OA and Switch noise are shown. Values given in dB(V/$\sqrt{Hz}$).

		Reticon chip	Discrete component version
SPICE Simulation	OA	-110	-125
	Switch	-110	-138
	Total	-103	-125
z-Domain transfer function method	OA	-101	-119
	Switch	-101	-129
	Total	-98	-119
Laboratory tests	Total	-99	-118

9.4 SUMMARY FOR CHAPTERS 8 AND 9

Three methods have been used successfully to predict the noise behaviour of SC circuits - a time domain approach using TCAPS, SPICE modelling and z-domain analysis. The time domain approach accurately predicted the noise generated in an integrator. However, application to higher order filters requires care with the spectral estimation algorithms used, and further investigation is necessary before this approach can be used with confidence. The validity of the SPICE modelling and z-domain analysis was confirmed by comparing the results with experimental tests performed on two filters, each realized in fabricated and discrete component form.

The effect of capacitor size on the switch noise became very evident when comparing the two structures. The small size of the capacitors in the fabricated structures greatly increased the noise contribution of the switches. This is seen in Tables 9.3 and 9.4 where OA noise dominates in the discrete component structures while switch noise dominates in the fabricated structures.

The increase in switch noise is slightly offset by a simultaneous increase in OA noise. The explanation for this is found in the OA 1/f noise contribution. For the discrete component structures it is submerged beneath the undersampled broadband noise while, in the fabricated structures, the 1/f noise corner frequency was seen to be larger than the sampling frequency, thus causing undersampling of this noise. This effect is more evident in the 7th order filter, where the difference in capacitor size between the two versions is smaller than with the Biquad filter. The relative contributions of OA and switch noise in the fabricated 7th order filter are therefore similar.

For the analysis and simulation of noise within the SC filters, it was necessary to obtain characteristics for the OAs. Existing methods for the calculation of the equivalent input voltage and current noise of an OA were found to lack consistency. A new model was therefore developed for this purpose and tests conducted on the OAs confirmed its validity. Measurements of the equivalent input noise current above 100 kHz were found to be unpredictable. This was, however, assumed to be as a result of parasitic effects in the testing arrangement. Accordingly, this region was ignored when characterizing the equivalent input current noise of the OAs.

Chapter 10

INTERPOLATION AND DECIMATION IN SC FILTERS

10.1 NEED FOR INTERPOLATION/DECIMATION

The frequency spectrum of a sampled signal consists of the original base-band positive and negative frequency spectrum repeated at integer multiples of the sampling frequency F_S , as shown in Fig. 10.1. If the original signal contains unwanted frequency components above the Nyquist limit $F_S/2$, these may be folded into the base-band region upon sampling. This "aliasing" is usually prevented by incorporating an anti-aliasing filter (AAF) at the input prior to sampling.

If a low-pass SC filter characteristic is assumed and aliasing allowed in the stop-band region ($f_p < f < F_S/2$), then the required response of the AAF is as shown in Fig. 10.2. As f_p approaches $F_S/2$, this response becomes comparable to that of the SC filter. In order to relax the AAF requirement in such cases, a higher sampling frequency may be chosen as shown in Fig. 10.3. There are, however, disadvantages to using high sampling frequencies, as listed in the chapter on noise. Briefly, these include:

- large capacitor ratios resulting in: poorer accuracy, larger chip area and increased sensitivity to parasitics.
- the need for high speed OAs and switches.

One solution to these problems is to change the sampling frequency where necessary. In this way the AAF requirements may be eased by high frequency sampling at the input stage ("oversampling" [116])

while the rest of the filter is made to operate at a lower frequency. Lowering the sampling frequency within an SC filter is termed Decimation, whereas increasing this frequency is referred to as Interpolation.

Interpolation and decimation may be effectively employed in SC filters. The advantages (small capacitor spread and simple hardware) of a low sampling frequency to pole frequency ratio can thus be gained in filters containing widely spaced pole frequencies. This is achieved by regulating the sampling to pole frequency ratio within each stage of the filter. For example, decimation is used in the circuit of Fleischer & Laker et. al. [117], to give a four to one improvement in the capacitor ratios of the high pass sections. The AAF requirement at the same time is relaxed in this circuit by the use of oversampling.

The techniques of interpolation and decimation are well established [118,119,120]. In addition to the use of interpolation and decimation within SC filters, programmable sampling rate conversion circuits may be realized, using SC structures.

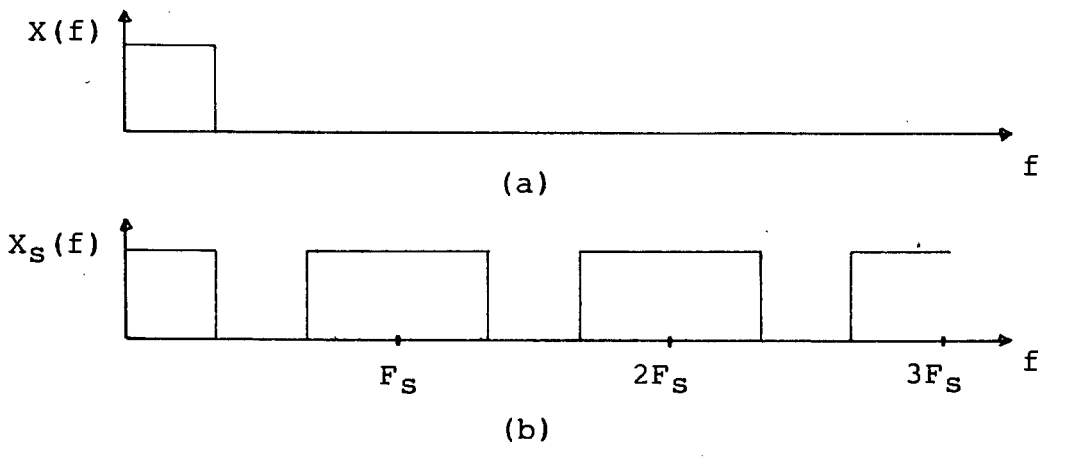

Fig. 10.1 Frequency spectrum of a continuous signal before (a) and after (b) sampling.

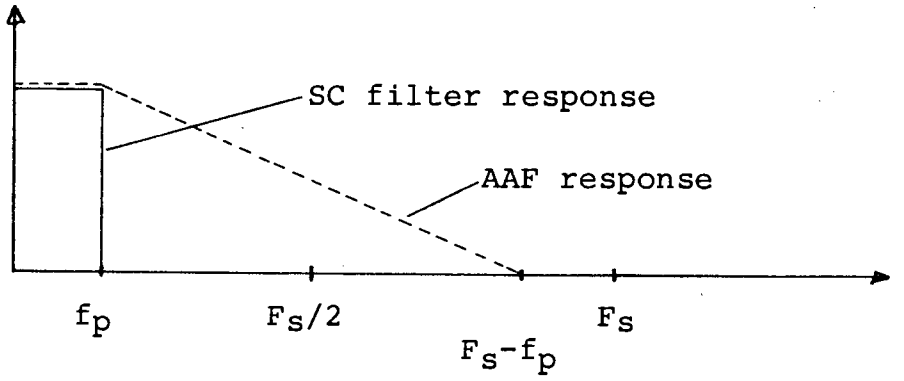

Fig. 10.2 Anti-aliasing filter requirement for a low-pass SC filter.

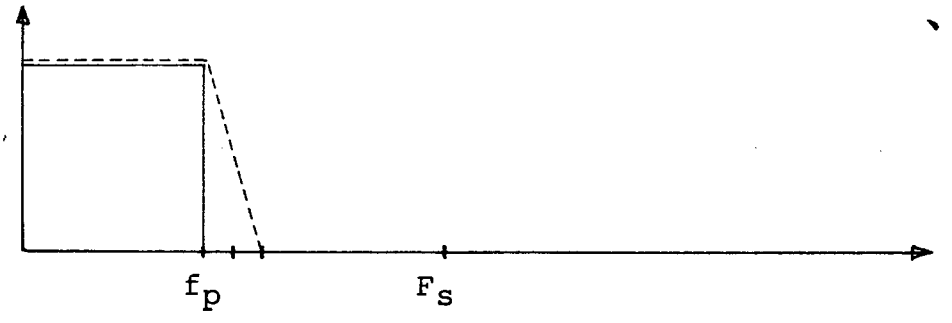

(a)

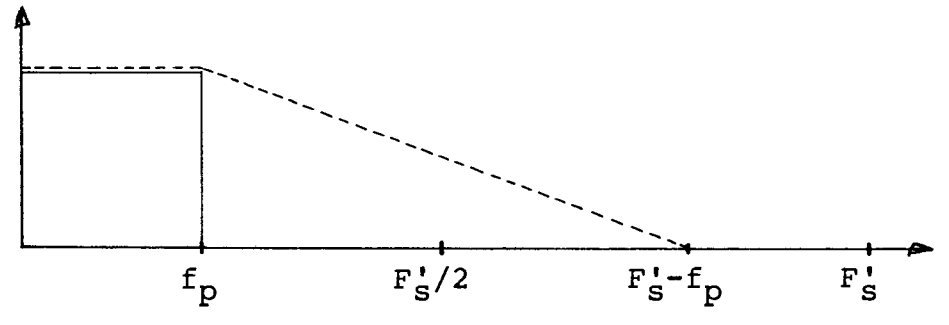

(b)

Fig. 10.3 Relaxing the AAF requirement of a low-pass SC filter by increased sampling frequency.

10.2 INTERPOLATION

10.2.1 TIME DOMAIN REPRESENTATION OF LINEAR INTERPOLATION

Consider the sampled and held signal $x_n = x(nT')$ $(n=0,\pm L,\pm 2L,\ldots)$. Its linear interpolation is given by $y_n = y(nT')$ $(n=0, \pm 1, \pm 2,\ldots)$ as shown in Fig. 10.4 where

$$y_n - y_{n-1} = \frac{x_n - x_{n-L}}{L} \qquad \ldots(10.1)$$

L is the interpolation ratio, with the new sampling period

$$T' = T/L \qquad \ldots(10.2)$$

Inherent in the operation is a constant delay of $(L-1)T'$ as seen in the diagram.

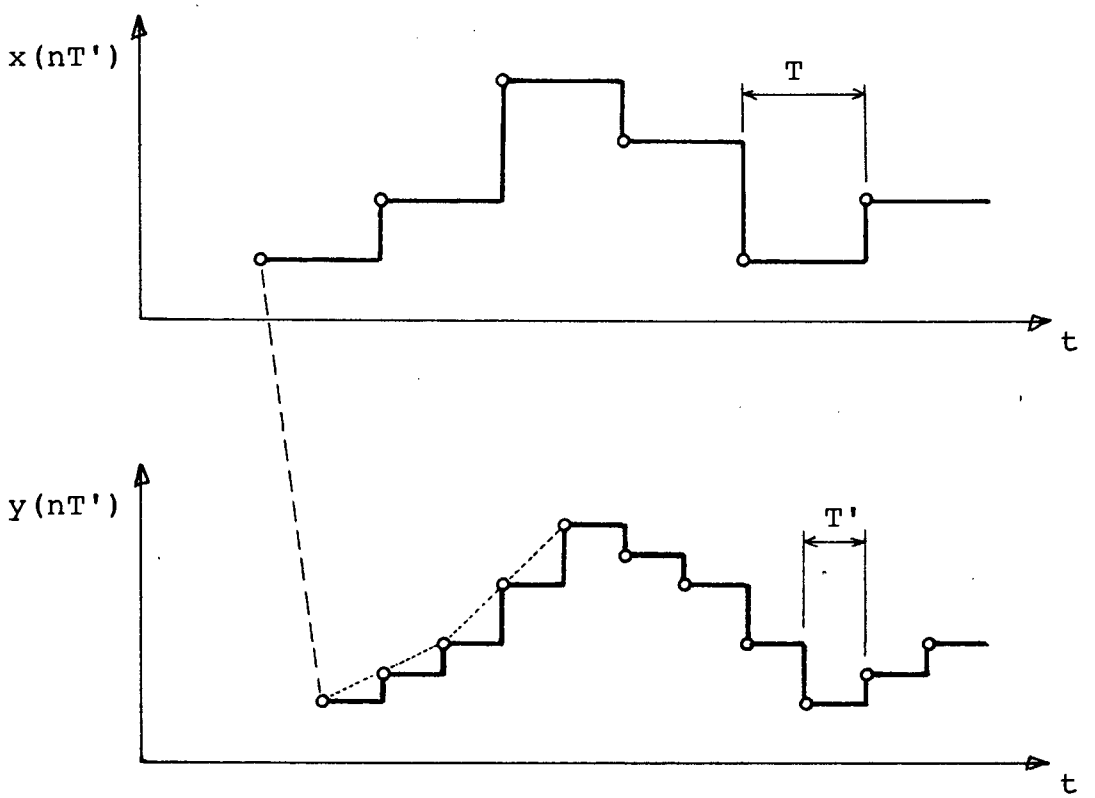

Fig. 10.4 Sampled and held signal x(nT') and its linear interpolation y(nT'), with L=2.

Taking the z-Transform of equation (10.1) and letting $z = e^{j\omega T'}$ yields

$$H(z) = \frac{Y(z)}{X(z)} = \frac{1}{L}\,\frac{(1 - z^{-L})}{(1 - z^{-1})} \qquad \ldots(10.3)$$

$$\left|H(e^{j\omega T'})\right| = \frac{1}{L}\left|\frac{\sin(\frac{\omega T' L}{2})}{\sin(\frac{\omega T'}{2})}\right| \qquad \ldots(10.4)$$

For the more general case of x_n sampled but not held one obtains

$$\left|H(e^{j\omega T'})\right| = \frac{1}{L}\left|\frac{\sin(\frac{\omega T' L}{2})}{\sin(\frac{\omega T'}{2})}\right|^2 \qquad \ldots(10.5)$$

Linear interpolation can be easily implemented in SC form as demonstrated by Gregorian & Nicholson [121] and Ghaderi, Temes & Law [122], where Fig. 10.5 is an example from this reference. The circuit is ideally suited for use as a general purpose interpolator. The circuit topology and type of the clocking scheme is simple and remains the same for all values of L. For $C_1 = C_3$ and $C_2 = C_4$ the maximum capacitor spread is L.

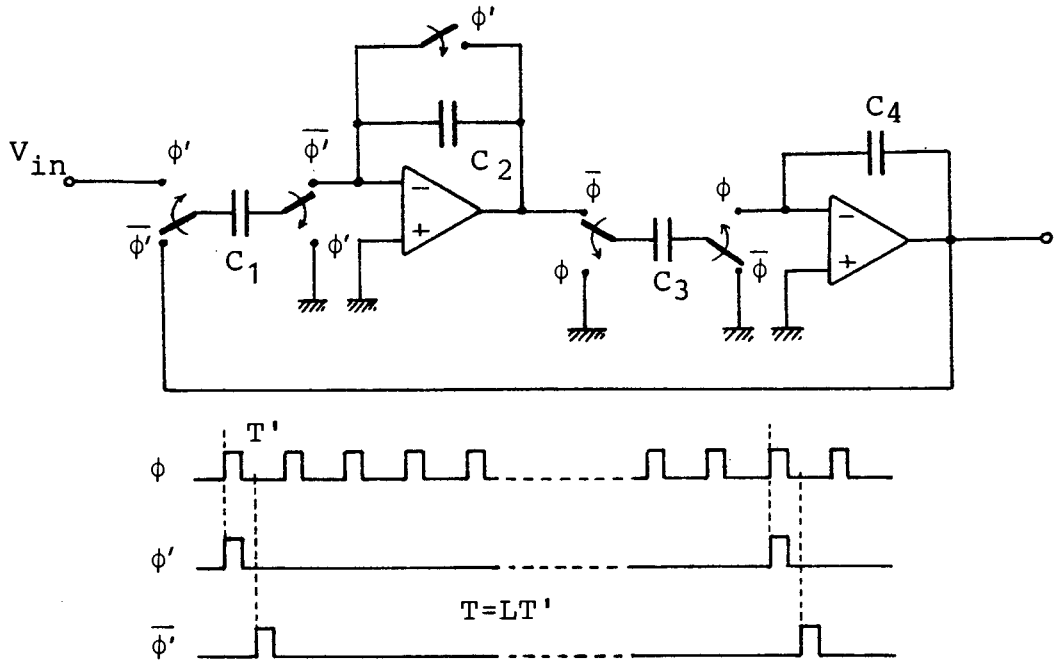

Fig. 10.5 Switched Capacitor interpolator of Ghaderi, Temes & Law [122], $C_2 C_4 = L(C_1 C_3)$.

10.2.2 INTERPOLATION IN THE FREQUENCY DOMAIN

Knowledge about the effect interpolation has on the frequency spectrum of a sampled signal can be directly applied when designing interpolation filters. Schafer & Rabiner [118] have shown that interpolation by a factor L implies:

(i) the creation of (L-1) zero-valued sample points between each of the original samples, and

(ii) the ideal low-pass filtering of this new signal with suitable pass-band gain.

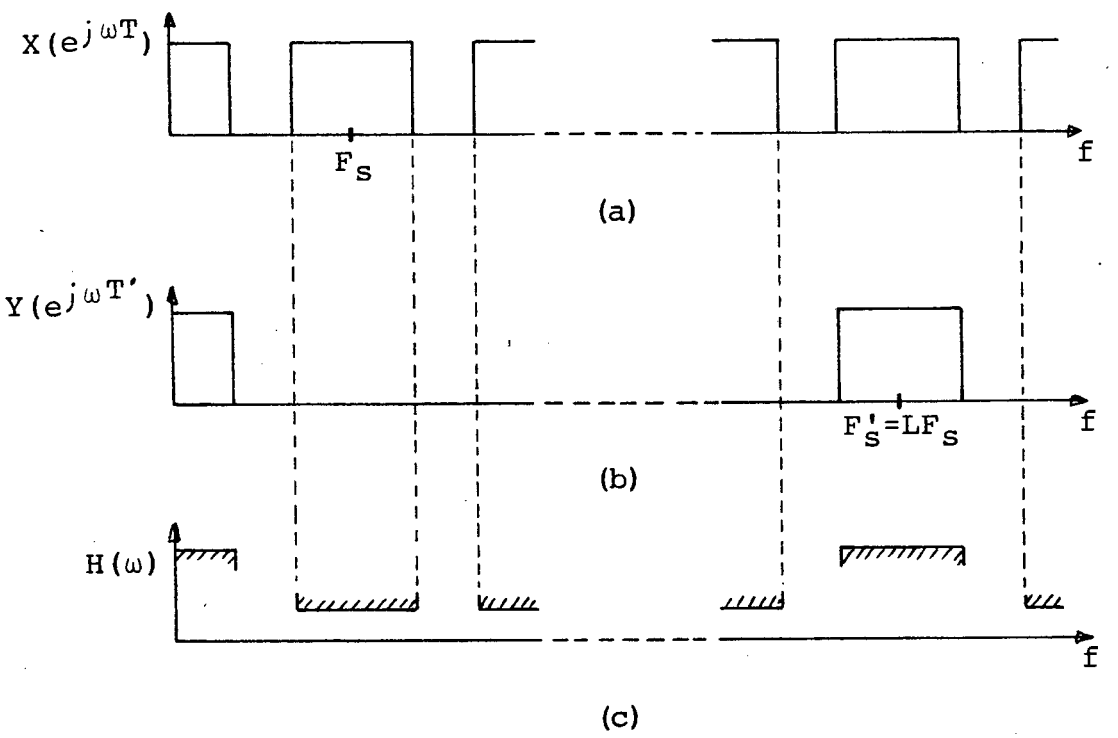

Fig. 10.6 Frequency spectrum of a sampled signal before (a) and after (b) ideal interpolation by factor L. (c) Multi-stop-band filter requirement.

In this filter design it must be ensured that all base-band spectrum replicas lying between the base-band and interpolated sampling frequency are removed while leaving the base-band signal spectrum intact as shown in Figs. 10.6(a) and 10.6(b). For a band-limited signal, the extended stop-band of the low-pass filter can be replaced by a multiple stop-band characteristic [118]. This eases the filter requirement as shown in Fig. 10.6(c).

For linear interpolation the spectral function was seen to be

$$|H(e^{j\omega T'})|^2 = \frac{1}{L^2}\left|\frac{\sin(\frac{\omega T'L}{2})}{\sin(\frac{\omega T'}{2})}\right|^4 \qquad ...(10.6)$$

Unfortunately this function does not fulfil the second requirement, namely that of ideal low-pass filtering. As a result, linear interpolation is only accurate for high sampling to signal frequency ratios. For low sampling to signal frequency ratios, the filter must be designed so as to approximate this characteristic more closely.

10.2.3 SIGNAL RECOVERY

In the limiting case, interpolation takes the form of ideal low-pass analog filtering where the interpolation ratio $L = \infty$. High frequency components within a sampled and held signal are suppressed yielding a continuous signal approximation relating to the fundamental frequencies as shown in Fig. 10.7 . Unless the signal is needed in its sampled and held form, SC networks generally would require such a filter at their output. If simple low-order smoothing is not sufficient, greater efficiency and more accurate recovery can be obtained with the use of conversion

filters as described by Fettweis [123]. Khalil & Pandel [124] discuss the design of such conversion filters for use in SC network test set-ups, where minimum distortion and maximum energy transfer is required.

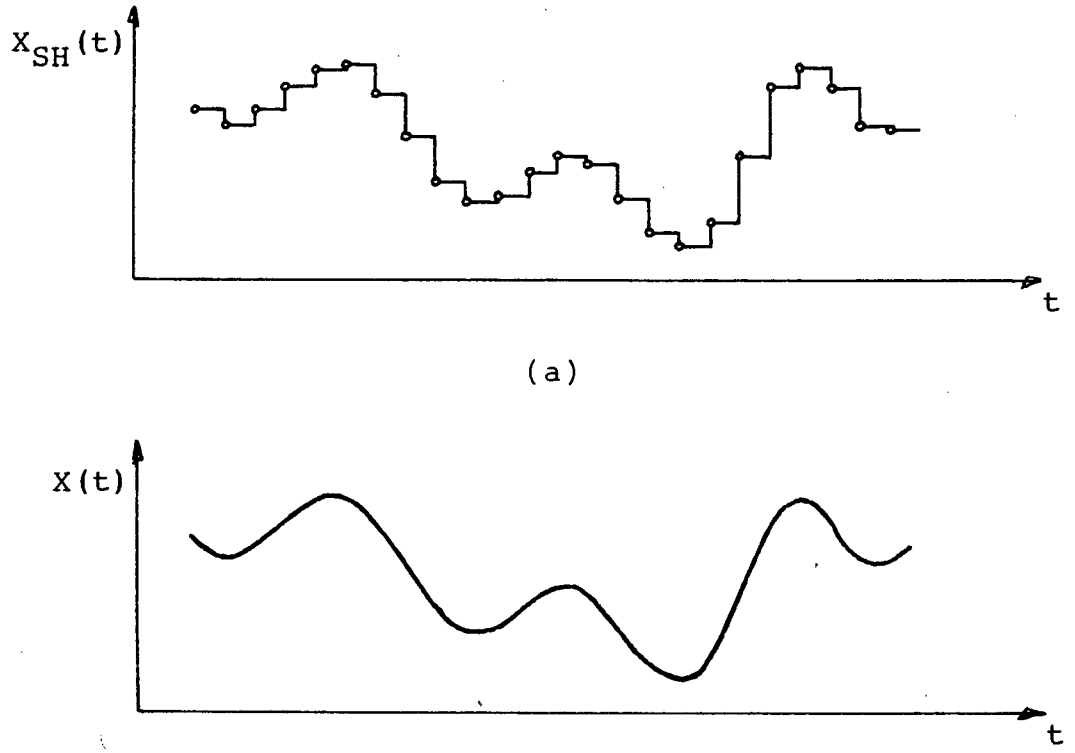

Fig. 10.7 Sampled and held signal before (a) and after (b) low-pass analog filtering.

10.3 DECIMATION

To reduce the sampling frequency by a factor M entails producing one sample for every M samples of the input signal. The usual method employed is to output every Mth sample ("decimation sampling") as depicted in Fig. 10.8 [118,119,125].

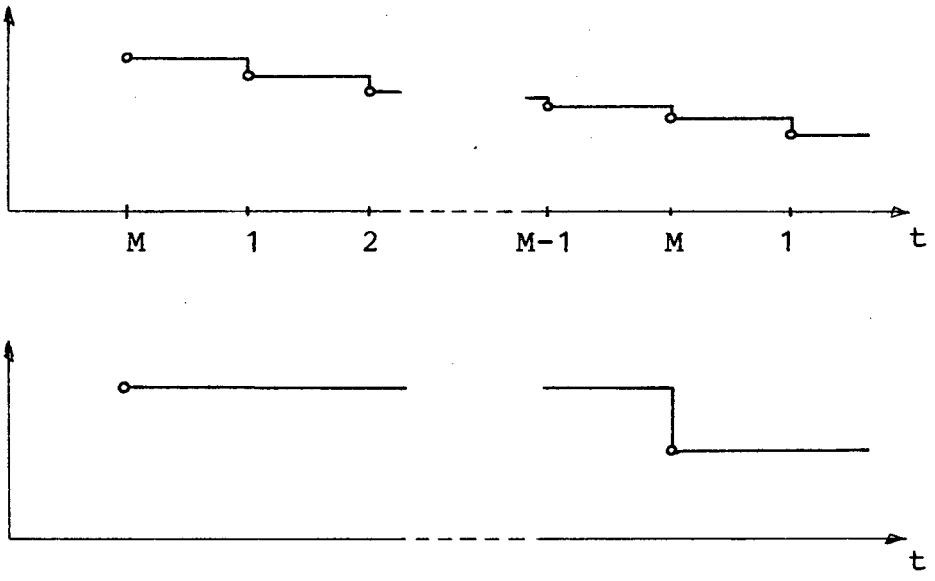

Fig. 10.8 Decimation of a sampled and held signal by M.

In the frequency domain this results in the input spectrum being reproduced around integer multiples of the new sampling frequency as shown in Fig. 10.9 . Band-limiting of the input signal may be necessary in order to prevent aliasing during this process. Generally, therefore, decimation should include a low-pass filter with the ideal characteristic given by equation (10.12). Multiple stop-band type filters may however be used instead of the low-pass type when band-limited signals are concerned. The cosine filtering principles described by Berger & Coutures [126] are an example relating to the aforementioned situation.

$$H(\omega) = \begin{cases} 1 & \omega < \pi F_S/M \\ 0 & \omega > \pi F_S/M \end{cases} \qquad \ldots(10.12)$$

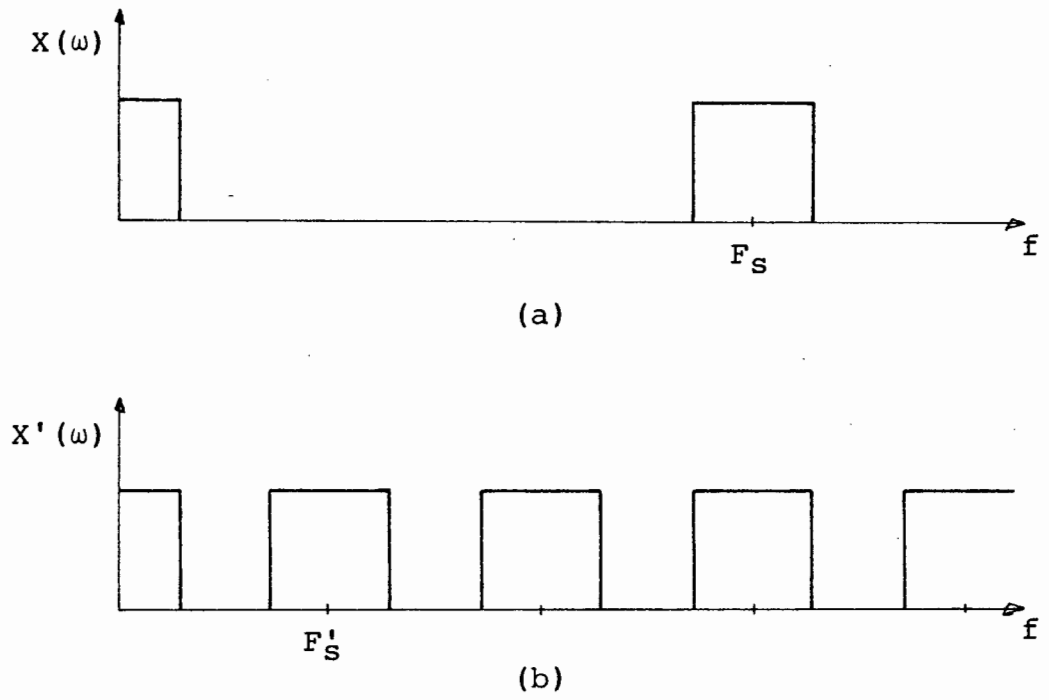

Fig. 10.9 Freqency spectrum of a sampled signal before (a) and after (b) decimation by factor M=3.

This type of filtering may also be achieved as a matter of course by the decimation process used; where, instead of simply preserving every Mth sample, some form of summing and averaging of the input samples is employed. This averaging has a band-limiting effect which depends on the particular method followed. Berger & Coutures [126] and Séquin [127] examine a few of these summing and averaging methods for decimation of signals within CCD filters. Significant improvement in the roll-off characteristic of the decimator is shown by averaging over two cycles. In addition, the stop-band can be extended by weighting each of the original samples. Although this weighting is possible in SC filters, it would require separate input capacitors for each sample as well as a complex clocking scheme. Simple SC averaging decimators are also possible and have been effectively used by von Grünigen et. al. [128], a typical circuit of which is given in Fig. 10.10.

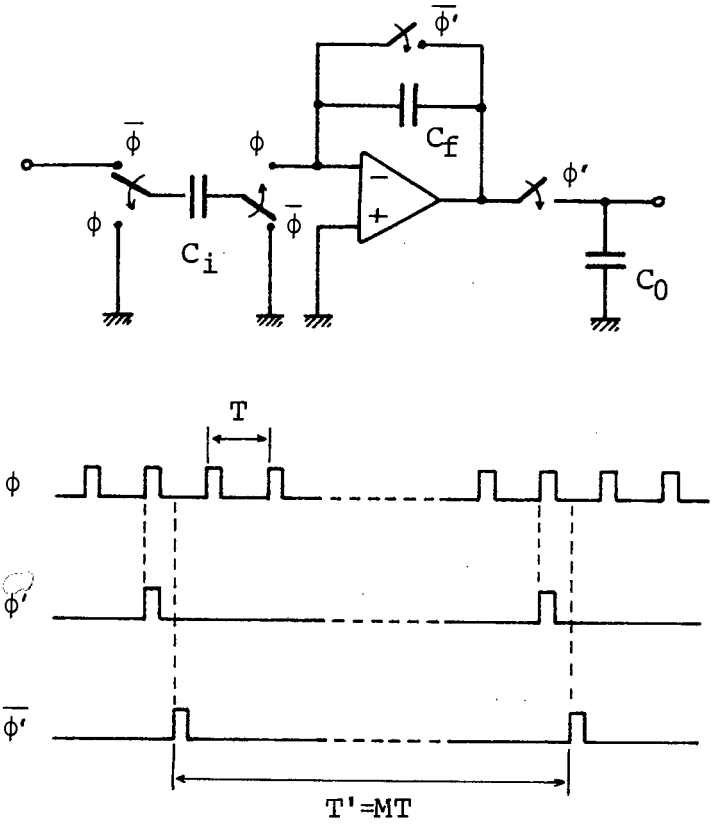

Fig. 10.10 SC averaging decimation filter of von Grünigen et. al. [128]

10.4 INTERPOLATION/DECIMATION BY RATIONAL FACTORS

In Fig. 10.11 interpolation and decimation is summarised showing the filtering function associated with each operation. It has been assumed in the previous sections that the conversion ratios L and M are integers. This is in keeping with classical interpolation and decimation theory where the sampled nature of the processes requires integer conversion [118]. Conversion of the sampling frequency by a rational factor (L/M) is achieved by first interpolating to LF_S followed by decimation to $(LF_S)/M$. Application of decimation as a first step would place severe band-limiting requirements on the signal). The filtering function of each operation may be combined to provide more efficient realisation procedures as \shown in Fig. 10.12.

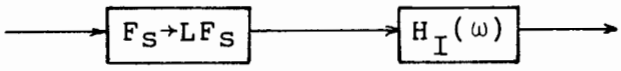

(a)

(b)

Fig. 10.11 Interpolation (a) and decimation (b) by integer factors.

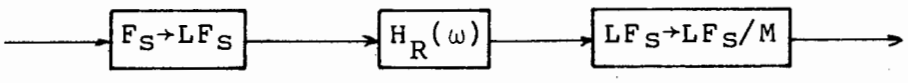

Fig. 10.12 Sampling frequency conversion by a rational factor (L/M).

Paul & Woods [129] have extended the principles of multiple stop-band interpolation and decimation filters to include this combination, known as an "intersection filter". It has stop-bands extending only over the regions required by both the interpolation and decimation operations. A rational factor SC interpolation/ decimation filter could be constructed by cascading the circuits in Figs. 10.5 and 10.10 provided an appropriate clocking scheme is used.

10.6 SUMMARY

The sampling frequency chosen within an SC network influences the design of the network and the hardware to be used. Conversion of this sampling frequency within different sections of a network is therefore an important consideration for optimum design and performance.

A brief summary of the use of interpolation and decimation for sampling frequency conversion has been presented. The advantages of, and need for, this conversion in SC networks are discussed and suitable application examples are included. Because of their sampled-data nature and operation within the charge domain, SC networks lend themselves to interpolation and decimation. Thus, dedicated sampling rate conversion filters can be implemented very efficiently in SC form. Many of the existing design principles for these filters equally apply when SC structures are used.

The question of programmability of SC networks has also been addressed. This can be used to great advantage in applications such as digital modulation conversion circuits.

Chapter 11

CONCLUSION

A general approach, including novel optimization techniques, for the prewarping of arbitrary SC filter response requirements has been presented, allowing effective compensation for the non-linear frequency warping normally associated with these filters.

Previously, classical prewarping has been applied in the case of piecewise-constant-magnitude responses, where the pass-band and stop-band edge frequencies are adjusted so as to provide the necessary compensation. This has enabled the design of SC filters that satisfy these response requirements, with the only restriction on the maximum signal frequency being the Nyquist Limit. However, the non-linearity of the warping becomes especially evident in filters with non-piecewise-constant-magnitude responses, and where the pass-band frequencies are not substantially less than the sampling frequency.

If prewarping is applied in these cases, as has been done for second order SC filters, exact correspondence between the desired and SC filter response can only be assured at the prewarping frequency. Deviation of the SC filter response from the desired response will increase as distance from this frequency increases (provided that, as the frequency approaches dc, the responses will again correspond with each other). Therefore, except in the case of narrow-band filter applications or filters that have a piecewise-constant-magnitude response, the non-linear nature of the warping requires that high sampling to signal frequency ratios be employed (eg. $F_S/f>15$).

11.1 POLE/ZERO PREWARPING

The first method developed, to enable effective compensation for warping of arbitrary filter responses without these restrictions, is that of pole/zero prewarping, where adjustment is applied individually to the poles and zeros of the original response function. In this way the effective location of each pole and zero in the SC filter is made to coincide with its desired location at a frequency within the region where it has most influence on the magnitude response.

The advantage of the pole/zero prewarping procedures developed lies in expressions, derived in conjunction with the prewarping expressions, that conveniently allow prediction of the amount of error each prewarped pole and zero contributes to the magnitude response at all other frequencies.

This enables selective optimization of the amount of prewarping that is applied to each pole and zero during the design procedure. A sixth order elliptic low-pass SC filter, designed to have 0.18 dB ripple in the pass-band, is shown to exhibit a maximum pass-band ripple of 0.2 dB using this optimization technique, while applying the same prewarping approach to each pole and zero shows greater deviation, with the pass-band ripple in this case being 0.39 dB.

Variation in the amount of the prewarping is achieved by way of three distinct approaches ("Center Frequency" (CF), "Selectivity" (S), and "Complex Mapping" (CM) prewarping). These were derived by examining: (i) the pole and zero mappings that occur in a filter upon transformation from the analog to digital domain, and (ii) the effective locations of these poles and zeros in the SC

filter when subject to continuous frequency signals.

One of the problems associated with pole/zero prewarping, where each pole and zero is prewarped by a differing amount, is that the unique relationship between the original locations of the poles and zeros is altered, thus distorting the shape of the original filter magnitude response. This is shown most clearly in filter response functions having special properties associated with the inter-relationships between the pole and zero locations, such as the sixth order elliptic filter example, which exhibits equiripple in the pass-band and stop-band regions.

Expressions for the prediction of the magnitude error contributed by each pole and zero were derived for CF, S and CM prewarping. These are given in the case of simple and complex pair poles for both the LDI and Bil transformations. (It was observed that corresponding expressions for the FD and BD transformations, using CM prewarping, are identical to those of the LDI transformation.)

In order to gain a graphical picture of the effect each prewarping method has on a filter response, the error contribution expressions were poltted showing the dependency of the error on the signal frequency, the pole frequency and the pole selectivity. CM prewarping was seen to exhibit an error characteristic associated with low distortion of the filter magnitude response shape, while those of CF and S prewarping have error characteristics associated with reduced magnitude error in the vicinity of the poles and zeros of the filter response.

Also evident, upon examination of the error plots, is the significantly greater directional variation, and steeper gradients of the error contours, seen in the case of the Bil transformation

when compared with the LDI transformation. This causes filter responses realized with Bil structures to show greater distortion of the required magnitude response shape. In addition, the error contour values are generally larger for the Bil transformation than for the LDI transformation. Considering the magnitude deviation of a pole/zero prewarped response, it can therefore be argued that the LDI transformation generally, will give better results than the Bil transformation.

The Forward-Difference (FD) and Backward-Difference (BD) transformations were also examined and seen to exhibit Q-enhancement and Q-degradation respectively. In the FD case, restrictions are necessary on the pole locations to ensure stable realizations, while in the BD case similar restrictions apply if the poles are to remain stable upon prewarping.

Pole/zero prewarping is also possible when using FD and BD structures. Expressions for CM prewarping using these transformations were derived and applied successfully to a third order Chebyshev filter. Results are shown to be identical to those obtained using the LDI transformation. This is to be expected, since the pole error expressions for these transformations are identical to those of the LDI transformation.

The drawback associated with the FD and BD transformations is that prewarping alters the original response function substantially and, indeed, may alter the form of this function, thus requiring the circuit to be re-designed. There is also the possibility, with BD structures, that unrealizable responses will result following prewarping. In both transformations, the large amount of prewarping necessary may also adversely affect optimal properties associated with the original circuit, such as minimum component

spread and low sensitivity to component value variation. It is suggested here that the LDI and Bil transformations be employed wherever possible to avoid these disadvantages.

The third order filter example is one given by Brugger & Hosticka [92] who, for designs based on the BD transformation, derive prewarping expressions corresponding to CM prewarping. Since no mention is made in this paper, of the results obtainable using other transformations, the example is extended to include LDI, Bil and FD realizations, thus enabling comparison of the four transformations when using CM prewarping.

In addition to allowing selection of different pole/zero prewarping approaches for optimization of the SC filter magnitude response, knowlege of the distortion expected in the prewarped SC filter also allows other techniques, such as increasing the order of the filter, to be used in further reducing the distortion. This technique is demonstrated in a tenth order SC speech synthesis filter where, over a bandwidth of 5 kHz (with a sampling frequency of 16 kHz), the maximum magnitude error is below 0.5 dB, attained through the use of pole/zero prewarping in conjunction with an additional cascaded second order section. For an additional first order cascaded section, the corresponding error value was 2 dB, while, through the use of pole/zero prewarping without such optimization, a maximum magnitude error of 6 dB resulted.

Although pole/zero prewarping is seen to enable very good SC filter approximations of piecewise-constant-magnitude response functions, it would not normally be used in such cases, since prewarping of the pass-band and stop-band edge frequencies in the

classical way prior to selection of the filter parameters is both simple, reliable and sufficiently accurate. Any special properties of the response function, such as equiripple in the pass-band or stop-band regions, can be maintained through the appropriate choice of a new function to satisfy the prewarped specifications. In most applications it is convenient to use look-up tables for this purpose, which give the component values of a standard structure.

By contrast, pole/zero prewarping requires knowlege of the original filter response function, after which the circuit must be synthesised from the prewarped version of this function. In addition, the prewarping stage may require optimization techniques for reduction of the remaining magnitude distortion. If the filter is designed on the basis of an existing analog circuit, care may also be needed in the circuit synthesis and choice of component values, in order to preserve any optimal characteristics in the original filter, such as gain equalization or component spread minimization.

Pole-zero prewarping would, however be indicated for piecewise-constant-magnitude responses where an existing analog response function is known, but where look-up tables for the classically prewarped specifications are not available. For non-piecewise-constant-magnitude response examples, such as that of the 10th order speech synthesis filter, pole/zero prewarping is ideally suited. Specifications will often be given in terms of pole and zero locations that extend over a relatively wide band. Pole/zero prewarping is easily applied and is seen to approximate closely the desired response in such cases.

In both non-piecewise and piecewise-constant-magnitude filter applications, the techniques developed for optimizing the pole/zero prewarping , are shown to be most effective. Development of a computer aided design package to include the error analysis and these optimization techniques did not fall within the scope of this present study. However, the successful development of such a program package in the future would be of great benefit, not only in SC filter design, but in any sampled-data system. Ideally, this would be an interactive optimization package, where a ceratin amount of user decision making was present.

For the elimination of the termination errors in ladder filters, Lee & Chang [54] have discussed methods for the use of LDI structures in filters whose overall response exhibits Bilinear properties. In future, a powerful extension to the present methods of optimizing pole/zero prewarping may be gained by using a similar concept, where the LDI and Bil transformations would be utilized jointly within the same filter. By careful assignment of each pole and zero to either an LDI or Bil structure, distortion could be greatly reduced, since the overall positive error, generally contributed by LDI transformed poles, could be largely cancelled out by negative error generally contributed by the Bil transformed poles.

11.2 "COMPLEMENTARY FREQUENCY CONVERSION" (COFREC) FILTERING

A second novel approach to the problem of warping effects in SC filters has also been described and studied. In extending the use of SC filters to higher frequencies, it is suggested that the frequency warping effects in these filters be eliminated by

introducing a pair of "Complementary Frequency Conversion" (COFREC) filters. This involves prewarping the signal rather than the filter function, as is the case with classical prewarping.

The operation, which must be performed on the spectrum of the signal so as to include all frequency components, is accomplished in real time by using Surface Acoustic Wave (SAW) Fast Fourier Transform (FFT) devices in the COFREC filter design.

One of the advantages associated with COFREC filtering is that provision can be made for the prewarping operations to track the SC filter sampling frequency. This will provide, for the first time, the ability to compensate for the effects of warping in programmable SC filters that operate with variable sampling frequency.

Since the SAW devices will operate with the pass-band center frequency situated at a multiple of the SC filter sampling frequency, a convenient choice for the SC filter would be that of a pseudo n-path structure. This class of SC filter also operates at a multiple of the sampling frequency, and would therefore be a first choice for applications in high frequency SC networks incorporating SAW COFREC filters.

Two approaches to the fabrication of the COFREC filters are examined. For applications where these filters are to be incorporated in an SC filter design, it would be desirable to use silicon substrate thin-film technology, where the SC filter, the COFREC filters and the associated control circuitry would all be fabricated on a single chip.

Use of COFREC filters as stand alone devices, for inclusion at the input and output of an existing SC circuit, is also possible. In

this case a hybrid package may be used with the SAW devices fabricated in the technology most suited to their particular requirements. Such a packaged device may also have wide-ranging application in other sampled-data systems.

11.3 NOISE IN SC NETWORKS

The noise behaviour of SC circuits differs from that of analog circuits, owing to their sampled-data nature. In most cases the frequency spectrum of noise signals generated within the circuit will extend beyond the sampling frequency, thus causing a large degree of undersampling to take place.

The two primary sources of noise within SC circuits are the operational amplifiers (OAs) and the switches. Models for these are presented so that appropriate noise sources can be included in association with each switch and OA within the circuit. The total resulting noise is then calculated by considering the transfer path that each source sees to the output. Depending on the complexity of the circuit, analysis of these transfer paths could be a lengthy procedure, making simulation of the process for arbitrary circuits desirable. Unfortunately, at the commencement of this research no SC computer simulation program was available that possessed this ability.

A new procedure was therefore developed involving a time domain simulation of the SC circuit using TCAPS. Time samples of band-limited white noise and 1/f noise were generated for inclusion in the circuit description, and a number of spectral estimation algorithms tested for conversion of the output noise signal to the frequency domain. The success of this procedure, using the Yule-Walker Auto-Regressive (AR) algorithm, was

demonstrated for an SC integrator. However, extension to a Biquadratic filter yielded poor results, due to the time-varying properties of this circuit when subjected to noise signals of frequencies greater than the sampling frequency.

Two alternative methods for conversion of the output time signal to the frequency domain (the Autocorrelation algorithm and a windowed periodogram method) were more successful in predicting the output noise. However, these methods were not consistent in the levels of noise that they predicted. Further investigation, resulting in a spectral estimation method that can be employed successfully with the time domain noise simulation, could prove very useful. However, it is considered that the comparative ease with which noise sources may be specified in the frequency domain, and the lack of any operation necessary on the output, will make frequency domain noise simulation, where available, a more efficient choice.

For simulation of the noise behaviour within the Biquadratic filter and a 7th order elliptic filter, an existing method using SPICE was employed. These results were compared with those obtained using a z-domain analysis procedure. Very close agreement with the experimental results was achieved with the latter, for both fabricated and discrete component versions, while, for the SPICE simulation, consistently lower levels of noise ($\approx$ 7dB) were predicted. Both methods predicted similar proportions of noise due to the OAs and switches.

Inclusion of the OA 1/f noise was found to be important in the simulation of the fabricated versions, since, in this case, the 1/f corner frequency was larger than the sampling frequency, resulting in the undersampling of this contribution. Also, the

effect of capacitor size on the switch noise was seen, where the small size of the capacitors in the fabricated filters, caused the switch noise contribution to be greatly increased.

In addition to providing verification of predicted noise behaviour, the experimental tests were used to compare the results of discrete component and fabricated versions of the same filter. This may have led to the development of methods whereby the expected noise behaviour of a fabricated filter could be simulated experimentally, using a discrete component version of the filter. However, as was demonstrated, very different behaviour is possible between the two versions, resulting from the different characteristics of the circuits. This method of prediction is therefore not recommended.

For the design of low noise SC filters it is now clear that the size of the capacitors should be maintained as large as is economically possible, and that low noise OAs should be used. Further methods for the reduction of the noise are also available, such as those of "correlated-double sampling" and "chopper stabilization". Also, reduction of the OA gain-bandwidth product will reduce the amount of undersampling. However, this may adversely affect the high frequency performance of the filter.

11.4 INTERPOLATION AND DECIMATION IN SC FILTERS

As SC filters are used increasingly in large system applications, such as data communication processing, the need for sampling rate conversion, both within a filter and at the interface between processing operations, becomes more apparent. This may be required by the processing operation itself, whereby signal modulation conversion is effected, or else it may be employed to aid design

efficiency and performance.

Large sampling to signal frequency ratios allow accurate signal approximation with negligible warping. However, these desirable characteristics will be at the expense of large capacitor ratios and stringent hardware specifications. Decimation (reduction) of the sampling frequency may therefore be necessary to give a more efficient design, while interpolating (increasing) the sampling frequency may be necessary for signal recovery or for relaxation of the anti-aliasing filter requirements.

In addition, SC filters with their sampled-data properties, are considered ideally suited to the design of programmable sampling rate conversion filters and for use in the operations of digital communications signal processing. Circuit examples are given of SC interpolation and decimation filters, showing the ease with which these operations may be accomplished using such circuits.

APPENDIX 1

POLE ERROR CONTRIBUTION EXPRESSIONS FOR THE LDI AND BILINEAR TRANSFORMATIONS USING DIFFERENT POLE/ZERO PREWARPING APPROACHES

	Real Pole	
	LDI	Bil
CF	$\dfrac{1+(f/f_0)^2}{1+\dfrac{\sin^2(\pi f/F)}{\sin^2(\pi f_0/F)}}$	$\dfrac{1+(f/f_0)^2}{1+\dfrac{\tan^2(\pi f/F)}{\tan^2(\pi f_0/F)}}$
S	$\dfrac{1+(f/f_0)^2}{1+(\dfrac{1}{\pi f_0/F})^4\sin^2(\pi f/F)\sin^2(\pi f_0/F)}$	$\dfrac{1+(f/f_0)^2}{1+(\dfrac{1}{\pi f_0/F})^4\tan^2(\pi f/F)\tan^2(\pi f_0/F)}$
CM	$\dfrac{1+(f/f_0)^2}{1+\dfrac{\sin^2(\pi f/F)}{\sinh^2(\pi f_0/F)}}$	$\dfrac{1+(f/f_0)^2}{1+\left[1+\cosh(2\pi f_0/F)\right]^2\dfrac{\sin^2(\pi f/F)}{\sinh^2(2\pi f_0/F)}}$

$$e_p = \log_{10}[\quad]$$

	Complex Pole Pair:LDI
CF	$\dfrac{(1-f^2/f_0^2)^2+f^2/f_0^2/Q^2}{\left[1-\dfrac{\sin^2(\pi f/F)}{\sin^2(\pi f_0/F)}\right]^2+\left[\dfrac{\sin^2(\pi f/F)}{Q^2\sin^2(\pi f_0/F)}\right]}$
S	$\dfrac{\left[(1-f^2/f_0^2)^2+f^2/f_0^2/Q^2\right]\left[(\frac{\pi f_0}{F})^4+(4Q^2-1)\sin^4(\frac{\pi f_0}{F})\right]^2}{\left[(\frac{\pi f_0}{F})^4+(4Q^2-1)\sin^4(\frac{\pi f_0}{F})-4Q^2\sin^2(\frac{\pi f}{F})\sin^2(\frac{\pi f_0}{F})\right]^2+16Q^2(\frac{\pi f_0}{F})^4\sin^2(\frac{\pi f}{F})\sin^2(\frac{\pi f_0}{F})}$
CM	$\dfrac{\left[(1-f^2/f_0^2)^2+f^2/f_0^2/Q^2\right]\left[\cosh(\sigma T)-\cos(\omega_p T)\right]^2}{\left[\cosh^2(\sigma T)+\cos^2(\omega_p T)+\cos^2(\omega T)-2\cosh(\sigma T)\cos(\omega_p T)\cos(\omega T)-1\right]}$

	Complex Pole Pair:Bil
CF	$\dfrac{(1-f^2/f_0^2)^2+f^2/f_0^2/Q^2}{\left[1-\dfrac{\tan^2(\pi f/F)}{\tan^2(\pi f_0/F)}\right]^2+\dfrac{\tan^2(\pi f/F)}{Q^2\tan^2(\pi f_0/F)}}$
S	$\dfrac{\left[(1-f^2/f_0^2)^2+f^2/f_0^2/Q^2\right]\left[(\frac{\pi f_0}{F})^4+(4Q^2-1)\tan^4(\frac{\pi f_0}{F})\right]^2}{\left[(\frac{\pi f_0}{F})^4+(4Q^2-1)\tan^4(\frac{\pi f_0}{F})-4Q^2\tan^2(\frac{\pi f}{F})\tan^2(\frac{\pi f_0}{F})\right]^2+16Q^2(\frac{\pi f_0}{F})^4\tan^2(\frac{\pi f}{F})\tan^2(\frac{\pi f_0}{F})}$
CM	$\dfrac{\left[(1-f^2/f_0^2)^2+f^2/f_0^2/Q^2\right]\left[\sinh^2(\sigma T)+\sin^2(\omega_p T)\right]^2}{\left[\sinh^2(\sigma T)+\sin^2(\omega_p T)-\tan^2(\frac{\omega T}{2})\left[\cos(\omega_p T)+\cosh(\sigma T)\right]^2\right]^2+4\sinh^2(\sigma T)\tan^2(\frac{\omega T}{2})\left[\cos(\omega_p T)+\cosh(\sigma T)\right]^2}$

APPENDIX 2

POLE ERROR CONTRIBUTION PLOTS FOR THE LDI AND BILINEAR TRANSFORMATIONS USING DIFFERENT POLE/ZERO PREWARPING APPROACHES

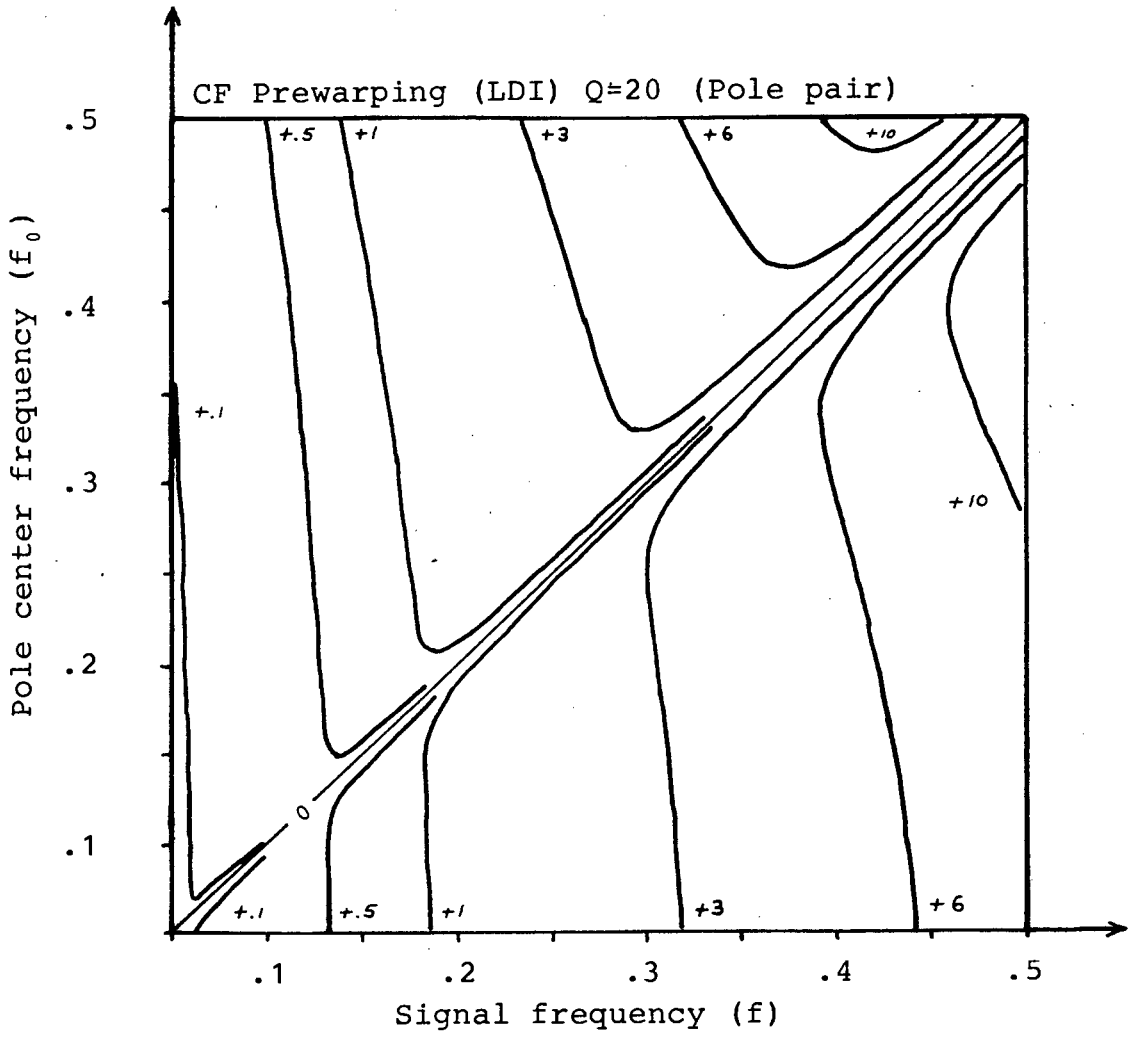

(Contour values in dB)

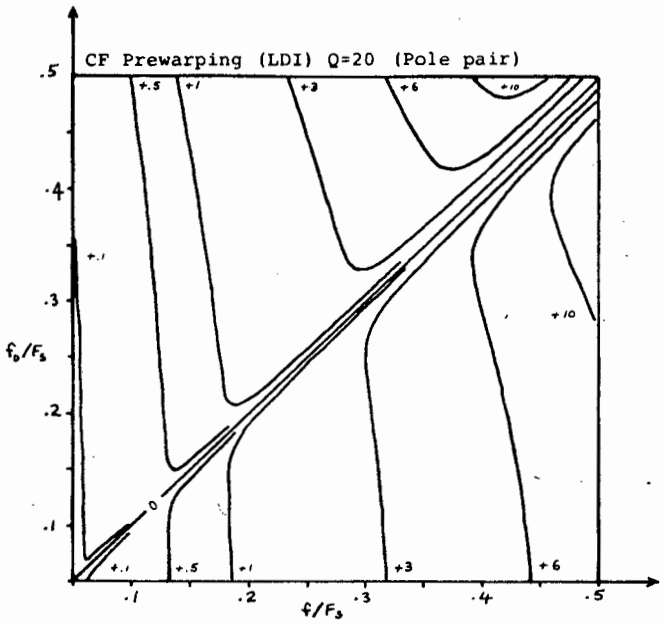
CF Prewarping (LDI) Q=20 (Pole pair)
f_0/F_s
f/F_s
.5
.4
.3
.2
.1
.1
.2
.3
.4
.5
+.5
+1
+3
+6
+10
+.1
0

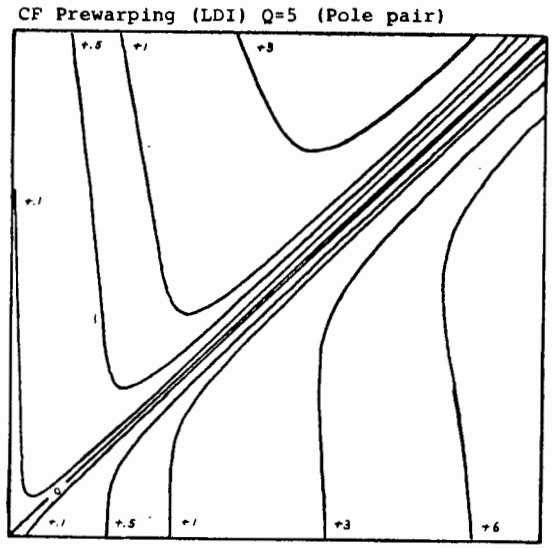
CF Prewarping (LDI) Q=5 (Pole pair)
+.5
+1
+3
+.1
0
+.1
+.5
+1
+3
+6

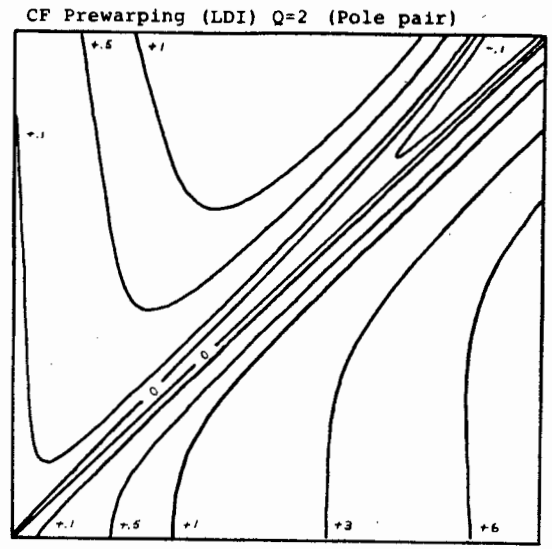
CF Prewarping (LDI) Q=2 (Pole pair)
+.5
+1
-.1
+.1
0
0
+.1
+.5
+1
+3
+6

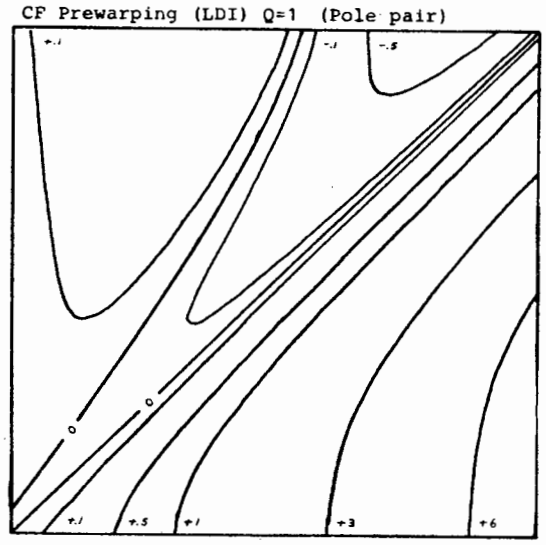
CF Prewarping (LDI) Q=1 (Pole pair)
+.1
-.1
-.5
0
0
+.1
+.5
+1
+3
+6

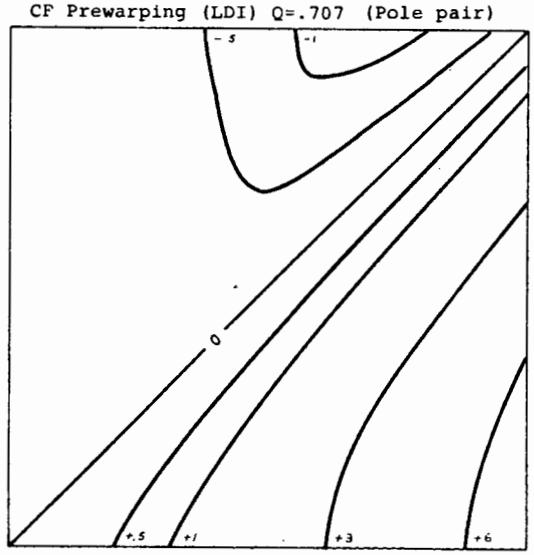
CF Prewarping (LDI) Q=.707 (Pole pair)
-.5
-.1
0
+.5
+1
+3
+6

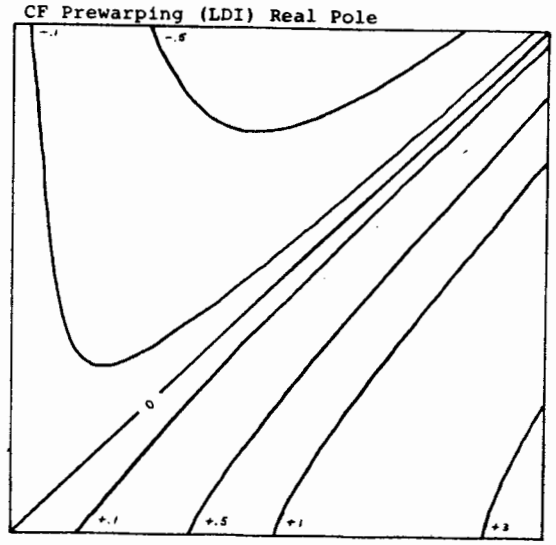
CF Prewarping (LDI) Real Pole
-.1
-.5
0
+.1
+.5
+1
+3

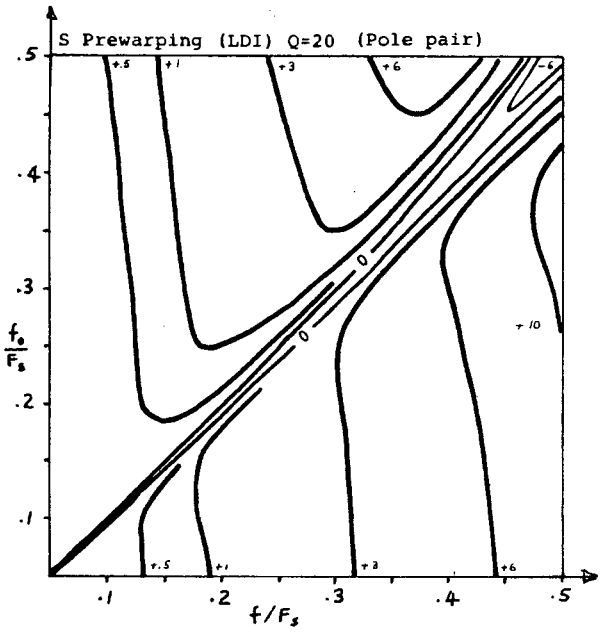
S Prewarping (LDI) Q=20 (Pole pair)
.5
.4
.3
.2
.1
$\frac{f_o}{F_s}$
+.5
+1
+3
+6
-6
0
0
+10
.1
.2
.3
.4
.5
f/Fs

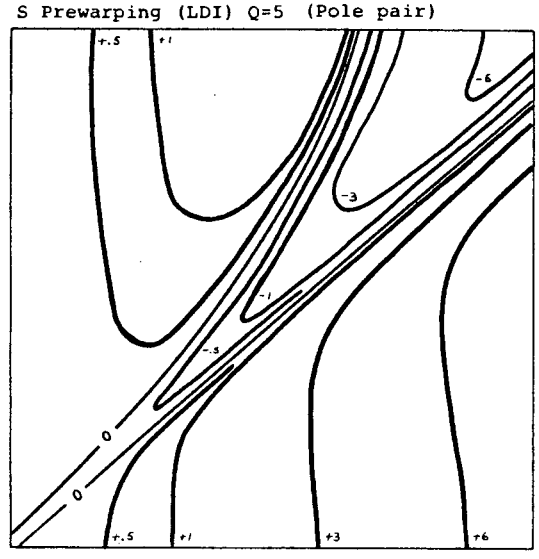
S Prewarping (LDI) Q=5 (Pole pair)
+.5
+1
-6
-3
-1
-.5
0
0
+.5
+1
+3
+6

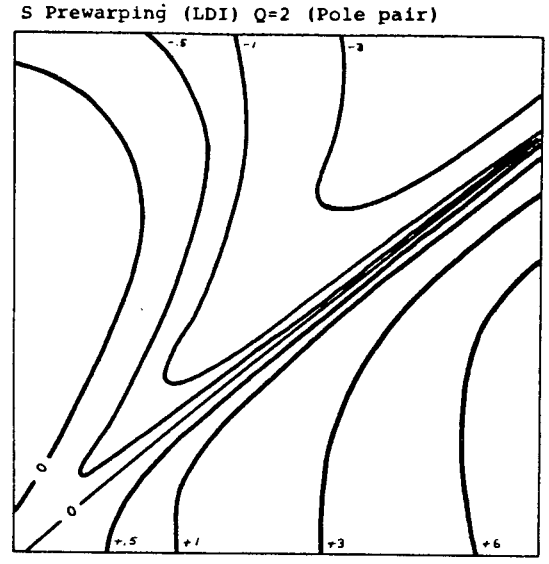
S Prewarping (LDI) Q=2 (Pole pair)
-.5
-1
-3
0
0
+.5
+1
+3
+6

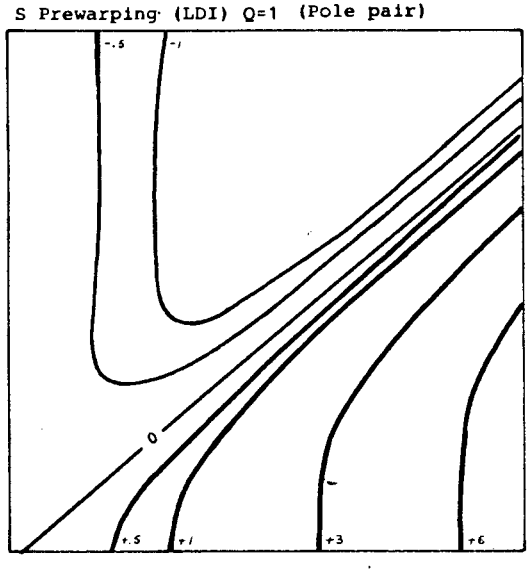
S Prewarping (LDI) Q=1 (Pole pair)
-.5
-1
0
+.5
+1
+3
+6

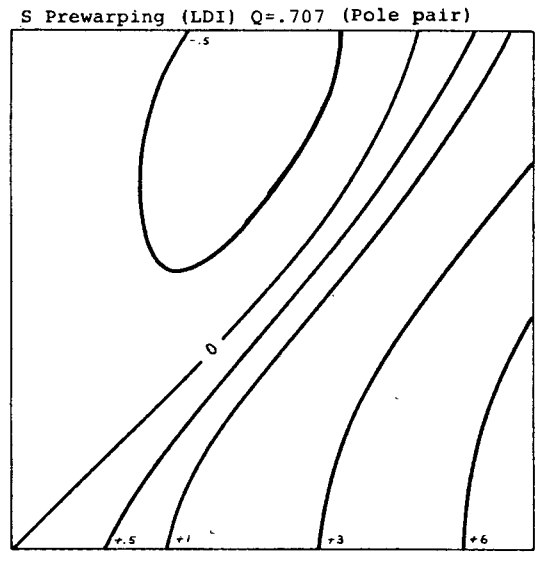
S Prewarping (LDI) Q=.707 (Pole pair)
-.5
0
+.5
+1
+3
+6

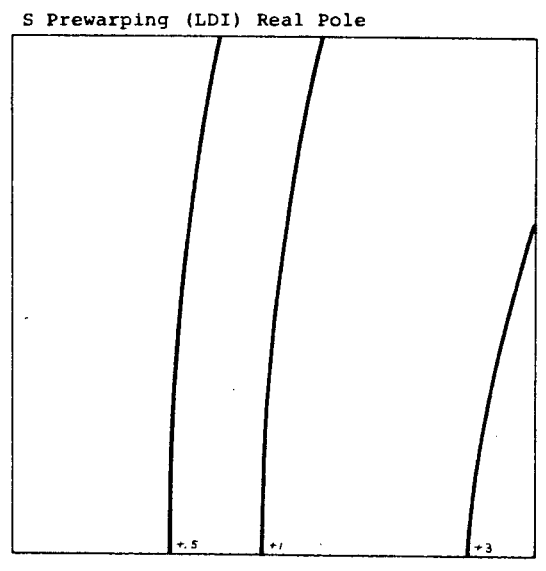
S Prewarping (LDI) Real Pole
+.5
+1
+3

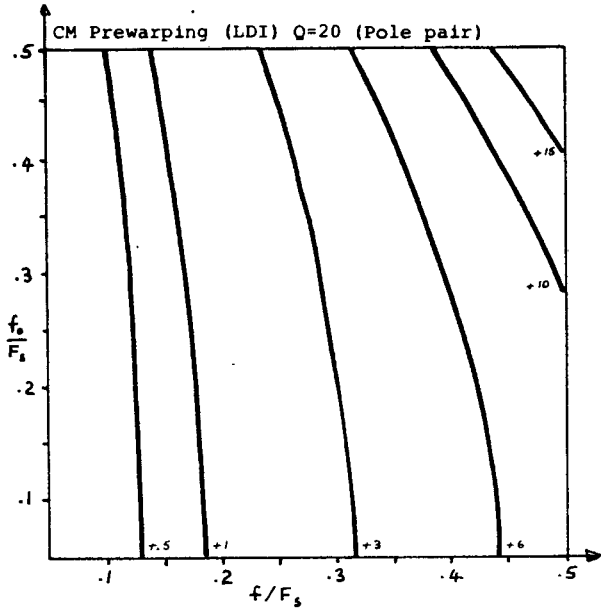
CM Prewarping (LDI) Q=20 (Pole pair)
.5
.4
.3
.2
.1
$\frac{f_c}{F_s}$
+.5
+1
+3
+6
+10
+15
.1
.2
.3
.4
.5
f/F_s

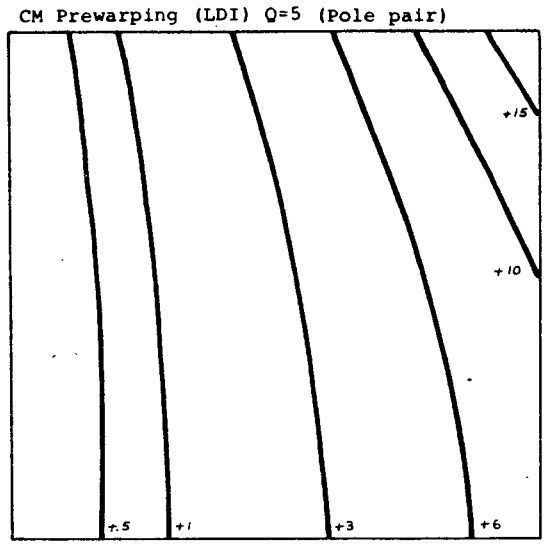
CM Prewarping (LDI) Q=5 (Pole pair)
+15
+10
+.5
+1
+3
+6

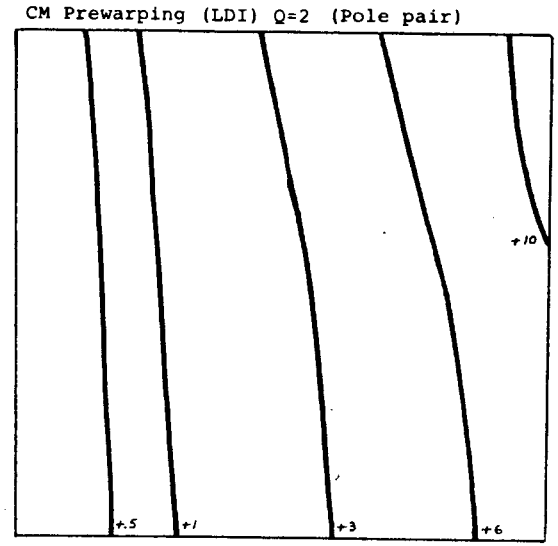
CM Prewarping (LDI) Q=2 (Pole pair)
+10
+.5
+1
+3
+6

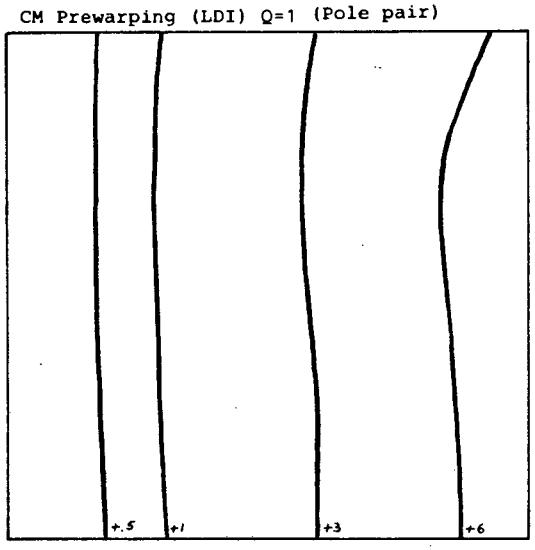
CM Prewarping (LDI) Q=1 (Pole pair)
+.5
+1
+3
+6

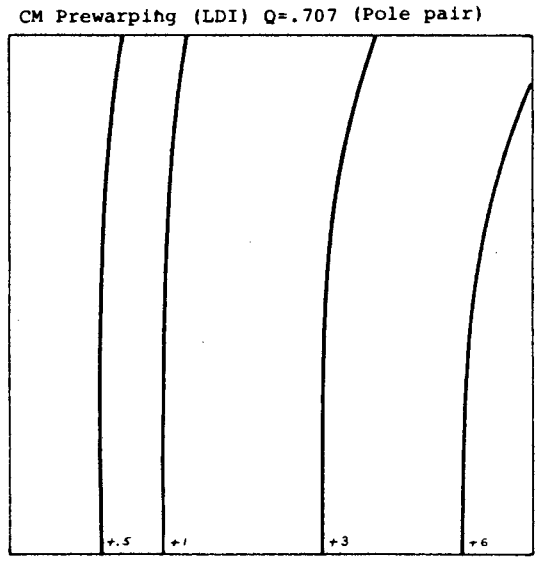
CM Prewarping (LDI) Q=.707 (Pole pair)
+.5
+1
+3
+6

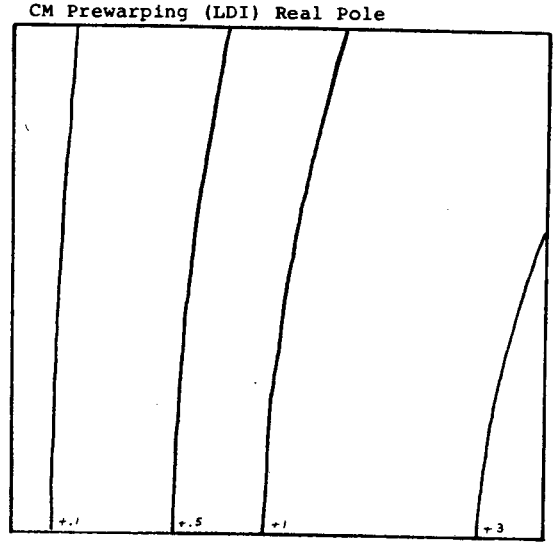
CM Prewarping (LDI) Real Pole
+.1
+.5
+1
+3

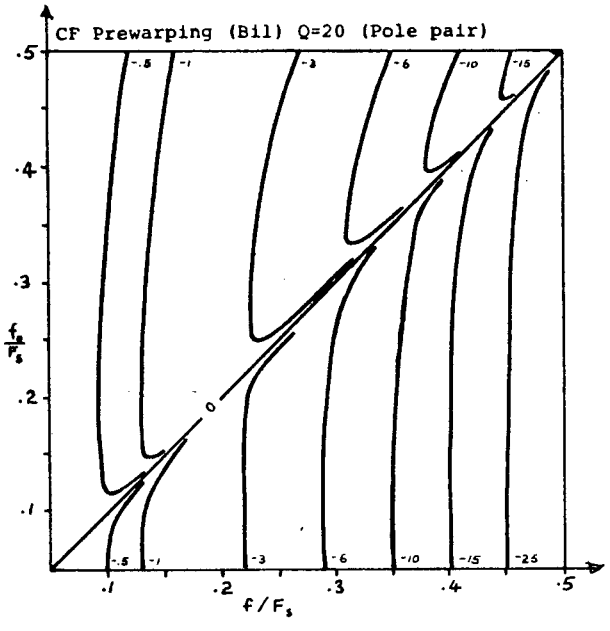
CF Prewarping (Bil) Q=20 (Pole pair)
.5
.4
.3
.2
.1
$\frac{f_a}{F_s}$
-.5
-1
-3
-6
-10
-15
-25
0
.1
.2
.3
.4
.5
f/F_s

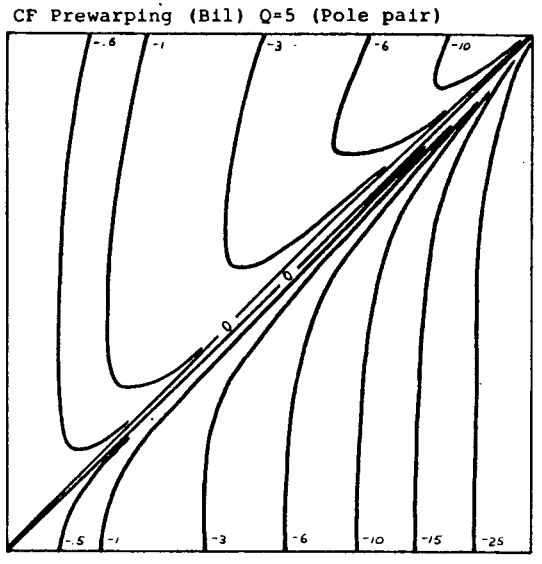
CF Prewarping (Bil) Q=5 (Pole pair)
-.5
-1
-3
-6
-10
-15
-25
0

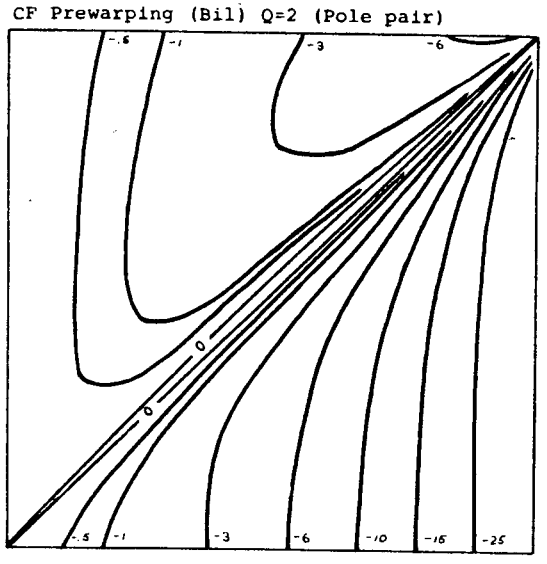
CF Prewarping (Bil) Q=2 (Pole pair)
-.5
-1
-3
-6
-10
-15
-25
0

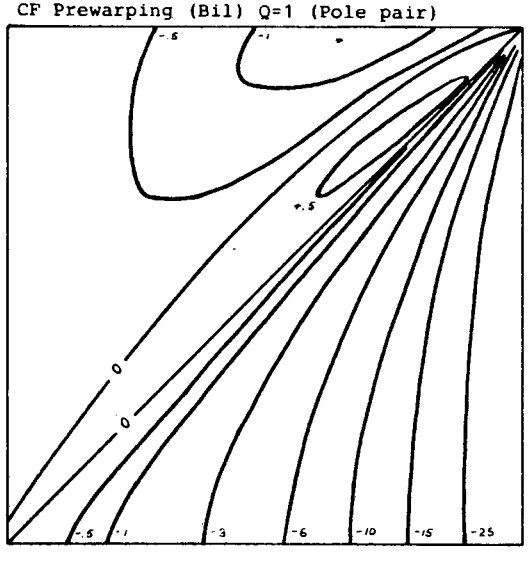
CF Prewarping (Bil) Q=1 (Pole pair)
-.5
-1
-3
-6
-10
-15
-25
0
0
0

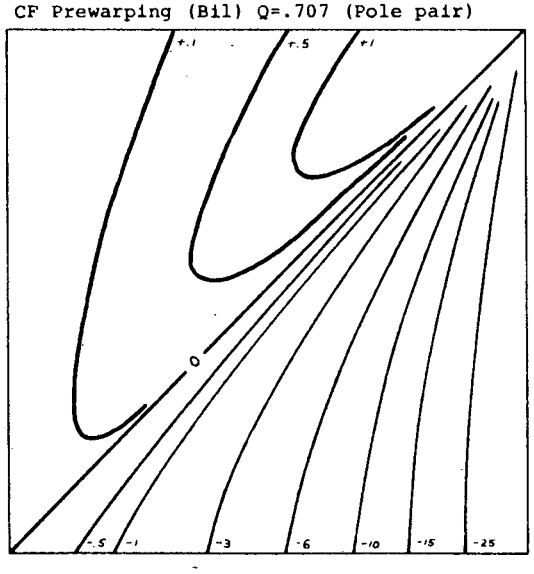
CF Prewarping (Bil) Q=.707 (Pole pair)
+.1
+.5
+1
-.5
-1
-3
-6
-10
-15
-25
0

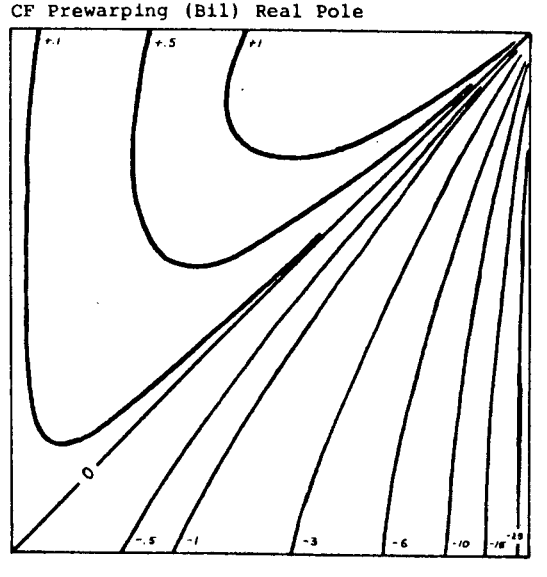
CF Prewarping (Bil) Real Pole
+.1
+.5
+1
-.5
-1
-3
-6
-10
0

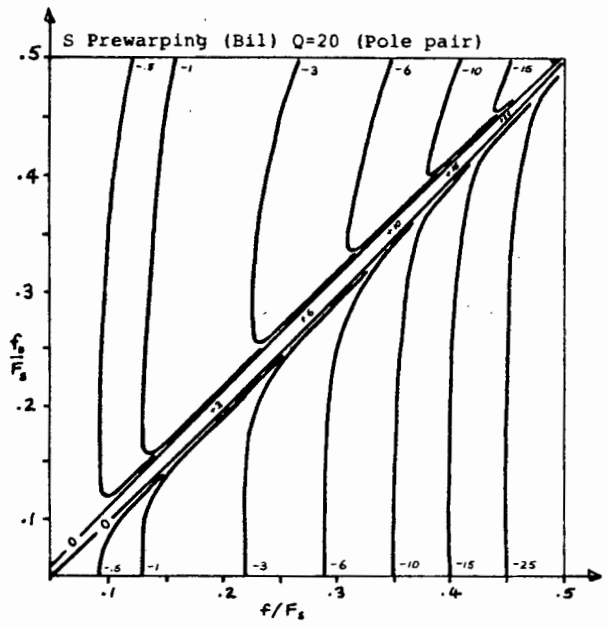
S Prewarping (Bil) Q=20 (Pole pair)
.5
.4
.3
.2
.1
$\frac{f_s}{F_s}$
0
-.5
-1
-3
-6
-10
-15
-25
+3
+6
+10
+15
.1
.2
.3
.4
.5
f/F_s

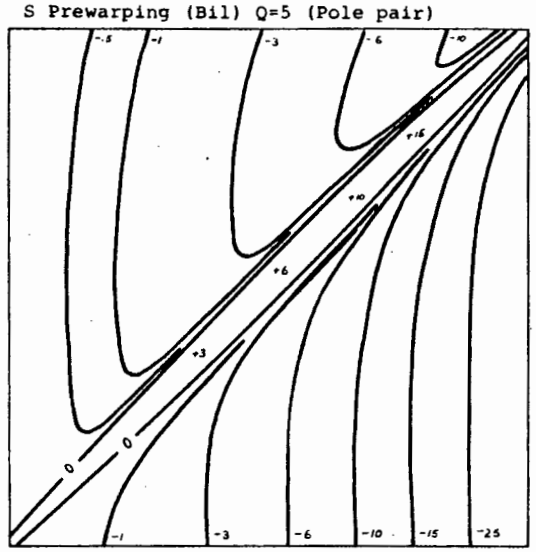
S Prewarping (Bil) Q=5 (Pole pair)
-.5
-1
-3
-6
-10
+15
+10
+6
+3
0
0
-1
-3
-6
-10
-15
-25

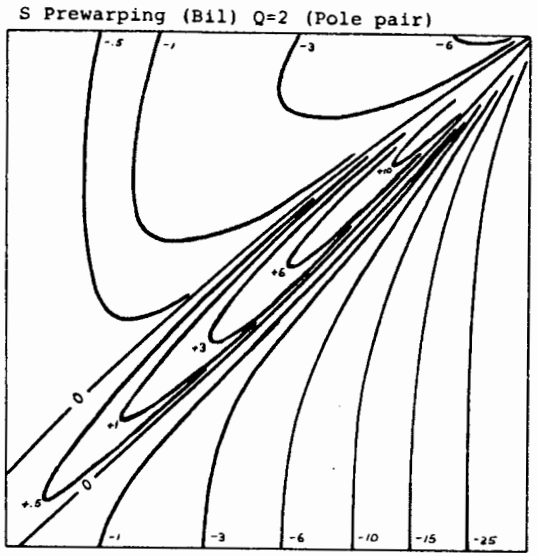
S Prewarping (Bil) Q=2 (Pole pair)
-.5
-1
-3
-6
+10
+6
+3
0
+1
0
+.5
-1
-3
-6
-10
-15
-25

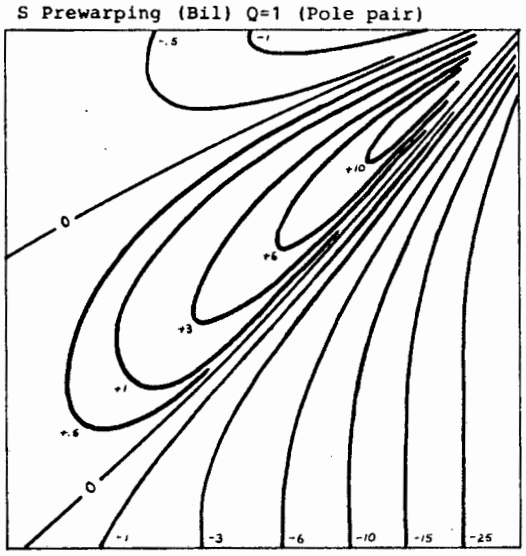
S Prewarping (Bil) Q=1 (Pole pair)
-.5
-1
+10
+6
+3
+1
+.5
0
0
-1
-3
-6
-10
-15
-25

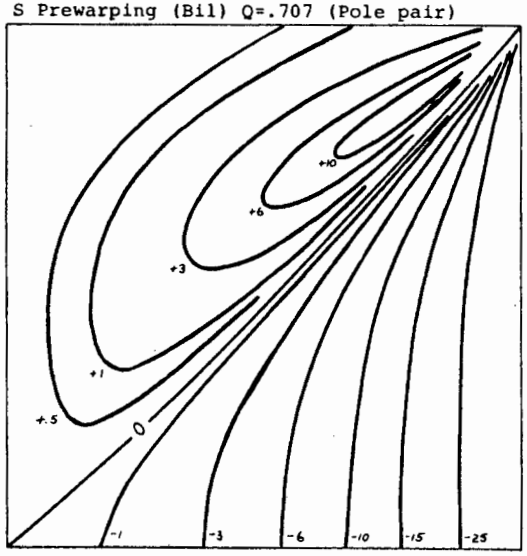
S Prewarping (Bil) Q=.707 (Pole pair)
+10
+6
+3
+1
+.5
0
-1
-3
-6
-10
-15
-25

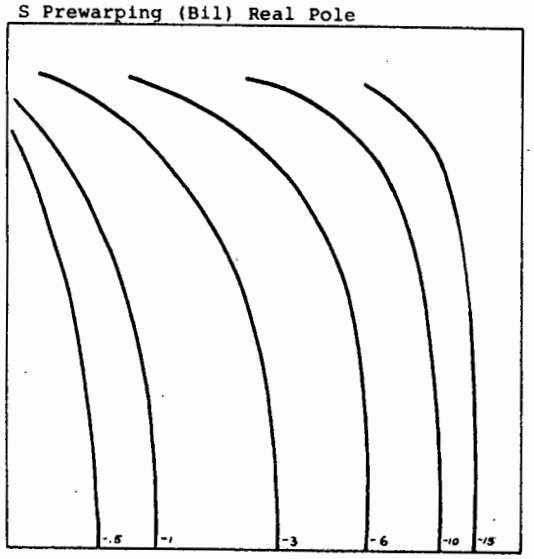
S Prewarping (Bil) Real Pole
-.5
-1
-3
-6
-10
-15

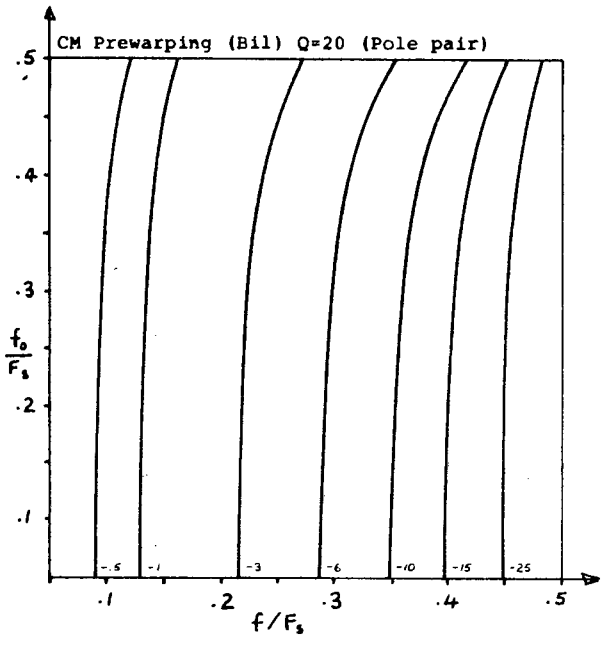
CM Prewarping (Bil) Q=20 (Pole pair)
.5
.4
.3
$\frac{f_0}{F_s}$
.2
.1
-.5
-1
-3
-6
-10
-15
-25
.1
.2
.3
.4
.5
f/F_s

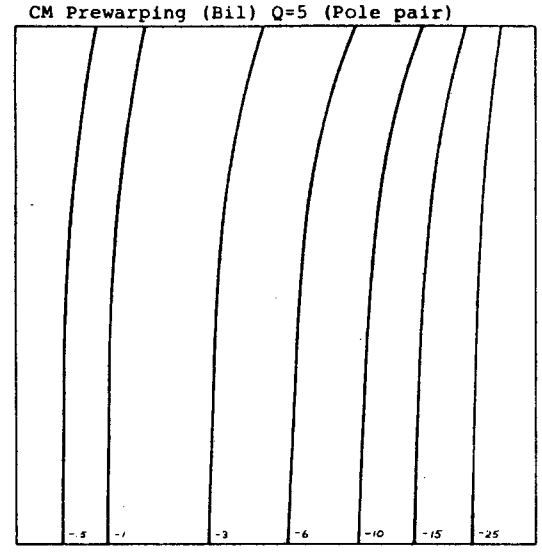
CM Prewarping (Bil) Q=5 (Pole pair)
-.5
-1
-3
-6
-10
-15
-25

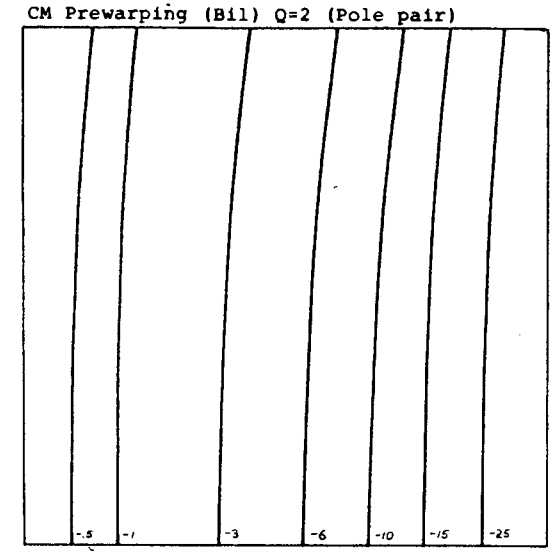
CM Prewarping (Bil) Q=2 (Pole pair)
-.5
-1
-3
-6
-10
-15
-25

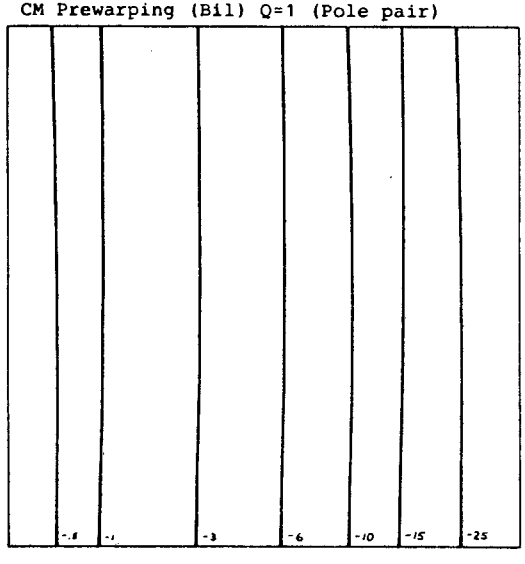
CM Prewarping (Bil) Q=1 (Pole pair)
-.5
-1
-3
-6
-10
-15
-25

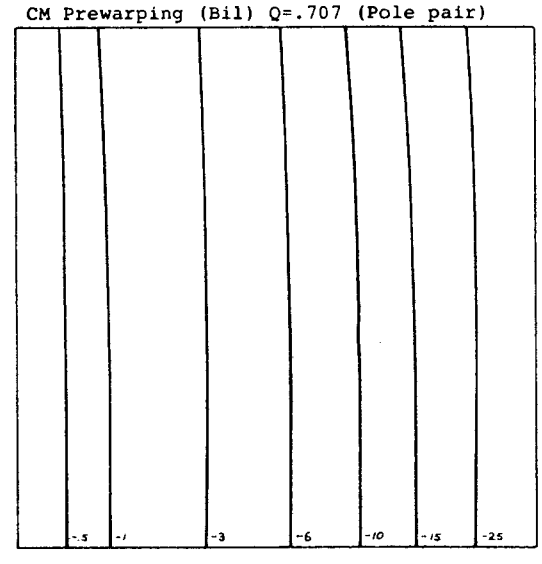
CM Prewarping (Bil) Q=.707 (Pole pair)
-.5
-1
-3
-6
-10
-15
-25

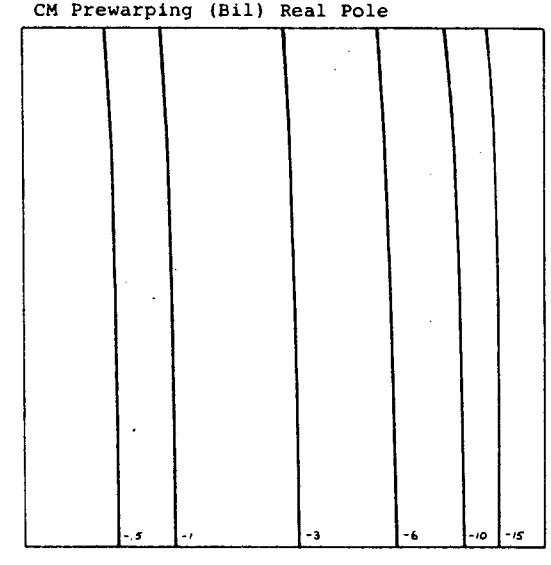
CM Prewarping (Bil) Real Pole
-.5
-1
-3
-6
-10
-15

REFERENCES

[1] D.L.Fried, "Analog Sampled-Data Filters", IEEE J. SolidState Circuits, vol.SC-7, no.4, pp 302-304, August 1972.

[2] J.T.Caves et. al. , "Sampled Analog Filtering using Switched Capacitors as Resistor Equivalents", IEEE J. Solid-State Circuits, vol.SC-12, no.6, pp 592-599, December 1977.

[3] B.J.Hosticka, R.W.Brodersen, P.R.Gray, "MOS Sampled Data Recursive Filters using Switched Capacitor Integrators", IEEE J. Solid-State Circuits, vol.SC-12, no.6, pp.600-608, December 1977.

[4] R.W.Brodersen, P.R.Gray, D.A.Hodges, "MOS Switched Capacitor Filters", Proc. IEEE, vol.67, no.1, pp 61-75, January 1979.

[5] J.Cornu, "LSI Techniques for Telecommunication", Elec. Communication, vol.55, no.4, pp 376-381, April 1980.

[6] W.Twaddell, "Switched-Capacitor-Array Introductions Herald Semi-custom Analog Flexibility", EDN, pp.45-48, February 17, 1983.

[7] R.L.Geiger, P.E.Allen, D.T.Ngo, "Switched-Resistor Filters A Continuous Time Approach to Monolithic MOS Filter Design", IEEE Trans. Circuits Syst., vol.CAS-29, no.5, pp.306-315, May 1982.

[8] M.Banu, Y.Tsividis, "Fully Integrated Active RC Filters in MOS Technology", IEEE J. Solid-State Circuits, vol.SC-18, no.6, pp.644-651, December 1983.

[9] J.Khoury, Y.Tsividis, M.Banu, "Use of MOS Transistor as a Tunable Distributed RC Filter Element", Electron. Lett., vol.20, no.4, pp.187-188, February 1984.

[10] A.Fettweis, "Basic Principles of SC Filters Using Voltage Inverter Switches", AEU, Band 33, Heft 1, pp.13-19, January 1979.

[11] ————————, "SC Filters Using Voltage Inverter Switches : Further Design Principles", AEU, Band 33, Heft 3, pp.107-114, March 1979.

[12] A.Fettweis, D.Herbst, J.A.Nossek, "Floating Voltage Inverter Switches for SC Filters", AEU, Band 33, Heft 9, pp.376-377, September 1979.

[13] G.C.Temes, H.J.Orchard, M.Jahanbegloo, "SC Filter Design Using the Bilinear z-Transform", IEEE Trans. Circuits Syst., vol.CAS-25, no.12, pp.1039-1044, December 1978.

[14] G.M.Jacobs et. al., "Design Techniques for MOS SC Ladder Filters", IEEE Trans. Circuits Syst., vol.CAS-25, no.12, pp.1014-1021, December 1978.

[15] S.O.Scanlan, "Analysis and Synthesis of SC State-Variable Filters", IEEE Trans. Circuits Syst., vol.CAS-28, no.2, pp.85-93, February 1981.

[16] M.S.Lee, G.C.Temes, C.Chang, M.B.Ghaderi, "Bilinear SC Ladder Filters", IEEE Trans. Circuits Syst., vol.CAS-28, no.8, pp.811-821, August 1981.

[17] D.J.Allstot, K-S.Tan, "Simplified MOS SC Ladder Structures", IEEE J. Solid-State Circuits, vol.SC-16, no.6, pp.724-729, December 1981.

[18] G.C.Temes, M.Jahanbegloo, "SC Circuits Bilinearly Equivalent to Floating Inductor or FDNR", Electron. Lett., vol.15, no.3, pp.87-88, February 1979

[19] U.W.Brugger, B.J.Hosticka, G.S.Moschytz, "SC Simulation of Floating Inductors Using Gyrators", Electron. Lett., vol.15, no.16, pp.494-496, August 1979.

[20] J.A.Nossek, G.C.Temes, "SC Filter Design Using Bilinear Element Modelling", IEEE Trans. Circuits Syst., vol.CAS-27, no.6, pp.481-491.
[21] T.R.Viswanathan et. al., "Switched-Capacitor Transconductance and Related Building Blocks", IEEE Trans. Circuits Syst., vol.CAS-27, no.6, pp.502-508, June 1980.
[22] B.J.Hosticka, G.S.Moschytz, "SC Filters Using FDNR-like Super Capacitances", IEEE Trans. Circuits Syst., vol.CAS-27, no.6, pp.569-573, June 1980.
[23] F.Ueno, T.Inoue, I.Oota, "Realization of Closely Coupled Inductors Using SC Circuits", IEEE Trans. Circuits Syst., vol.CAS-29, no.1, pp.52-53, January 1982.
[24] M.Cooperman, C.W.Kapral, "Integrated Switched-Capacitor FDNR Filter", IEEE J. Solid-State Circuits, vol.SC-18, no.4, pp.378-383,August 1983.
[25] E.Luder, G.Spahlinger, "Performance of Various Types of Switched-Capacitor Filters", AEU, Band 36, Heft 2, pp.57-62, February 1982.
[26] K.R.Laker, "Equivalent Circuits for the Analysis and Synthesis of SC Networks", Bell Syst. Tech. J., vol.58, no.3, pp.729-769, March 1979.
[27] P.E.Fleischer, K.R.Laker, "A Family of Active SC Building Blocks", Bell Syst. Tech. J., vol.58, no.10, pp.2235-2269, December 1979.
[28] K.Martin, "Exact Design of SC Bandpass Filter Using Coulped-Biquad Structures", IEEE Trans. Circuits Syst., vol.CAS-27, no.6, pp.469-474, June 1980.
[29] J.A.Nossek, G.C.Temes, "SC Filter Design Using Bilinear Element Modelling", IEEE Trans. Circuits Syst., vol.CAS-27, no.6, pp.481-491, June 1980.
[30] R.Gregorian, "SC Filter Design Using Cascaded Sections", IEEE Trans. Circuits Syst., vol.CAS-27, no.6, pp.515-521, June 1980.
[31] U.W.Brugger, D.C.von Grunigen, G.S.Moschytz, "A Comprehensive Procedure for the Design of Cascaded SCFs", IEEE Trans. Circuits Syst., vol.CAS-28, no.8, pp.803-810, August 1981.
[32] H.C.Patangia, J.Cartinhour, "2-Phase Circulating Shift Register for SC N-Path Filters", Electron. Lett., vol.18, no.11, pp.444-445, May 1982.
[33] J.Pandel, "Principles of Pseudo N-Path SCFs Using Recharging Devices", AEU, Band 36, Heft 5, pp.177-187, May 1982.
[34] M.B.Ghaderi, J.A.Nossek, G.C.Temes, "Narrow-Band Switched-Capacitor Bandpass Filters", IEEE Trans. Circuits Syst., vol.CAS-29, no.8, pp.557-571, August 1982.
[35] D.C.von Grunigen et. al., "An Integrated CMOS Switched-Capacitor Bandpass Filter Based on N-Path and Frequency-Sampling Principles", IEEE J. Solid-State Circuits, vol.SC-18, no.6, pp.753-761, December 1983.
[36] E.Simonyi, A.Heszberger, "Design of Recursive CCD and Multiple-Loop Feedback SC Filters using Wave Matrix Techniques", Proc. ISCAS, Chicago, pp.762-765, May 1979.
[37] J.Pandel, "SC Elements for VIS-SCFs with Reduced Influences of Parasitic Capacitors", AEU, Band 35, Heft 3, pp.121-130, March 1981.
[38] J.Mavor et. al., "A Prototype SC Voltage-Wave Filter Realized in NMOS Technology", IEEE J. Solid-State Circuits, vol.SC-16, no.6, pp.716-723, December 1981.
[39] D.J.Allstot, R.W.Brodersen, P.R.Gray, "An Electrically-

Programmable SC Filter", IEEE J. Solid-State Circuits, vol.SC-14, no.6, pp.1034-1041, December 1979.

[40] D.B.Cox, L.T.Lin, R.S.Florek, H-F.Tseng, "A Real-Time Programmable SC Filter", IEEE J. Solid-State Circuits, vol.SC-15, no.6, pp.972-977, December 1980.

[41] K.Martin, A.S.Sedra, "SC Building Blocks for Adaptive Systems", IEEE Trans. Acous. Speech Signal Processing, vol.ASSP-29, no.3, pp.736-744, June 1981.

[42] U.Kleine et. al., "Real-Time Programmable Unit-Element SC Filter for LPC Synthesis", Electron. Lett., vol.17, no.17, pp.600-602, August 1981.

[43] C.F.Kurth, G.S.Moschytz, "Nodal Analysis of SC Networks", IEEE Trans. Circuits Syst., vol.CAS-26, no.2, pp.93-105, February 1979.

[44] M.L.Liou, Y-L.Kuo, "Exact Analysis of SC Circuits with Arbitrary Inputs", IEEE Trans. Circuits Syst., vol.CAS-26, no.4, pp.213-223, April 1979.

[45] Y-L.Kuo, M.L.Liou, J.W.Kasinskas, "An Equivalent Circuit Approach to the Computer-Aided Analysis of SC Circuits", IEEE Trans. Circuits Syst., vol.CAS-26, no.9, pp.708-714, September 1979.

[46] Y.P.Tsividis, "Analysis of SC Networks", IEEE Trans. Circuits Syst., vol.CAS-26, no.11, pp.935-947, November 1979.

[47] M.L.Liou, Y-L.Kuo, C.F.Lee, "A Tutorial on Computer-Aided Analysis of Switched-Capacitor Circuits", Proc. IEEE, vol.71, no.8, pp.987-1005, August 1983.

[48] G.C.Temes, "MOS SC Filters History and State of the Art", Proc. European Conf. Circuit Theory and Design, The Hague, September 1981.

[49] R.Gregorian, K.W.Martin, G.C.Temes, "Switched-Capacitor Circuit Design", Proc. IEEE, vol.71, no.8, pp.941-966, August 1983.

[50] D.J.Allstot, W.C.Black, "Technological Design Considerations for Monolithic MOS Switched-Capacitor Filtering Systems", Proc. IEEE, vol.71, no.8, pp.967-986, August 1983.

[51] M.S.Lee, C.Chang, "Low Sensitivity SC Ladder Filters", IEEE Trans. Circuits Syst., vol.CAS-27, no.6, pp.475-480, June 1980.

[52] R.D.Davis, T.N.Trick, "Optimum Design of Low-Pass SC Ladder Filters", IEEE Trans. Circuits Syst., vol.CAS-27, no.6, pp.522-527, June 1980.

[53] T.C.Choi, R.w.Brodersen, "Considerations for High-Frequency SC Ladder Filters", IEEE Trans. Circuits Syst., vol.CAS-27, no.6, pp.545-552, June 1980.

[54] M.S.Lee, C.Chang, "SCFs Using the LDI and Bilinear Transforms", IEEE Trans. Circuits Syst., vol.CAS-28, no.4, pp.265-270, April 1981.

[55] K.Haug, "Design, Analysis and Optimization of SCFs Derived from Lumped Analog Models", AEU, Band 35, Heft 7/8, pp.279-287, July/August 1981.

[56] P.V.Ananda Mohan, V.Ramachandran, M.N.S.Swamy, "Terminations for Component-Simulation-Type SC Ladder Filters", Electron. Lett., vol.19, no.1, pp.29-30, January 1983.

[57] E.Luder, "SCFs Insensitive to Parasitics", AEU, vol.34, no.12, pp.501-506, December 1980.

[58] G.Fischer, G.S.Moschytz, "High-Q SC Biquad with a Minimum Capacitor Spread", Electron. Lett., vol.18, no.25, pp.1087-1089, December 1982.

[59] P.van Peteghem, W.Sansen, "T-Cell SC Integrator Synthesises Very Large Capacitor Ratios", Electron. Lett., vol.19, no.14, pp.541-543, July 1983.
[60] G.C.Temes, R.Gregorian, "Compensation for Parasitic Capacitances in SC Filters", Electron. Lett., vol.15, no.13, pp.377-379, June 1979.
[61] K.Martin, "Improved Circuits for the Realization of SC Filters", IEEE Trans. Circuits Syst., vol.CAS-27, no.4, pp.237-244, April 1980.
[62] P.E.Fleischer, A.Ganesan, K.R.Laker, "Parasitic Compensated SC Circuits", Electron. Lett., vol.17, no.24, pp.929-931, October 1981.
[63] K.Martin, "New Clock Feedthrough Cancellation Technique for Analog MOS Circuits", Electron. Lett., vol.18, no.1, pp.39-40, January 1982.
[64] P.V.Ananda Mohan, V.Ramachandran, M.N.S.Swamy, "Parasitic-Compensated Second-Order SCFs", Electron. Lett., vol.18, no.12, pp.531-533, June 1982.
[65] I.A.Young, D.A.Hodges, "MOS SC Analog Sampled-Data Direct-Form Recursive Filters", IEEE J. Solid-State Circuits, vol.SC-14, no.6, pp.1020-1033, December 1979.
[66] G.C.Temes, "Finite Amplifier Gain and Bandwidth Effects in SC Filters", IEEE J. Solid-State Circuits, vol.SC-15, no.3, pp.358-361, June 1980.
[67] K.Martin, A.S.Sedra, "Effects of the Op Amp Finite Gain and Bandwidth on the Performance of SCFs", IEEE Trans. Circuits Syst., vol.CAS-28, no.8, pp.822-829, August 1981.
[68] R.L.Geiger, E.Sanchez-Sinencio, "Op Amp Gain-Bandwidth Product Effects on the Performance of SC Networks", IEEE Trans. Circuits Syst., vol.CAS-29, no.2, pp.96-106, February 1982.
[69] M.Sasikumar, K.Radhakrishna, M.A.Reddy, "Active Compensation in the Switched Capacitor Biquad", Proc. IEEE, vol.71, no.8, pp.1008-1009, August 1983.
[70] S.Eriksson, K.Chen, "Offset-Compensated Switched-Capacitor Leapfrog Filters", Electron. Lett., vol.20, no.18, August 1984.
[71] E.Sanchez-Sinencio, J.Silva-Martinez, R.L.Geiger, "Biquadratic SC Filters with Small GB Effects", IEEE Trans. Circuits Syst., vol.CAS-31, no.10, pp.876-883, October 1984.
[72] L.T.Bruton, "Low Sensitivity Digital Ladder Filters", IEEE Trans. Circuits Syst., vol.CAS-22, no.3, pp.168-176, March 1975.
[73] E.Lueder, H.Lanfer, "Equivalent Sampled Data Filter Structures and some of their Properties", Proc. ISCAS, New York, pp.752-755, May 1978.
[74] D.Herbst et. al., "Integrated CMOS SC Filter with 170 kHz Cuttoff Frequency", Electron. Lett., vol.17, no.5, pp.205-207, March 1981.
[75] K.Matsui, T.Matsuura, K.Iwasaki, "2 Micron CMOS Switched-Capacitor Circuits for Analog Video LSI", Proc. ISCAS, pp.241-244, May 1982.
[76] G.Fischer, G.S.Moschytz, "SC Integrator for High-Frequency Applications", Electron. Lett., vol.19, no.13, pp.495-496, June 1983.
[77] T.C.Choi et. al., "High-Frequency CMOS Switched-Capacitor Filters for Communications Applications", IEEE J. Solid-State Circuits, vol.SC-18, no.6, pp.652-664, December 1983.

[78] G.Fischer, G.S.Moschytz, "On the Frequency Limitations of SC Filters", IEEE J. Solid-State Circuits, vol.SC-19, no.4, pp.510-518, August 1984.
[79] A.Antoniou, "Design of Elliptic Digital Filters : Prescribed Specifications", Proc. IEE, vol.124, no.4, pp.341-344, April 1977.
[80] E.Hokenek, U.W.Brugger, G.S.Moschytz, "New Frequency Transformation for the Accurate Design of SC Ladder Filters", Electron. Lett., vol.18, no.6, pp.276-278, March 1982.
[81] C.R.W.Campbell, "Frequency Transformations in Switched Capacitor Filters", Research Review, Dept. Elec. Electron. Eng., Univ. of Cape Town, vol.6, no.2, pp.68-74, March/April 1982.
[82] C.R.W.Campbell, K.M.Reineck, "A Novel Prewarping Technique for the Design of Wideband SC Filters", Proc. 26th Midwest Symp. Circuits Syst., Puebla, Mexico, pp.594-596, August 1983.
[83] C.R.W.Campbell, K.M.Reineck, "A Pole/Zero Prewarping Procedure in SC Filter Design", IEEE Trans. Circuits Syst., vol.CAS-31, no.9, pp.821-825, September 1984.
[84] M.A.Jack, P.M.Grant, J.H.Collins, "The Theory, Design and Applications of Surface Acoustic Wave Fourier-Transform Processors", Proc. IEEE, vol.68, no.4, pp.450-468, April 1980.
[85] A.J.Slobodnik, "Surface Acoustic Waves and SAW Materials", Proc. IEEE, vol.64, no.5, pp.581-595, May 1976.
[86] A.J.Slobodnik, T.L.Szabo, K.R.Laker, "Miniature Surface-Acoustic-Wave Filters", Proc. IEEE, vol.67, no.1, pp.129-146, January 1979.
[87] F.S.Hickernell, "Zinc-Oxide Thin-Film Surface-Wave Transducers", Proc. IEEE, vol.64, no.5, pp.631-635, May 1976.
[88] O.Yamazaki, T.Mitsuyu, K.Wasa, "ZnO Thin-Film SAW Devices", IEEE Trans. Sonics Ultrasonics, vol.SU-27, no.6, pp.369-379, November 1980.
[89] L.A.Coldren, "Characteristics of Zinc-Oxide-on-Silicon Signal Processing and Storage Devices", Proc. IEEE, vol.64, no.5, pp.769-771, May 1976.
[90] W.J.Ghijsen, A.Venema, "Optimal Transducer Design for the Generation of SAW in Silicon Substrates", Sensors and Actuators, vol.3, pp.51-61, 1982.
[91] M.Hikita, et. al., "Miniature 90 MHz Low-Loss Narrowband SAW Filter Using New Resonant Configuration", Electron. Lett., vol.19, no.22, pp.944-945, October 1983.
[92] U.W.Brugger, B.J.Hosticka, "A Prewarping Scheme for the Design of SCFs", Proc. ISCAS, Houston, pp.317-320, May 1980.
[93] A.I.Zverev, "Handbook of Filter Synthesis", J.Wiley & Sons, USA.
[94] K.Steiglitz, "On the Simultaneous Estimation of Poles and Zeros in Speech Analysis", IEEE Trans. Acous. Speech Signal Processing, vol.ASSP-25, no.3, pp.229-234, June 1977.
[95] C-A.Gobet, A.Knob, "Noise Analysis of Switched Capacitor Networks", IEEE Trans. Circuits Syst., vol.CAS-30, no.1, pp.37-43, January 1983.
[96] N.Fliege, S.Tatari, "Noise Spectrum in Systems with Periodically Operated Switches", Proc. ISCAS, New York, pp.757-761, May 1978.
[97] C-A.Gobet, A.Knob, "Noise Analysis of Switched Capacitor

Networks", Proc. ISCAS, Chicago, pp.856-859, May 1981.
[98] B.Furrer, W.Guggenbuhl, "Noise Analysis of Sampled-Data Circuits", AEU, Band 35, Heft 11, pp.426-430, November 1981.
[99] J.H.Fischer, "Noise Sources and Calculation Techniques for SCFs", IEEE J. Solid-State Circuits, vol.SC-17, no.4, pp.742-752, August 1982.
[100] M.H.White et. al., "Characterization of Surface Channel CCD Image Arrays at Low Light Levels", IEEE J. Solid-State Circuits, vol.SC-9, no.1, pp.1-12, February 1974.
[101] K-C.Hsieh et. al., "A Low-Noise Chopper-Stabilized Differential SC Filtering Technique", IEEE J. Solid-State Circuits, vol.SC-16, no.6, pp.708-715, December 1981.
[102] F.W.Stephenson et. al., "Noise Modelling of Switched Capacitor Filters", IBM Fed. Syst. Div. contract report no.108081, research undertaken at Virginia Polytechnic Inst. & S.U., Blacksburg, September 1982.
[103] F.W.Stephenson et. al., "Noise Modelling of Switched Capacitor Filters", IBM Fed. Syst. Div. contract report no.YD-277246, research undertaken at Virginia Polytechnic Inst. & S.U., Blacksburg, May 1983.
[104] F.W.Stephenson et. al., "Analytical Techniques for Switched-Capacitor Filters", IBM Fed. Syst. Div. contract report no.YD-260624, research undertaken at Virginia Polytechnic Inst. & S.U., Blacksburg, September 1983.
[105] B.Furrer, W.Guggenbuhl, "Noise Analysis of a Switched-Capacitor Biquad", Proc. ISCAS, pp.460-463, May 1982.
[106] C-A.Gobet, "Spectral Distribution of a Sampled 1st Order Lowpass Filtered White Noise", Electron. Lett., vol.17, no.19, pp.720-721, September 1981.
[107] J.Velazquez-Ramos et. al., "Noise Analysis of Analog and Digital Circuits using Autoregressive Power Spectrum Estimation", IEEE Trans. Circuits Syst., vol.CAS-30, no.3, pp.193-195, March 1983.
[108] C-A.Gobet, A.Knob, "Noise Generated in SC Networks", Electron. Lett., vol.16, no.19, pp.734-735, September 1980.
[109] L.T.Bruton, F.N.Trofimenkoff, D.H.Treleaven, "Noise Performance of Low-Sensitivity Active Filters", IEEE J. Solid-State Circuits, vol.SC-8, no.1, pp.85-91, February 1973.
[110] J.Zurada, M.Bialko, "Noise and Dynamic Range of Active Filters with Op Amps", IEEE Trans. Circuits Syst., vol.CAS-22, no.10, pp.805-809, October 1975.
[111] R.Whitehead, "Operational Amplifier Noise Prediction", Harris Corp. Application Note #519, May 1976.
[112] T.S.Bernardi, "Designing Low Noise Op-Amp Based Systems:Part I", Electron. Eng., pp.43-47, July 1982.
———————, "Designing Low Noise Op-Amp Based Systems:Part II", Electron. Eng., pp.33-41, August 1982.
[113] A.Ryan, T.Scranton, "D-C Amplifier Noise Revisited", Analog Dialog, vol.18, no.1, pp.3-10, January 1984.
[114] D.F.Stout, "Handbook of Operational Amplifier Circuit Design", McGraw-Hill Book Co., USA, 1976.
[115] W.G.Jung, "Op Amp Cookbook"
[116] K.Martin, A.S.Sedra, "Easing Prefiltering Requirements of SC Filters", Electron. Lett., vol.16, no.16, pp.613-614, July 1980.
[117] P.E.Fleischer et. al., "An NMOS Analog Building Block for Telecommunication Applications", IEEE Trans Circuits Syst., vol.CAS-27, no.6, pp.552-559, June 1980.

[118] R.W.Schafer, L.R.Rabiner, "A Digital Signal Processing Approach to Interpolation", Proc. IEEE, vol.61, no.6, pp.692-702, June 1973.
[119] R.E.Crochiere, L.R.Rabiner, "Optimum FIR Digital Filter Implementations for Decimation, Interpolation and NarrowBand Filtering", IEEE Trans. Acous. Speech Signal Processing, vol.ASSP-23, no.5, pp.444-456, October 1975.
[120] ————————, "Interpolation and Decimation of Digital Signals - A Tutorial Review", Proc. IEEE, vol.69, no.3, pp.300-331, March 1981.
[121] R.Gregorian, W.E.Nicholson, "SC Decimation and Interpolation Circuits", IEEE Trans. Circuits Syst., vol.CAS-27, no.6, pp.509-514, June 1980.
[122] M.B.Ghaderi, G.C.Temes, S.Law, "Linear Interpolation using CCDs or SC Filters", IEE Proc., vol.128 Pt.G, no.4, pp.213-215, August 1981.
[123] A.Fettweis, A.Khalil, "Optimal Low-Sensitivity Anti-Aliasing and Conversion Filters", IEEE Trans. Circuits Syst., vol.CAS-27, no.6, pp.559-566, June 1980.
[124] A.Khalil, J.Pandel, "Interpolation Circuits as a Test-Aid for SC Filters and Digital Filters", AEU, Band 35, Heft 4, pp.182-184, April 1981.
[125] D.S.R.Gunawardena, A.H.Kayran, R.A.King, "Some Properties of Multidimensional Sampling Rate Conversion", Electron. Lett., vol.18, no.8, pp.321-323, April 1982.
[126] J-L.Berger, J-L.Coutures, "Cancellation of Aliasing in CCD Low-Pass Filters", IEEE J. Solid-State Circuits, vol.SC-12, no.6, pp.617-625, December 1977.
[127] C.H.Sequin, "Antialiasing Inputs for CCDs", IEEE J. Solid-State Circuits, vol.SC-12, no.6, pp.609-616, December 1977.
[128] D.C.von Grunigen, U.W.Brugger, G.S.Moschytz, "Simple SC Decimation Circuit", Electron. Lett., vol.17, no.1, pp.30-31, January 1981.
[129] I.Paul, J.W.Woods, "Intersection Filters for General Decimation/Interpolation", IEEE Trans. Acous. Speech Signal Processing, vol.ASSP-29, no.4, pp.934-936, August 1981.